

Chapter 3

Synthesis of Linear Arrays and Apertures

In this chapter we develop techniques for choosing the weighting of each sensor output in order to obtain a frequency-wavenumber response and beam pattern with desirable properties. The weighting process is also referred to as shading or tapering in the literature. In this chapter we restrict our attention to linear arrays. In Chapter 4, we consider planar array configurations.

The frequency-wavenumber response $\Upsilon(\omega, \mathbf{k})$ is the Fourier transform of the weights w_n , so there is a large body of mathematical results available. For linear arrays with equal spacing, $\Upsilon(\omega : \mathbf{k})$ has exactly the form of the discrete Fourier transform (DFT) so the techniques from equivalent temporal problems such as finite impulse response (FIR) filters and spectral estimation windows can be used directly. For planar arrays with equal spacing, the corresponding 2-D techniques can be used. For linear arrays whose sensors are located at arbitrary points on a line, the design problem is more difficult because we are no longer sampling on a uniform lattice.

Although there is a mathematical duality with the time domain problem, there are important differences between array processing and time domain processing that shape our conclusions:

- (i) The spatial dimension of the array normally has an absolute constraint due to the structure supporting it (e.g., a radio tower, a mast on a ship, the fuselage of an airplane, a satellite bus, a towed array). Even if it is possible to extend the array, it will be much more expensive than obtaining more time samples.
- (ii) The cost per sensor is significant in many cases because of the sensor

itself and associated electronics. Therefore, even if space is available, we choose to increase the processing complexity in order to reduce the number of sensors. There is a large incentive to optimize processing performance.

- (iii) In some cases, it is difficult to maintain amplitude and phase calibration of the sensors for a number of reasons (e.g., mutual coupling, environmental changes) and overall array calibration due to changes in sensor location. In Section 2.6, we saw how these changes placed a limit on the null depth in the beam pattern. We find many other cases in which calibration errors are the limiting factor in array performance. In contrast, time samples are very uniform in most applications.
- (iv) In the time domain, for a given signal and noise model, one can vary the number of samples to change performance. However, in the array problem, we have two dimensions: N , the number of sensors, and K , the number of samples that can be varied to change performance.

Therefore, although duality is an important factor that we will exploit, the array processing problem must be studied in its own context.

In this chapter, we examine a number of different techniques for design of linear, equally spaced arrays. Linear arrays are the traditional focus of texts on classical array processing. The design of weighting for linear arrays reveal many of the important concepts in array processing. Many of the ideas extend to more general geometries, although the mathematics becomes more involved (in some cases, the mathematics does not extend to higher dimensions).

Recall from our discussion in Chapter 1 that our ultimate goal is to design array processors that adapt their configuration to match the incoming data and are optimized in a statistical sense. However, it is important to have a thorough understanding of classical (or deterministic) beamformer design for several reasons:

- (i) The classical array design provides a basis for comparison for any proposed adaptive design. If we derive some “optimum array processor,” we should show its improvement over the classical array processor.
- (ii) In many cases, we will find that the “optimum array processor” has one of the beamformers that we design using deterministic techniques as a basic building block in its implementation.
- (iii) In some cases, understanding the deterministic design points out areas where statistical techniques may be useful.

We consider several approaches to the selection of weighting functions for linear apertures and linear arrays:

(i) Spectral Weightings (3.1)

This approach exploits the Fourier transform relationships between the frequency-wavenumber response function and the weighting function and the parallelism with windows and tapers used in the spectral analysis of time series.

(ii) Array Polynomials and the z -Transform (3.2)

This approach, which originated with Schelkunoff [Sch43], develops a polynomial representation of a linear array and leads to a z -transform relationship. We can then analyze and synthesize patterns by positioning the zeros of the array polynomial.

(iii) Pattern Sampling in Wavenumber Space (3.3)

This approach specifies the desired values of the pattern on a grid in wavenumber space. For apertures, it utilizes the sampling theorem. For arrays, it leads to a DFT relationship.

(iv) Minimum Beamwidth for Specified Sidelobe Level (3.4)

This approach attempts to find an array weighting function that minimizes the beamwidth for a given maximum sidelobe level. It leads us to the Dolph-Chebychev and Taylor weightings, which are widely used in practice.

(v) Least Squares Error Pattern Synthesis (3.5)

This approach specifies a desired pattern in frequency-wavenumber space and attempts to find a weighting function to achieve it. The approach uses the Fourier transform for apertures or the Fourier series for arrays to obtain a minimum mean-square error approximation to the desired pattern.

(vi) Minimax Design (3.6)

This approach utilizes a technique that was developed to design finite impulse response (FIR) filters. It specifies a maximum allowable variation in the height of the main lobe (e.g., $1 - \delta_p \leq B_\psi(\psi) \leq 1 + \delta_p$) and a maximum allowable height in the sidelobe region, δ_s , and finds a solution to meet these criteria.

(vii) Null Steering (3.7)

This approach assumes that there are certain points in wavenumber space where there are interfering signals (e.g., jammers). We design weightings so that the frequency-wavenumber response is zero in these directions.

(viii) Asymmetric Beams (3.8)

All of the beams discussed up to this point assume that the desired target direction is known. If we are required to estimate the target direction, then beam patterns with different characteristics, specifically a significant non-zero slope in the pointing direction, are useful. We develop this type of beam in Section 3.8 and discuss its properties.

(ix) Spatially Non-uniform Linear Arrays (3.9)

In this section, we discuss linear arrays with non-uniform element spacing. We develop several synthesis techniques. We also introduce the idea of minimally redundant linear arrays.

(x) Beamspace Processing (3.10)

In later chapters of the text, we find that, in many applications, it is useful to preprocess the array data to form a set of beams that span the space of interest and then do further processing in these output beams. We introduce this idea in Section 3.10 and develop it in detail in later chapters.

(xi) Broadband Arrays(3.11)

In this section, we develop linear array spacings that are useful when the signals of interest are broadband.

The structure of the chapter is shown in Table 3.1.

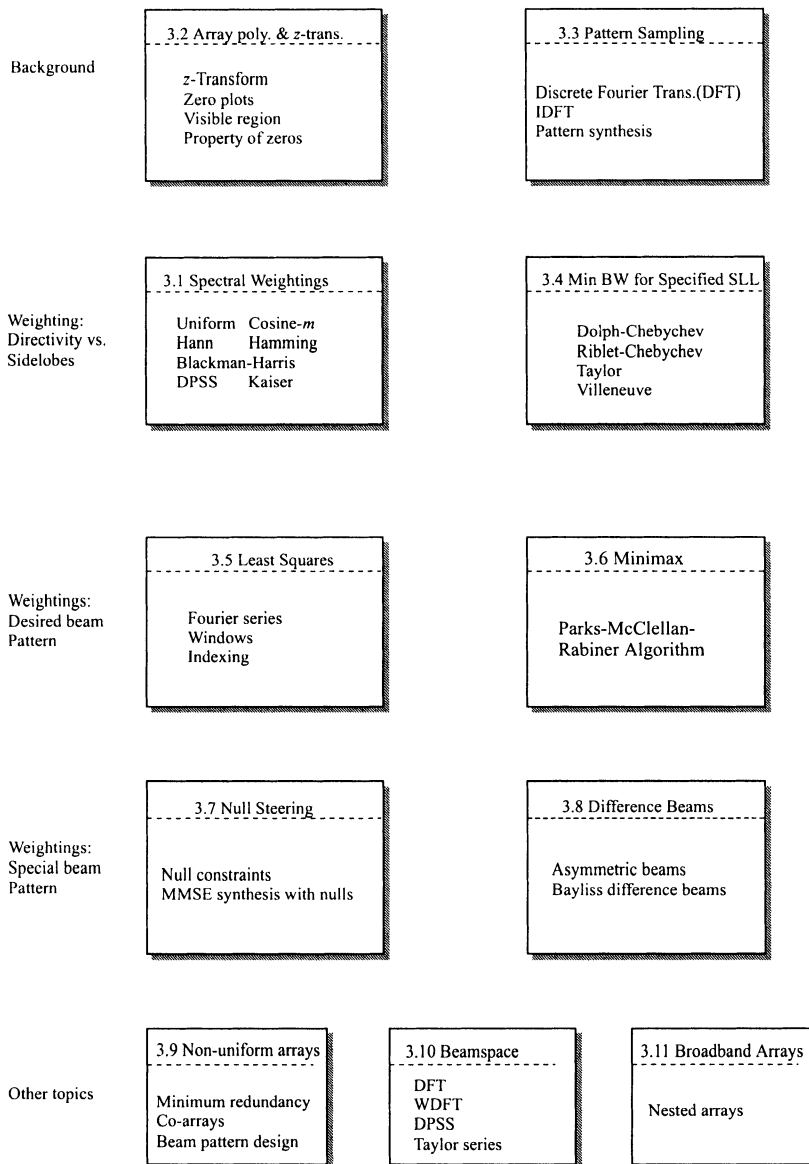


Table 3.1 Structure of Chapter 3.

The techniques are drawn from the classical antenna literature and the digital filter design literature. Representative texts in the antenna area are Elliot [Ell81], Kraus [Kra88], Balanis [Bal82], Milligan [Mil85], Johnson [Joh93], Steinberg [Ste76], Ziomek [Zio95], Ma [Ma74], Mailloux [Mai94], Weeks [Wee68], Stutzman and Thiele [ST81], and the four volume handbook

edited by Lo and Lee [LL93a], [LL93b], [LL93c], [LL93d].

Representative texts in the digital filter area are Oppenheim and Schafer [OS89], Proakis et al. [PRLN92], Rabiner and Gold [RG75], and Mittra and Kaiser [MK93]. We use examples from these references and other sources.

3.1 Spectral Weighting

There are several classes of array weightings that are equivalent to various windows or tapers used in the spectral analysis of time series. Their design depends explicitly upon the Fourier transform relationship for the weighting and the frequency-wavenumber response for a linear array with a sensor spacing less than or equal to $\lambda/2$; consequently, grating lobes and spatial aliasing become unimportant and Fourier transform theory for continuous functions can be used directly.

The starting point is the Fourier transform pair in (2.215) and (2.216),

$$\Upsilon(\omega, k) = \int_{-\infty}^{\infty} w_a^*(z) e^{-jkz} dz \quad (3.1)$$

and

$$w_a^*(z) = \frac{1}{2\pi} \int_{-\infty}^{\infty} \Upsilon(\omega, k) e^{jkz} dk, \quad (3.2)$$

where we have suppressed the z subscript on k_z .

As a result of this transform relationship there is a very large body of literature for weight design, or pattern synthesis, for arrays of this construction. Some of the more important considerations are the following:

- The Fourier uncertainty principle specifies a lower limit on the product of the mean-square aperture extent and the mean-square response width.¹ Specifically, we have

$$\sqrt{\overline{\Delta l^2}} \sqrt{\overline{\Delta k^2}} > 1/2, \quad (3.3)$$

where $\overline{\Delta l^2}$ and $\overline{\Delta k^2}$ are respectively the normalized mean-square widths of the weighting and the response and are given by

$$\overline{\Delta l^2} = \frac{\int_{-L/2}^{L/2} z^2 |w_a(z)|^2 dz}{\int_{-L/2}^{L/2} |w_a(z)|^2 dz}, \quad (3.4)$$

¹The proof of the Fourier uncertainty principle requires zero-mean position of the weighting and of the response. The discussion refers to distributions about these means.

$$\overline{\Delta k^2} = \frac{\int_{-\infty}^{\infty} k^2 |\Upsilon(\omega, k)|^2 dk / 2\pi}{\int_{-\infty}^{\infty} |\Upsilon(\omega, k)|^2 dk / 2\pi}. \quad (3.5)$$

This uncertainty principle implies that a narrow, or a high-resolution, frequency-wavenumber response (e.g., small $\overline{\Delta k^2}$) requires a large mean-square weighting extent $\overline{\Delta l^2}$ that is bounded by $L^2/4$ for an array of finite extent. Consequently, there is a fundamental trade-off between the resolution of the response function and the extent of the aperture.

- Parseval's (or Plancherel's) theorem states

$$\int_{-\infty}^{\infty} |\Upsilon(\omega, k)|^2 \frac{dk}{2\pi} = \int_{-\infty}^{\infty} |w_a(z)|^2 dz. \quad (3.6)$$

This implies that high amplitude response functions such as those often generated for null placements or for sidelobe reduction lead to large values for the sum of the magnitude squared of the weighting. We have seen earlier that this decreases the white noise gain, A_w , and increases the sensitivity function, $T(\omega)$.

- The sidelobes decay asymptotically according to the order of the discontinuity in the aperture weighting. Uniform weighting leads to sidelobes that decay as $O(\frac{1}{n})$. Smooth weighting patterns lead to fast sidelobe decay. It is important to note that this is an asymptotic result and is not a statement about the maximum sidelobe level; there are several very useful weightings, such as Hamming and Taylor, that have step or derivative discontinuities. These weightings achieve low maximum sidelobes by using these discontinuities to cancel the high sidelobes near the main beam.

The value of this work extends beyond linear arrays. First, there are a number of important arrays that consist of sets of linear arrays; second, weightings for planar arrays are often pursued in terms of a product of linear array weightings in each dimension; finally, the design principles are often applicable to higher dimensions.

Our development in this section will focus on linear arrays. The analogous results for linear apertures follow directly. In Section 3.1, the problem of interest is to reduce the sidelobes while minimizing the increase in the main-lobe width (and the loss in directivity).

Our approach in this section is heuristic. We will try different weight vectors and analyze their performance. In Section 3.4, we will develop an analytic technique. We use the uniform weighting as a reference. We derived its beam pattern in Section 2.4 and repeat it for reference purposes.

3.1.1.1 Uniform weighting

From (2.77), the uniform weights are

$$w_n = \frac{1}{N}, \quad n = 0, \dots, N-1. \quad (3.7)$$

The resulting beam pattern in u -space is

$$B_u(u) = \frac{1}{N} \frac{\sin(\frac{\pi Nd}{\lambda} u)}{\sin(\frac{\pi d}{\lambda} u)}. \quad (3.8)$$

We focus our attention on a standard linear array, so (3.8) reduces to,

$$B_u(u) = \frac{1}{N} \frac{\sin(\frac{N\pi u}{2})}{\sin(\frac{\pi u}{2})}. \quad (3.9)$$

From (2.140), the directivity is

$$D = N. \quad (3.10)$$

All of the weightings that we are going to consider in this section are real and symmetric, so it is convenient to use the position of the n th element as the index,

$$\begin{aligned} \tilde{n} &= n - \frac{N-1}{2}, & n &= 0, 1, \dots, N-1, \\ \tilde{n} &= -\frac{N-1}{2}, \dots, \frac{N-1}{2}. \end{aligned} \quad (3.11)$$

We first consider various weightings constructed from cosine functions.

3.1.1.2 Cosine weightings

We consider the case when N is odd. The cosine weighting is

$$w(\tilde{n}) = \sin\left(\frac{\pi}{2N}\right) \cos\left(\pi \frac{\tilde{n}}{N}\right), \quad -\frac{N-1}{2} \leq \tilde{n} \leq \frac{N-1}{2}, \quad (3.12)$$

where the $\sin(\frac{\pi}{2N})$ term is a constant such that $B_u(0) = 1$. Writing the cosine in exponential form gives

$$w(\tilde{n}) = \sin\left(\frac{\pi}{2N}\right) \left[\frac{e^{j\frac{\pi\tilde{n}}{N}} + e^{-j\frac{\pi\tilde{n}}{N}}}{2} \right], \quad -\frac{N-1}{2} \leq \tilde{n} \leq \frac{N-1}{2}. \quad (3.13)$$

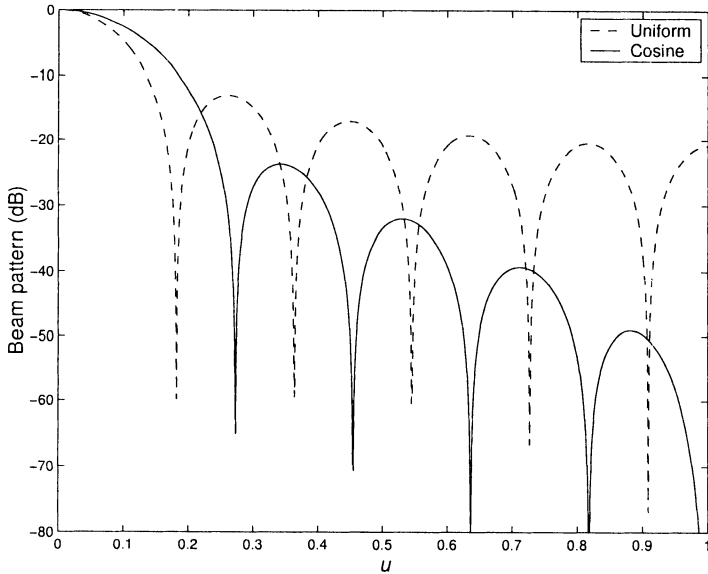


Figure 3.1 Beam pattern for uniform and cosine weighting: $N=11$.

Using the form of the array manifold vector in (2.70), the beam pattern is

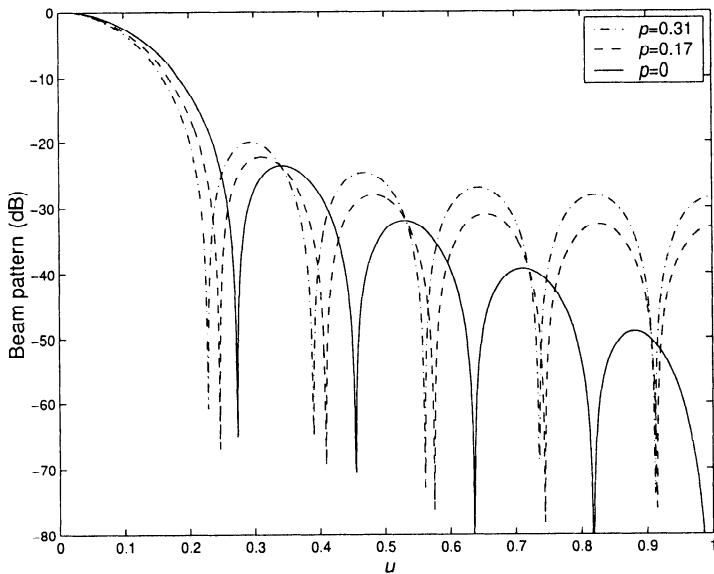
$$B_u(u) = \frac{1}{2} \sin\left(\frac{\pi}{2N}\right) \left\{ \sum_{\tilde{n}=-\frac{N-1}{2}}^{\frac{N-1}{2}} e^{j\frac{\pi\tilde{n}}{N}} e^{-j\tilde{n}\pi u} + \sum_{\tilde{n}=-\frac{N-1}{2}}^{\frac{N-1}{2}} e^{-j\frac{\pi\tilde{n}}{N}} e^{-j\tilde{n}\pi u} \right\}. \quad (3.14)$$

The first term corresponds to a conventional beam pattern steered to $u_s = 1/N$, and the second term corresponds to a conventional beam pattern steered to $u_s = -1/N$. Therefore,

$$B_u(u) = \frac{1}{2} \sin\left(\frac{\pi}{2N}\right) \left\{ \frac{\sin\left(\frac{N\pi}{2}(u - \frac{1}{N})\right)}{\sin\left(\frac{\pi}{2}(u - \frac{1}{N})\right)} + \frac{\sin\left(\frac{N\pi}{2}(u + \frac{1}{N})\right)}{\sin\left(\frac{\pi}{2}(u + \frac{1}{N})\right)} \right\}. \quad (3.15)$$

We will find this superposition of shifted conventional beams to be a common characteristic of many of the patterns that we develop. We show the beam pattern for an 11-element array using the cosine weighting in Figure 3.1. We show the conventional beam pattern as a reference. The sidelobes have been reduced but the main lobe is wider. The parameters for the two beam patterns are:²

²The parameter D_N is the normalized directivity of the array. It is normalized with respect to the directivity of a uniformly weighted array. For the standard linear array it is also the normalized white noise gain.

Figure 3.2 Beam pattern for raised cosine weighting: $N=11$.

Weighting	HPBW	BW_{NN}	First Sidelobe HT	D_N
Uniform	$0.89\frac{2}{N}$	$2.0\frac{2}{N}$	-13.0 dB	1
Cosine	$1.18\frac{2}{N}$	$3.0\frac{2}{N}$	-23.5 dB	0.816

3.1.1.3 Raised cosine

We can combine the rectangular uniform and the cosine weighting to obtain some of desireable features of each weighting. The corresponding array weighting is

$$w(\tilde{n}) = c(p) \left(p + (1-p) \cos \left(\pi \frac{\tilde{n}}{N} \right) \right), \quad \tilde{n} = -\frac{N-1}{2}, \dots, \frac{N-1}{2}, \quad (3.16)$$

where

$$c(p) = \frac{p}{N} + \frac{(1-p)}{2} \sin \left(\frac{\pi}{2N} \right) \quad (3.17)$$

is a constant so that $B_u(0) = 1$.

The beam patterns for the raised cosine weighting for $p = 0.31, 0.17$, and 0 are shown in Figure 3.2. As p decreases, the height of the first sidelobe decreases and the width of the mainlobe increases. The beam patterns have the following parameters:

p	HPBW	BW_{NN}	First Sidelobe HT	D_N
0.31	$1.03 \frac{2}{N}$	$2.50 \frac{2}{N}$	-20.0 dB	0.928
0.17	$1.09 \frac{2}{N}$	$2.70 \frac{2}{N}$	-22.0 dB	0.886
0	$1.18 \frac{2}{N}$	$3.00 \frac{2}{N}$	-23.5 dB	0.816

Thus, we have been able to narrow the HPBW and keep the first sidelobe much lower than the uniform distribution.

3.1.1.4 Cosine ^{m} weighting

We next consider a family of cosine weightings of the form $\cos^m(\pi\tilde{n}/N)$. The array weights are

$$w_m(n) = \begin{cases} c_2 \cos^2\left(\frac{\pi z}{L}\right), & m = 2, \\ c_3 \cos^3\left(\frac{\pi z}{L}\right), & m = 3, \\ c_4 \cos^4\left(\frac{\pi z}{L}\right), & m = 4, \end{cases} \quad (3.18)$$

where c_2, c_3 , and c_4 are normalization constants.

The weighting for $m = 2$ is sometimes called the Hann weighting.³ Once again, the beam pattern is computed using the exponential form of cosine function.

The beam patterns are shown in Figure 3.3. As m increases, the sidelobes decrease but the main lobe widens. The parameters for the beam patterns are:

m	HPBW	BW_{NN}	First Sidelobe HT.	D_N
2	$1.44 \frac{2}{N}$	$4 \frac{2}{N}$	-31.4 dB	0.667
3	$1.66 \frac{2}{N}$	$5 \frac{2}{N}$	-39.4 dB	0.576
4	$1.85 \frac{2}{N}$	$6 \frac{2}{N}$	-46.7 dB	0.514

3.1.1.5 Raised cosine-squared weighting

The raised cosine-squared family of weightings is given by

$$\begin{aligned} w(\tilde{n}) &= c_2(p) \left\{ p + (1-p) \cos^2\left(\frac{\pi\tilde{n}}{N}\right) \right\} \\ &= \frac{c_2(p)}{2} \left\{ (1+p) + (1-p) \cos\left(\frac{2\pi\tilde{n}}{N}\right) \right\}, \\ \tilde{n} &= -\frac{N-1}{2}, \dots, \frac{N-1}{2}, \end{aligned} \quad (3.19)$$

³The weighting is due to an Austrian meteorologist, von Hann. It is sometimes referred to as the Hanning weighting. We call it the Hann weighting.

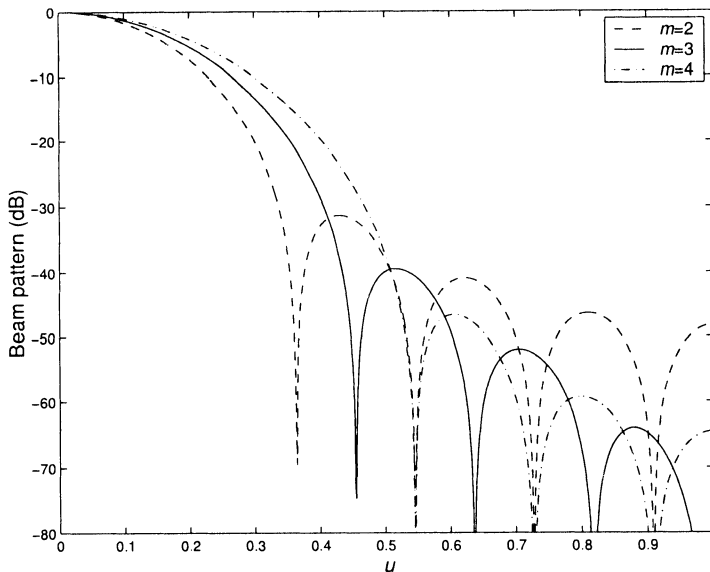


Figure 3.3 Beam patterns: cosine m weighting, $N=11$.

where $c_2(p)$ is the normalization constant. We consider the general case in the problems. In the text, we consider a specific weighting known as the Hamming weighting.

3.1.1.6 Hamming weighting

The Hamming weighting exploits the characteristics of the rectangular pattern and the cosine-squared pattern to place a null at the peak of the first sidelobe. The weighting function is

$$w(\tilde{n}) = g_0 + g_1 \cos\left(\frac{2\pi\tilde{n}}{N}\right), \quad \tilde{n} = -\frac{N-1}{2}, \dots, \frac{N-1}{2}. \quad (3.20)$$

The coefficients g_0 and g_1 are chosen to place a null at $u = 3/N$ and normalize the response at broadside to unity. The result is

$$w(\tilde{n}) = 0.54 + 0.46 \cos\left(\frac{2\pi\tilde{n}}{N}\right), \quad \tilde{n} = -\frac{N-1}{2} \leq n \leq \frac{N-1}{2}. \quad (3.21)$$

This corresponds to $p = 0.08$ in (3.19). The beam pattern is the sum of

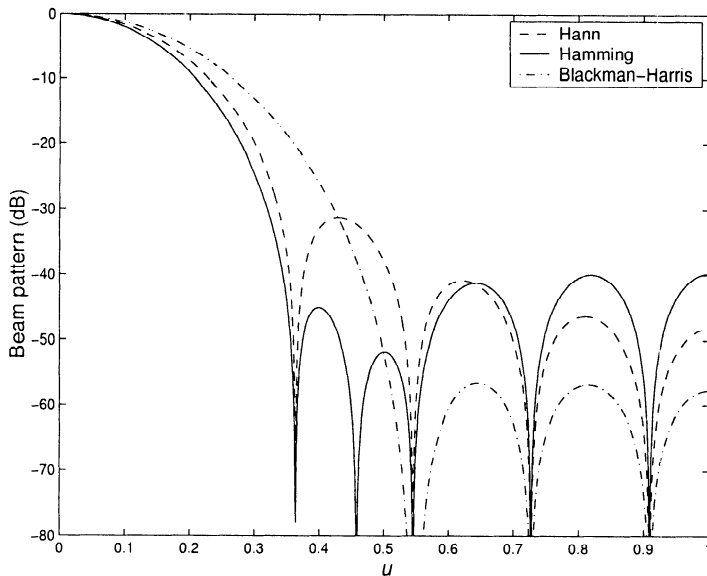


Figure 3.4 Beam patterns for Hann, Hamming, and Blackman-Harris weightings: $N=11$.

three conventional beam patterns:

$$B_u(u) = 0.54 \frac{\sin\left(\frac{N\pi u}{2}\right)}{\sin\left(\frac{\pi u}{2}\right)} + 0.23 \left[\frac{\sin\left(\frac{N\pi}{2}\left(u - \frac{2}{N}\right)\right)}{\sin\left(\frac{\pi}{2}\left(u - \frac{2}{N}\right)\right)} + \frac{\sin\left(\frac{N\pi}{2}\left(u + \frac{2}{N}\right)\right)}{\sin\left(\frac{\pi}{2}\left(u + \frac{2}{N}\right)\right)} \right]. \quad (3.22)$$

The Hamming weighting is shown in Figure 3.4. We also show the beam patterns for the Hann weighting (3.18) and the Blackman-Harris weighting, which we will derive next.

The first zero occurs at $u = 4/N$ and the height of the first non-zero sidelobe is -39.5 dB. There is a step discontinuity in the weighting that leads to an asymptotic falloff of the sidelobes of $O(\frac{1}{n})$; however, the first sidelobe is cancelled exactly and the remaining ones are low absolutely in spite of their relatively slow falloff. The directivity of the Hamming weighting is relatively high. In addition, we note that the beamwidth of the Hamming window is less than the beamwidth of the Hann weighting and its first sidelobe is lower. This is an exception to the general trend.

3.1.1.7 Blackman-Harris weighting

The Blackman-Harris weighting simply extends the procedure to higher order harmonics to provide nulls at the peaks of the first two sidelobes. The weighting function is

$$w(\tilde{n}) = 0.42 + 0.5 \cos\left(\frac{2\pi\tilde{n}}{N}\right) + 0.08 \cos\left(\frac{4\pi\tilde{n}}{N}\right), \tilde{n} = -\frac{N-1}{2}, \dots, \frac{N-1}{2}. \quad (3.23)$$

The beam pattern is a sum of conventional beam patterns,

$$B_u(u) = 0.42 \frac{\sin\left(\frac{N\pi u}{2}\right)}{\sin\left(\frac{\pi u}{2}\right)} + 0.25 \left[\frac{\sin\left(\frac{N\pi}{2}\left(u - \frac{2}{N}\right)\right)}{\sin\left(\frac{\pi}{2}\left(u - \frac{2}{N}\right)\right)} + \frac{\sin\left(\frac{N\pi}{2}\left(u + \frac{2}{N}\right)\right)}{\sin\left(\frac{\pi}{2}\left(u + \frac{2}{N}\right)\right)} \right] \\ + 0.04 \left[\frac{\sin\left(\frac{N\pi}{2}\left(u - \frac{2}{N}\right)\right)}{\sin\left(\frac{\pi}{2}\left(u - \frac{2}{N}\right)\right)} + \frac{\sin\left(\frac{N\pi}{2}\left(u + \frac{2}{N}\right)\right)}{\sin\left(\frac{\pi}{2}\left(u + \frac{2}{N}\right)\right)} \right], \quad (3.24)$$

and is shown in Figure 3.4. The parameters for the beam patterns are:

Weighting	HPBW	BW_{NN}	First Sidelobe HT.	D_N
Hann	$1.44\frac{2}{N}$	$4.0\frac{2}{N}$	-31.4 dB	0.664
Hamming	$1.31\frac{2}{N}$	$4.0\frac{2}{N}$	-39.5 dB	0.730
Blackman-Harris	$1.65\frac{2}{N}$	$6.0\frac{2}{N}$	-56.6 dB	0.577

The weightings up to this point have been based on various sinusoidal functions. We now look at other types of array weightings in an attempt to improve the beamwidth–sidelobe trade-off.

3.1.1.8 Prolate spheroidal functions ⁴

The problem of interest is to develop a weighting that will maximize the percentage of the total power that is concentrated in a given angular region. Thus, we want to maximize the ratio,

$$\alpha = \frac{\iint_{\Omega_1} |B(\theta, \phi)|^2 \sin \theta d\theta d\phi}{\int_0^\pi \sin \theta d\theta \int_0^{2\pi} d\phi |B(\theta, \phi)|^2}, \quad (3.25)$$

⁴Discrete prolate sequences have been applied to the FIR design problem by Tufts and Francis [TF70], Papoulis and Bertran [PB72], and Tufts [Tuf75]. They were applied to the aperture problem by Rhodes [Rho63]. Our discussion follows Prasad [Pra82].

where Ω_1 is a region around the mainbeam. For a linear array, this can be written as

$$\alpha = \frac{\int_{-\psi_0}^{\psi_0} |B_\psi(\psi)|^2 d\psi}{\int_{-\pi}^{\pi} |B_\psi(\psi)|^2 d\psi}, \quad (3.26)$$

where $\psi = \frac{2\pi}{\lambda}d \cos \theta$. From (2.51), we have

$$B_\psi(\psi) = \mathbf{w}^H \mathbf{v}_\psi(\psi). \quad (3.27)$$

The numerator can be written as

$$\begin{aligned} \alpha_N &= \int_{-\psi_0}^{\psi_0} \mathbf{w}^H \mathbf{v}_\psi(\psi) \mathbf{v}_\psi^H(\psi) \mathbf{w}^* d\psi \\ &= \mathbf{w}^H \left[\int_{-\psi_0}^{\psi_0} \mathbf{v}_\psi(\psi) \mathbf{v}_\psi^H(\psi) d\psi \right] \mathbf{w} \\ &= \mathbf{w}^H \mathbf{A} \mathbf{w}, \end{aligned} \quad (3.28)$$

where

$$\mathbf{A} \triangleq \int_{-\psi_0}^{\psi_0} \mathbf{v}_\psi(\psi) \mathbf{v}_\psi^H(\psi) d\psi. \quad (3.29)$$

The (m, n) element of \mathbf{A} is

$$\int_{-\psi_0}^{\psi_0} e^{jm\psi} e^{-jn\psi} d\psi = \frac{2 \sin((m-n)\psi_0)}{(m-n)} = 2\psi_0 \text{sinc}((m-n)\psi_0). \quad (3.30)$$

Similarly, the denominator is

$$\begin{aligned} \alpha_D &= \int_{-\pi}^{\pi} \mathbf{w}^H \mathbf{v}_\psi(\psi) \mathbf{v}_\psi^H(\psi) \mathbf{w} d\psi \\ &= \mathbf{w}^H \mathbf{B} \mathbf{w}, \end{aligned} \quad (3.31)$$

where

$$\mathbf{B} = \int_{-\pi}^{\pi} \mathbf{v}_\psi(\psi) \mathbf{v}_\psi^H(\psi) d\psi = 2\pi \mathbf{I}. \quad (3.32)$$

Thus,

$$\alpha = \frac{\mathbf{w}^H \mathbf{A} \mathbf{w}}{2\pi \mathbf{w}^H \mathbf{w}}. \quad (3.33)$$

To maximize α , we find the eigenvalues and eigenvectors of the matrix

$$2\pi \lambda \mathbf{w} = \mathbf{A} \mathbf{w}, \quad (3.34)$$

and choose the eigenvector corresponding to the largest eigenvalue λ_{max} .⁵ Using (3.30) in (3.34) and dropping the factor of 2, we have

$$\sum_{n=1}^N \frac{\sin((m-n)\psi_0)}{(m-n)} w_n = \pi\lambda w_m, \quad m = 1, 2, \dots, N. \quad (3.35)$$

The weightings (or sequences) obtained by solving (3.35) are called **discrete prolate spheroidal sequences (DPSS)** and the corresponding beam patterns are called **discrete prolate spheroidal functions**. They are discussed in detail by Slepian [Sle78]. The discrete prolate spheroidal sequences are also referred to as **Slepian sequences**. The sequence corresponding to the largest eigenvalue is referred to as the first Slepian sequence. They are the discrete analog to the continuous case discussed by Slepian, Landau, and Pollack in a series of *Bell System Technical Journal* articles [SP61], [Sle64], [Sle65], [SS65], [LP61], and [LP62]. For our present application, we do not need most of their properties. We discuss the DPSS functions in more detail in Chapter 5.

We now consider a simple example to illustrate the results.

Example 3.1.1⁶

We consider an 11-element array and solve (3.35) for various values of ψ_0 . In each case, the optimum weight vector \mathbf{w}_0 corresponds to the eigenvector corresponding to largest eigenvalue. The results are shown in Table 3.2. We show the first six normalized weights; the other five weights follow from symmetry. To simplify the plot we have normalized the weights so that $w_6 = 1$. The actual weights are normalized so that $B_u(0) = 1$.

Table 3.2 Normalized Weights Corresponding to Maximum Eigenvalues

ψ_0/π	w_1	w_2	w_3	w_4	w_5	w_6
0.025	0.975	0.984	0.991	0.996	0.999	1.000
0.06	0.865	0.912	0.950	0.978	0.994	1.000
0.10	0.678	0.785	0.875	0.943	0.986	1.000
0.20	0.274	0.466	0.665	0.839	0.958	1.000
0.40	0.043	0.168	0.391	0.670	0.907	1.000

In Figure 3.5, we show some representative discrete prolate spheroidal sequences for $\psi_0 = 0.1\pi, 0.2\pi$, and 0.4π .

The corresponding beam patterns are shown in Figure 3.6. As ψ_0 approaches zero, \mathbf{w}_0 approaches uniform weighting because we are maximizing the directivity. For $\psi_0 = 0.2\pi$, most of the energy is concentrated in the main beam with a slightly larger beamwidth and sidelobes of -20 dB and lower. For $\psi_0 = 0.4\pi$, the sidelobes are -53 dB, but the beam is much broader.

⁵The symbol λ denotes the eigenvalue. We also use λ for the wavelength but the meaning should be clear from the context.

⁶This example is similar to the result in Prasad [Pra82].

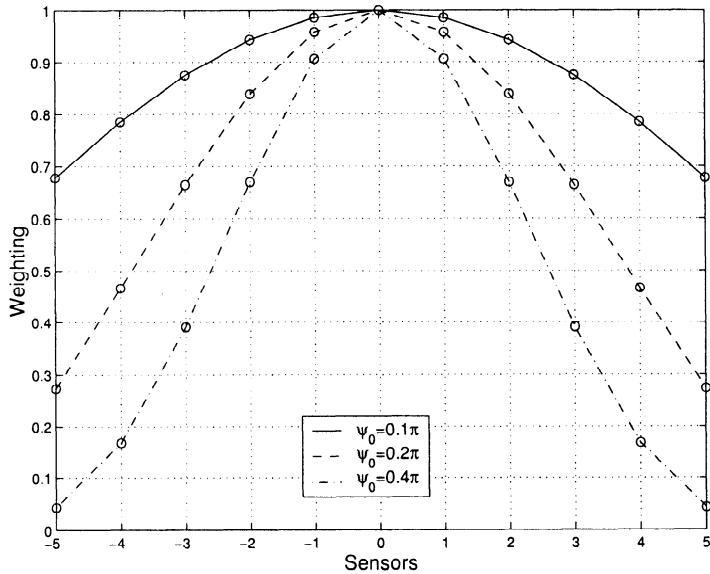


Figure 3.5 Discrete prolate spheroidal sequences: $\psi_0 = 0.1\pi$, 0.2π , and 0.4π .

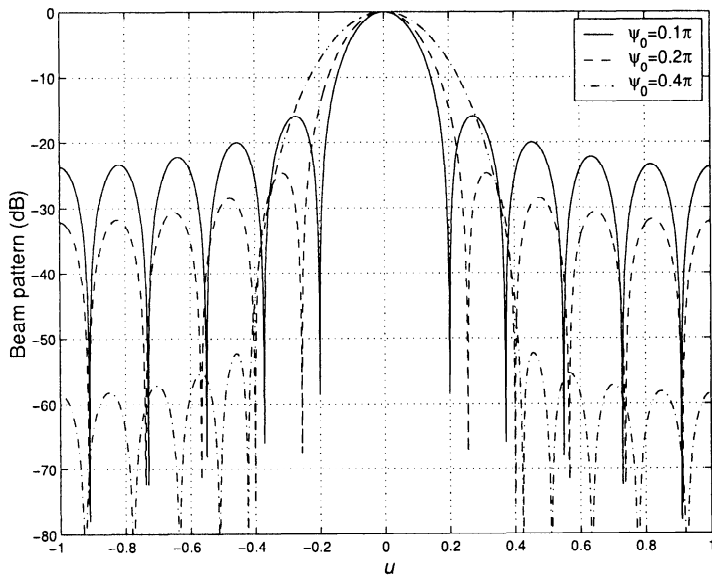


Figure 3.6 Beam patterns as a function of ψ_0 : DPSS weighting, $N=11$.

The beam pattern parameters for the DPSS weightings are:

		HPBW	BW_{NN}	First Sidelobe HT.	D_N
DPSS	$\psi_0 = 0.1\pi$	$0.02/N$	$1.40\pi/N$	-15.6 dB	0.981
	$\psi_0 = 0.2\pi$	$2.20/N$	$1.79\pi/N$	-24.7 dB	0.869
	$\psi_0 = 0.4\pi$	$2.86/N$	$2.97\pi/N$	-52.2 dB	0.665

3.1.1.9 Kaiser weightings

Kaiser [Kai74] proposed a relatively simple approximation to the prolate spheroidal sequences using Bessel functions. The weighting has found widespread usage in spectral analysis, FIR filter design, and other fields.

The Kaiser weights are

$$w(\tilde{n}) = I_0 \left(\beta \sqrt{1 - \left[\frac{2\tilde{n}}{N} \right]^2} \right), \quad -\frac{N-1}{2} \leq \tilde{n} \leq \frac{N-1}{2}, \quad (3.36)$$

where $I_0(x)$ is the modified Bessel function of zero-order [AS65]. The parameter β specifies a beam pattern trade-off between the peak height of the sidelobes and the beamwidth of the main lobe.

We now consider two examples to illustrate the behavior.

Example 3.1.2

Consider a standard 11-element linear array. The normalized ($w_6 = 1$) weights for $\beta = 3$ and 6 are shown in Figure 3.7(a). The resulting beam patterns are shown in Figure 3.7(b). For $\beta = 3$, the HPBW is $2.52/N$, the BW_{NN} is $1.12\pi/N$, and the highest sidelobe is -26 dB. For $\beta = 6$, the HPBW is $2.86/N$, the BW_{NN} is $1.68\pi/N$, and the highest sidelobe is -47 dB. Note that as β decreases, the weighting function approaches the uniform weighting.

Example 3.1.3

In this case, we fix β at 3 and investigate the behavior for $N = 11$, 21, and 41. The beam patterns are shown in Figure 3.8. All three cases have the same maximum sidelobe. Changing N changes the value of u where this maximum occurs.

The beam pattern parameters for the Kaiser weightings for $N = 11$ are:

		HPBW	BW_{NN}	First Sidelobe HT.	D_N
Kaiser	$\beta = 3$	$2.18/N$	$1.75\pi/N$	-23.7 dB	0.882
	$\beta = 6$	$2.80/N$	$2.76\pi/N$	-44.4 dB	0.683

This completes our initial discussion of array weight vectors that are designed to allow trade-off between the beamwidth of the main lobe and the height of sidelobes.

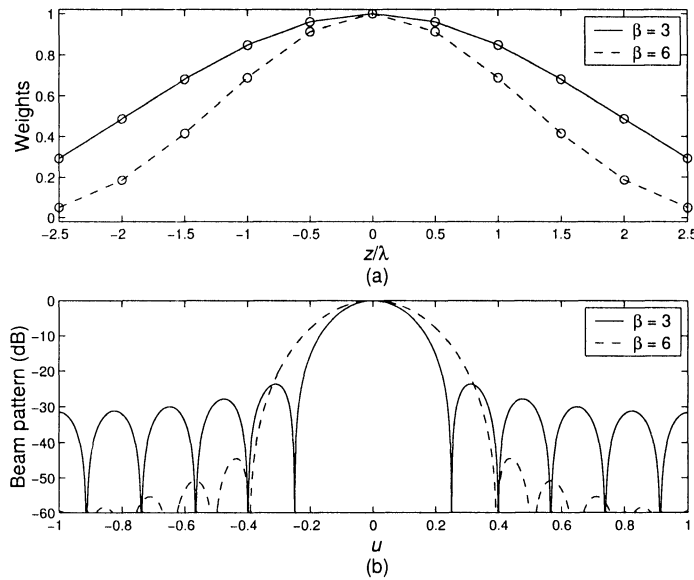


Figure 3.7 Kaiser weighting: (a) weighting for $\beta = 3$ and 6; (b) beam patterns for $\beta = 3$ and 6: $N=11$.

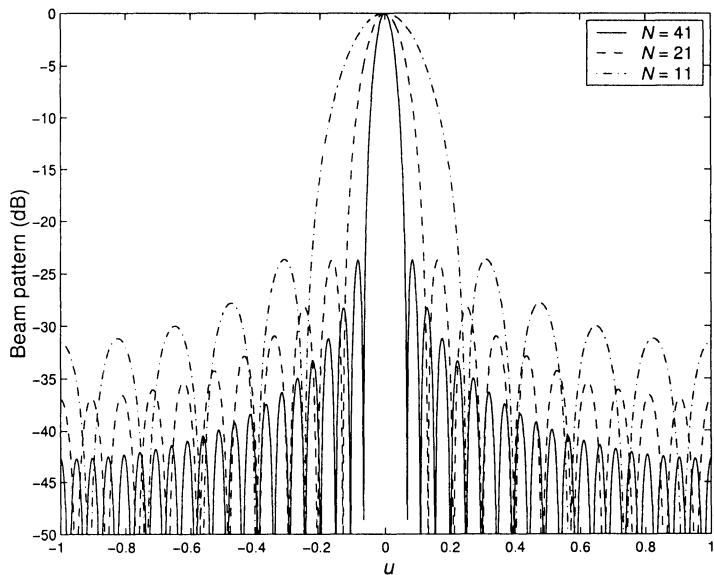


Figure 3.8 Beam patterns for Kaiser weighting; $\beta = 3$, $N = 11$, 21, and 41.

Other weight vectors are described in the comprehensive paper by Harris [Har78] on time-domain windows.

3.2 Array Polynomials and the z -Transform

For linear equally spaced arrays the beam pattern can be represented in terms of an **array polynomial**. In 1943, Schelkunoff [Sch43] utilized this representation to develop a theory of linear arrays. We utilize his work and introduce the z -transform representation.

3.2.1 z -Transform

From (2.71), the beam pattern can be written in ψ -space as

$$B_\psi(\psi) = e^{-j\left(\frac{N-1}{2}\right)\psi} \left(\sum_{n=0}^{N-1} w_n e^{-jn\psi} \right)^*. \quad (3.37)$$

Defining

$$z = e^{j\psi}, \quad (3.38)$$

we can write

$$B_z(z) = \sum_{n=0}^{N-1} w_n z^{-n}, \quad (3.39)$$

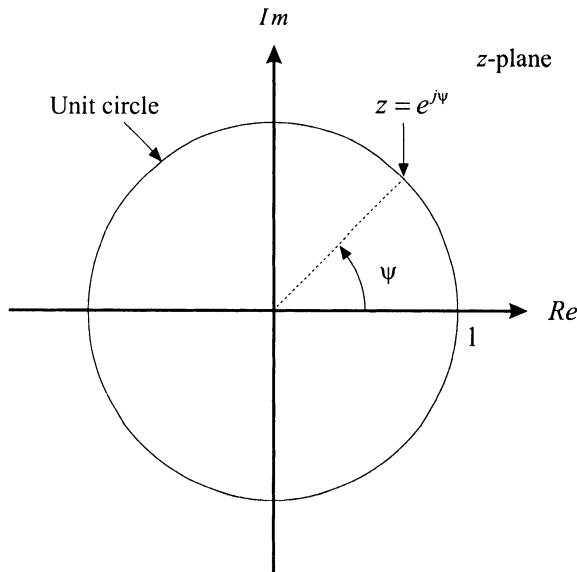
which is familiar as the z -transform. It maps the real variable ψ into a complex variable z with unit magnitude.

The transformation is shown in Figure 3.9. The variable ψ is the phase of the complex variable z . The beam pattern can be written as

$$B_\psi(\psi) = \left[z^{-\frac{N-1}{2}} B_z^*(z) \right]_{z=e^{j\psi}}. \quad (3.40)$$

Most discussions in the classical antenna literature focus on the case of real w_n . When we discuss optimum array design from a statistical standpoint in Chapter 6, we will usually have complex w_n . In Section 3.2.2, we restrict our attention to real weightings.⁷ In Section 3.2.3, we discuss some properties of the beam pattern in the vicinity of the zeros of $B_z(z)$.

⁷In Section 3.7, we consider a design problem that leads to complex weights.

Figure 3.9 z -Transform.

3.2.2 Real Array Weights

In this section, we assume the w_n are real and symmetrical.⁸ In the text, we analyze the case of symmetric weightings and N odd. We analyze the case of symmetric weightings and N even in the problems.

For symmetric weightings,

$$w(n) = w(N - 1 - n), \quad 0 \leq n \leq N - 1. \quad (3.41)$$

The z -transform is

$$B_z(z) = \sum_{n=0}^{N-1} w_n z^{-n}. \quad (3.42)$$

Because of the symmetry we can define

$$M = \frac{N - 1}{2}, \quad (3.43)$$

and write

$$\begin{aligned} B_z(z) &= z^{-M} \left\{ w(M) + w(M - 1) [z + z^{-1}] \right. \\ &\quad \left. + w(M - 2) [z^2 + z^{-2}] + \cdots + w(0) [z^M + z^{-M}] \right\}. \end{aligned} \quad (3.44)$$

⁸Many of the classical array weight vectors satisfy this assumption.

Letting $z = e^{j\psi}$,

$$\begin{aligned} B_z(e^{j\psi}) &= e^{-jM\psi} \{ w(M) + 2w(M-1)\cos\psi \\ &\quad + 2w(M-2)\cos 2\psi + \cdots + w(0)\cos(M\psi) \}. \end{aligned} \quad (3.45)$$

Using (3.40), the beam pattern is

$$B_\psi(\psi) = w(M) + 2 \sum_{m=1}^{M-1} w(m) \cos(M-m)\psi. \quad (3.46)$$

We can also write (3.46) as

$$B_\psi(\psi) = \sum_{n=0}^M \alpha_n \cos n\psi, \quad (3.47)$$

where

$$\alpha_n = \begin{cases} w(M), & n = 0, \\ 2w(M-n), & n \neq 0, \text{ for } N \text{ odd.} \end{cases} \quad (3.48)$$

We now explore the behavior of the zeros of $B_z(z)$. To find the zeros of $B_z(z)$, we observe that

$$B_z(z^{-1}) = z^{2M} B_z(z), \quad (3.49)$$

because of the symmetry of the coefficients. Therefore $B_z(z)$ and $B_z(z^{-1})$ have identical zeros. Since $B_z(z)$ has real coefficients, the zeros occur in complex conjugate pairs.

Thus, we can write $B_z(z)$ in factored form as⁹

$$B_z(z) = w(0) B_1(z) B_2(z) B_3(z), \quad (3.50)$$

where

$$B_1(z) = \prod_{i=1}^{N_1} \left[1 - \left(r_i + \frac{1}{r_i} \right) z + z^2 \right], \quad (3.51)$$

contains zeros in reciprocal pairs on the real axis. If $B_1(z)$ contains a zero at $z = +1$ or $z = -1$, then it will appear in pairs since $B_1(z)$ is of even order.

$$B_2(z) = \prod_{i=1}^{N_2} \left[1 - (2 \cos \theta_i) z + z^2 \right] \quad (3.52)$$

⁹We drop the z subscript on the right side for simplicity.

contains zeros occurring in complex conjugate pairs on the unit circle at $z = e^{\pm j\theta_i}$.

$$\begin{aligned} B_3(z) &= \prod_{i=1}^{N_3} \left\{ 1 - \left[2 \left(r_i + \frac{1}{r_i} \right) \cos \theta_i \right] z \right. \\ &\quad + \left[r_i^2 + \frac{1}{r_i^2} + 4 \cos^2 \theta_i \right] z^2 \\ &\quad \left. - \left[2 \left(r_i + \frac{1}{r_i} \right) \cos \theta_i \right] z^3 + z^4 \right\} \end{aligned} \quad (3.53)$$

contains zeros that occur in fours: complex conjugate pairs and reciprocal (with respect to the unit circle) pairs.

There are a total of $2M = N - 1$ zeros:

$$2M = 2N_1 + 2N_2 + 4N_3. \quad (3.54)$$

The **zeros on the unit circle** correspond to nulls in the beam pattern if they are in the visible region.

For N even,

$$M = \frac{N}{2} - 1, \quad (3.55)$$

and (3.50) becomes

$$B_z(z) = w(0)(1+z)B_1(z)B_2(z)B_3(z). \quad (3.56)$$

The $(1+z)$ corresponds to a zero at $z = -1$ and there are $2M$ additional zeros from $B_1(z)$, $B_2(z)$, and $B_3(z)$. There are always a total of $N - 1$ zeros.

The magnitude of $B(z)$ is

$$|B(z)| = |w_{N-1}| \prod_{n=1}^{2M} |z - z_n|. \quad (3.57)$$

This magnitude can be expressed as the product of the distances from a point z on the unit circle to the roots. Since the point $(1, 0)$ represents the MRA, the pattern is normalized by dividing by the product of the distances from $(1, 0)$ to the roots. Thus,

$$|B(z)| = \frac{|z - z_1| |z - z_2| \cdots |z - z_{N-1}|}{|1 - z_1| |1 - z_2| \cdots |1 - z_{N-1}|}, \quad (3.58)$$

and

$$\arg B(z) = \sum \arg(z - z_n) - \sum \arg(1 - z_n). \quad (3.59)$$

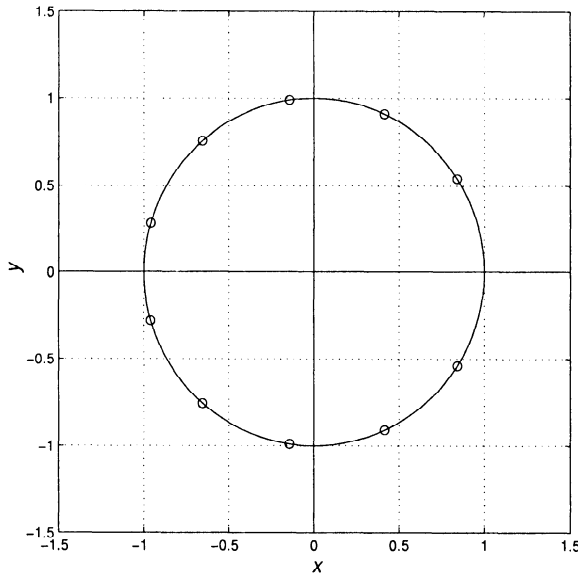


Figure 3.10 Zero plot for an 11-element array.

As z moves around the unit circle from $(1, 0)$ in a counterclockwise direction, ψ is moving 0 to $+kd$. When $d = \lambda/2$, ψ is moving from 0 to π , u is moving from 0 to 1, and θ is moving from 90° to 0° .

Example 3.2.1

Consider a standard 11-element array with uniform weighting. From (2.101), the zeros are located at

$$u_n = \pm \frac{n}{N} \cdot \frac{\lambda}{d}, \quad n = 1, 2, \dots, \frac{N-1}{2}, \quad (3.60)$$

or

$$u_n = \pm \frac{2n}{11}, \quad n = 1, \dots, 5. \quad (3.61)$$

The resulting z -plane plot is shown in Figure 3.10. Remember that the location of the first zero determines the beamwidth of the main lobe. Thus, we can develop techniques that constrain the first zero to be at a specified point and adjust the other zeros to obtain a desired pattern shape. Many of the commonly used patterns are developed in this manner.

In the next series of figures (Figures 3.11–3.13), we show the z -plane plots for some of the array weightings we derived in Section 3.1. They are grouped in the following sets:

- Figure 3.11: Cosine, cosine-squared
- Figure 3.12: Hamming, Blackman-Harris
- Figure 3.13: DPSS ($0.1\pi, 0.4\pi$)

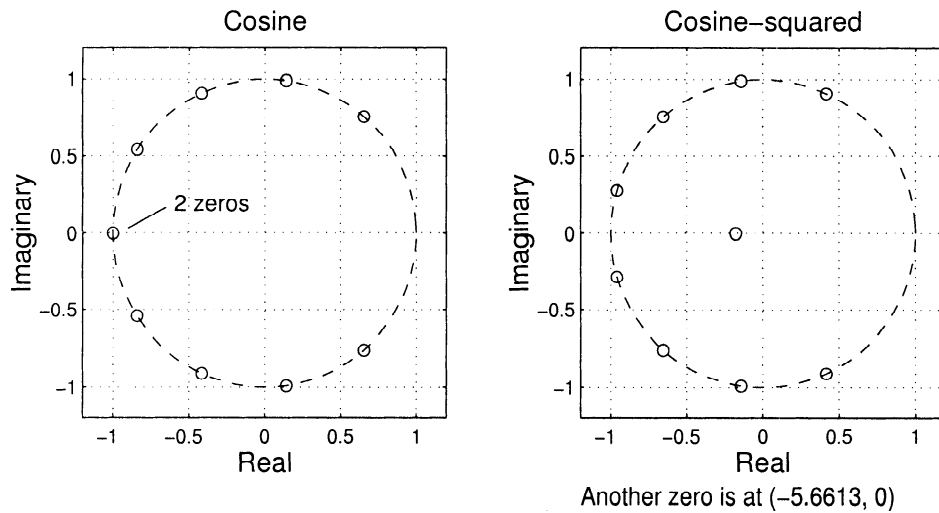


Figure 3.11 Zero plots for cosine and cosine-squared weightings.

In Figure 3.14, we show the effect of d on the z -plane plot for various values of d . The visible region represents the part of the circle corresponding to physically observable values of θ . The remainder of the circle corresponds to the virtual (or invisible) region that we have discussed previously.

For $d < \lambda/2$, the visible region does not cover the entire circle. For $d = \lambda/2$, the visible region corresponds exactly to the circle. For $d > \lambda/2$, the pattern overlaps and has grating lobes.

3.2.3 Properties of the Beam Pattern Near a Zero

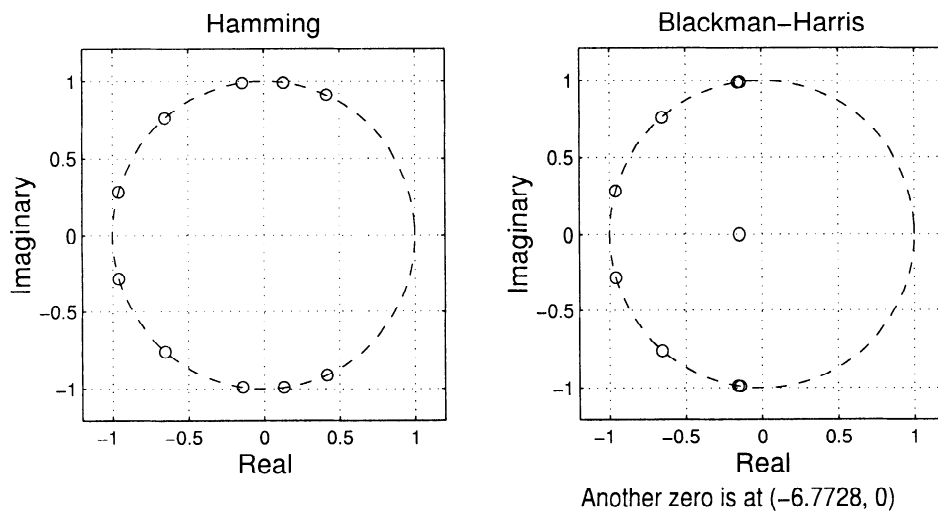
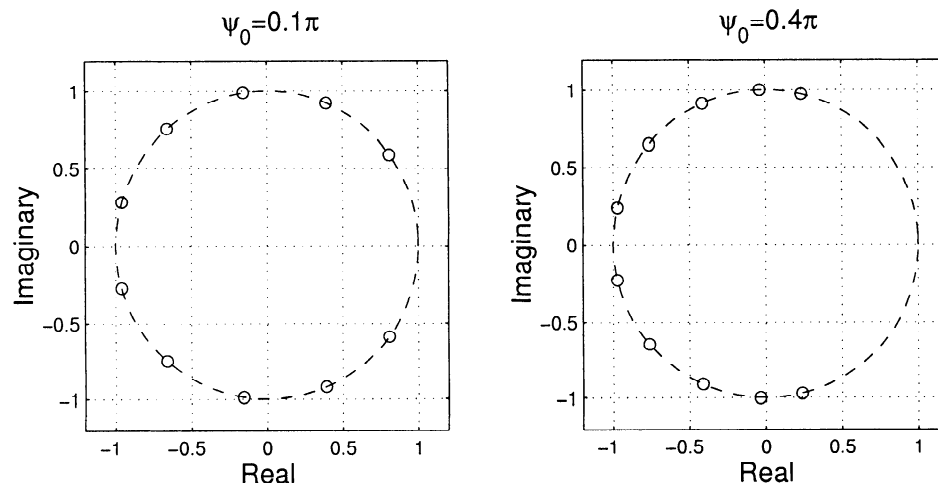
In this section we discuss the behavior of the beam pattern in the vicinity of a zero.¹⁰ Consider a linear aperture with uniform weighting. The beam pattern is

$$B_u(u) = \frac{\sin \alpha u}{\alpha u}, \quad (3.62)$$

where $\alpha = \pi L/\lambda$. The pattern in the vicinity the n th zero, u_n , is shown in Figure 3.15. It appears to be linear at the zero crossing. We want to recenter the pattern at u_n . Define

$$u_0 = u - u_n, \quad (3.63)$$

¹⁰This discussion follows pages 105–110 of Steinberg [Ste76].

Figure 3.12 Zero plots for Hamming, Blackman-Harris weightings.¹¹Figure 3.13 Zero plots for DPSS $(0.1\pi, 0.4\pi)$ weightings.

¹¹Note that the two inner zeros are both double zeros.

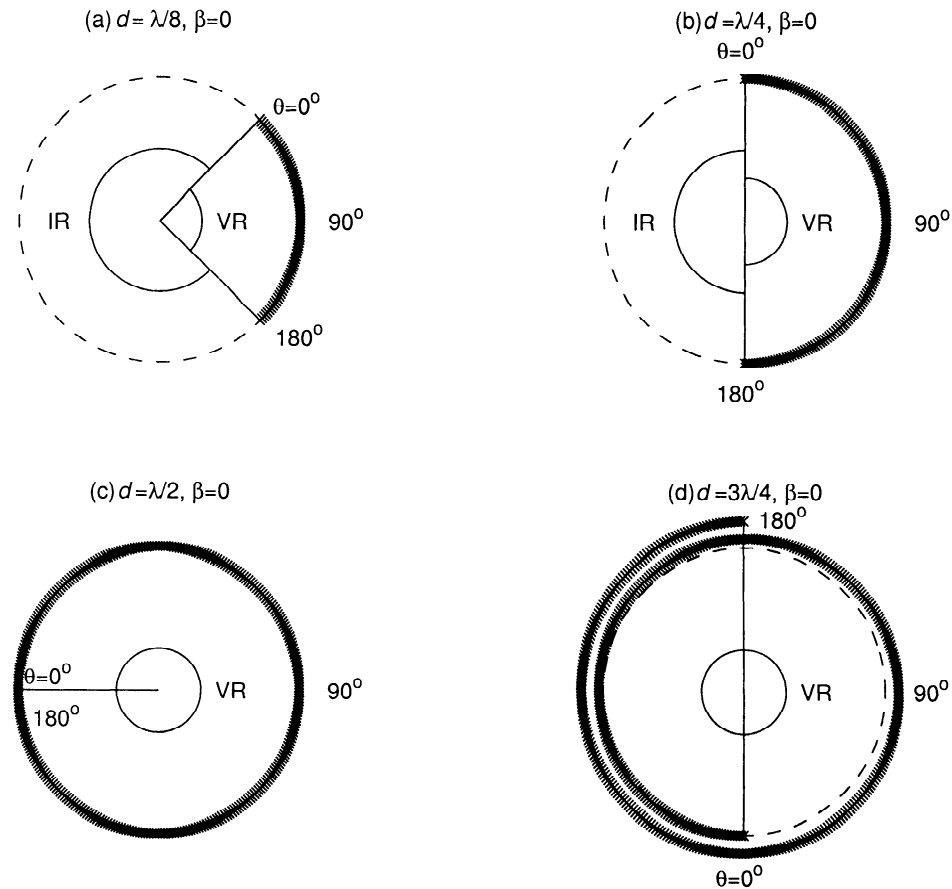


Figure 3.14 Visible region (VR) and invisible region (IR) boundaries for complex variable z .

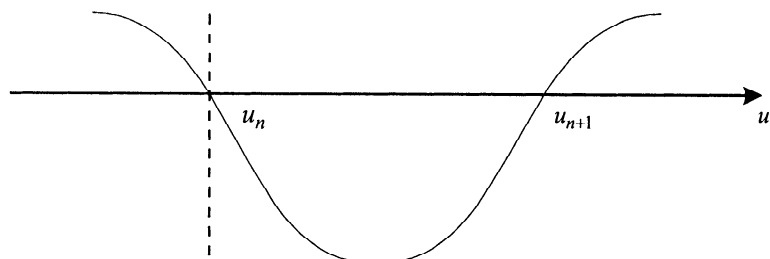


Figure 3.15 The beam pattern near a non-multiple zero.

and assume

$$u_n \gg \frac{\lambda}{L}. \quad (3.64)$$

Then,

$$\begin{aligned} B_{u_0}(u_0) &= B_u(u_0 + u_n) = \frac{\sin \alpha(u_0 + u_n)}{\alpha(u_0 + u_n)} \\ &= \frac{\sin \alpha u_0 \cos \alpha u_n + \cos \alpha u_0 \sin \alpha u_n}{\alpha(u_0 + u_n)}. \end{aligned} \quad (3.65)$$

Since $\sin \alpha u_n = 0$ and $\cos \alpha u_n = \pm 1$, we have

$$B_{u_0}(u_0) = \pm \frac{\sin \alpha u_0}{\alpha(u_0 + u_n)}. \quad (3.66)$$

In the region near the zero,

$$\sin \alpha u_0 \cong \alpha u_0, \quad (3.67)$$

and

$$u_0 \ll u_n, \quad (3.68)$$

so that (3.66) becomes

$$B_{u_0}(u_0) \simeq \pm \frac{u_0}{u_n}. \quad (3.69)$$

Thus the pattern is linear near the zero and the slope is inversely proportional to the coordinate of the zero in u -space.

To investigate the behavior near multiple zeros, we use the approximate radiation pattern of a triangularly weighted aperture

$$B_{u_0}(u_0) = \left(\frac{\sin \alpha u_0}{\alpha u} \right)^2. \quad (3.70)$$

The behavior in the neighborhood of u_n is quadratic

$$B_{u_0}(u_0) \simeq \left(\frac{u_0}{u_n} \right)^2. \quad (3.71)$$

Similar results follow for higher order zeros. The magnitude of $|B_{u_0}(u_0)|$ is sketched in Figure 3.16.

Several comments are in order:

- (i) A single zero creates a sharp null. If we are trying to null out an interfering source (perhaps a jammer), the performance will be sensitive to the exact location of the interfering source **and** its frequency.

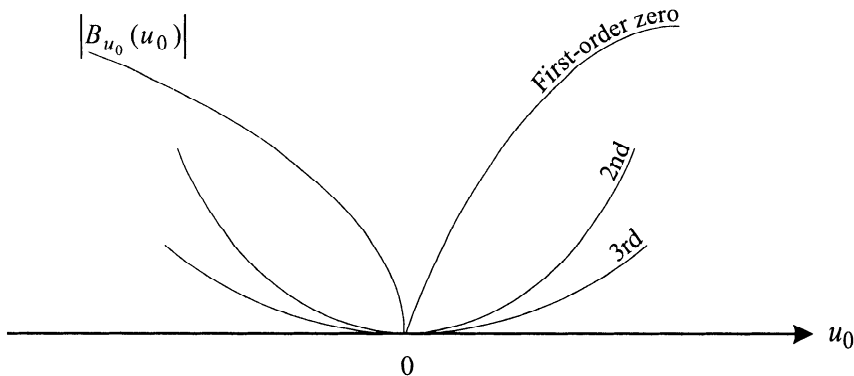


Figure 3.16 Beam pattern near first and higher order zeros.

- (ii) However, if we are trying to estimate the location of a source, it will be useful to work in the vicinity of a null. We see later (in Section 3.8) that a difference beam does exactly that.
- (iii) A double zero creates a wider null and is more robust to model variations or changes in the interferer's location. However, it utilizes 2 degrees of freedom per zero and limits the total number of nulls possible.

3.3 Pattern Sampling in Wavenumber Space

Woodward [Woo46] developed an antenna pattern synthesis technique based on the sampling theorem. We discuss it first for the case of continuous aperture and then for discrete arrays. For the discrete array case, it corresponds to a DFT relationship.

3.3.1 Continuous Aperture

Woodward's approach is based on the Fourier transform relationship between the wavenumber response and the aperture weighting. Rewriting (3.1) and (3.2) in u -space gives

$$\frac{1}{\lambda} \Upsilon_u(u) = \int_{-L/2}^{L/2} w^*(z_\lambda) e^{j2\pi u z_\lambda} dz_\lambda \quad (3.72)$$

and

$$w^*(z_\lambda) = \int_{-\infty}^{\infty} \frac{1}{\lambda} \Upsilon_u(u) e^{-j2\pi u z_\lambda} du, \quad (3.73)$$

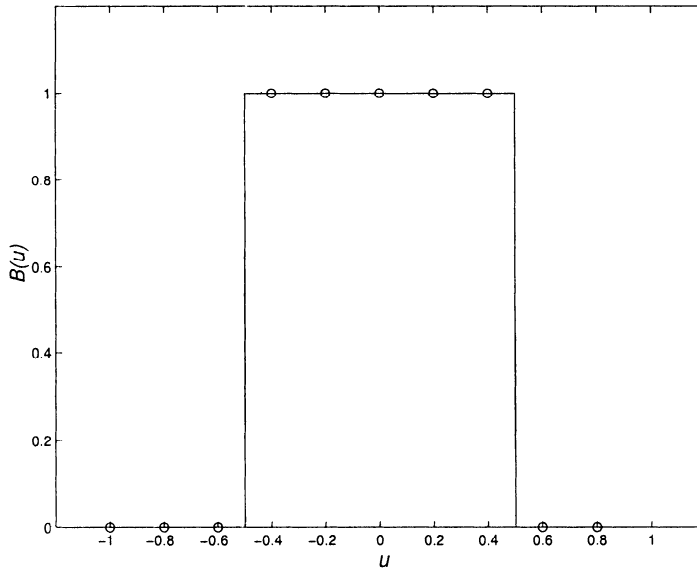


Figure 3.17 Pattern sampling.

where we have suppressed ω and $z_\lambda = z/\lambda$ is the normalized z -distance.

Since z_λ is limited to the range $\pm \frac{L}{2\lambda}$, then we can specify the aperture illumination function by sampling the antenna pattern in wavenumber space at intervals of¹²

$$\Delta u_s = \frac{\lambda}{L}. \quad (3.74)$$

For example, if the desired pattern is the rectangular pattern shown in Figure 3.17, we would sample at λ/L intervals and obtain a set of samples,

$$B_u(u_m), \quad m = 0, 1, \dots, N_s - 1, \quad (3.75)$$

where $u_m = (m\Delta u_s - 1)$, $m = 0, 1, \dots, N_s - 1$, and $N_s = \text{int}[2L/\lambda]$ ($\text{int}[x]$ denotes the largest integer less than x). In Figure 3.17, $L = 5\lambda$, so $\Delta u_s = 0.2$ (see (2.214)). To reconstruct $B_u(u)$, we use a sum of shifted sinc functions,

$$B_u(u) = \sum_{m=0}^{N_s-1} B_u(u_m) \text{sinc}\left(\frac{\pi L}{\lambda}(u - u_m)\right). \quad (3.76)$$

In this case, we have chosen the initial sample at $u = -1.0$. In this example, we could choose the initial sample to be anywhere in the interval $-1.0 \leq$

¹²This is identical to the Nyquist sampling criterion in the time-frequency context. If the signal is bandlimited $[-W \leq f \leq W]$, then the sampling interval $T = 1/2W$.

$u \leq -0.8$. The resulting synthesized pattern will be different. Note that the sampling is uniform in u -space (wavenumber space), not θ -space, and that the samples range over the entire visible u -space ($-1 \leq u \leq 1$). The nulls of the $\text{sinc}(u - u_m)$ functions occur at Δu_s so the coefficient of the sinc function is the value of the desired array response corresponding to the peak of the corresponding sinc function.

Each of the terms in (3.76) corresponds to a rectangular amplitude distribution multiplied by an exponential term to steer the beam. Thus,

$$w^*(z) = \frac{1}{L} \sum_{m=0}^{N_s-1} B_u(m) \exp\left[-j\left(m\frac{z}{L}\right)\right], \quad -\frac{L}{2} \leq z \leq \frac{L}{2}. \quad (3.77)$$

We consider a simple example to illustrate the procedure.

Example 3.3.1

The desired $B_{d\theta}(\theta)$ is uniform in the range: $60^\circ \leq \bar{\theta} \leq 120^\circ$, as shown in Figure 3.17. Let $L = 5\lambda$. Therefore the sampling interval in u -space is

$$\Delta u_s = \frac{\lambda}{5\lambda} = 0.2, \quad (3.78)$$

and there will be ten samples. The sample values are

$$B_u(u_m) = \begin{cases} 0, & m = 0, 1, 2, \\ 1, & m = 3, \dots, 7, \\ 0, & m = 8, 9. \end{cases} \quad (3.79)$$

Note that the value at $m = 10$ is determined by the value at $m = 0$ by the periodicity. The resulting synthesized pattern is shown in Figure 3.18.

3.3.2 Linear Arrays

The Woodward approach can also be used for linear arrays. We discuss the approach from two viewpoints. In this section, we use a straightforward modification of the continuous aperture case. In Section 3.3.3, we introduce the DFT as an intermediate step.

We first consider the case of a standard N -element linear array ($d = \lambda/2$). To relate to the continuous aperture,

$$Nd = L. \quad (3.80)$$

The sampling interval in u -space is $2/N$. As in the aperture case, we can choose the initial sample point. For purposes of discussion in the text, we will assume the samples are taken symmetrically about $u = 0$. Other initial sampling points can also be used. Thus,

$$u_m = \frac{2}{N} \left(m - \frac{N-1}{2} \right), \quad m = 0, 1, \dots, N-1. \quad (3.81)$$

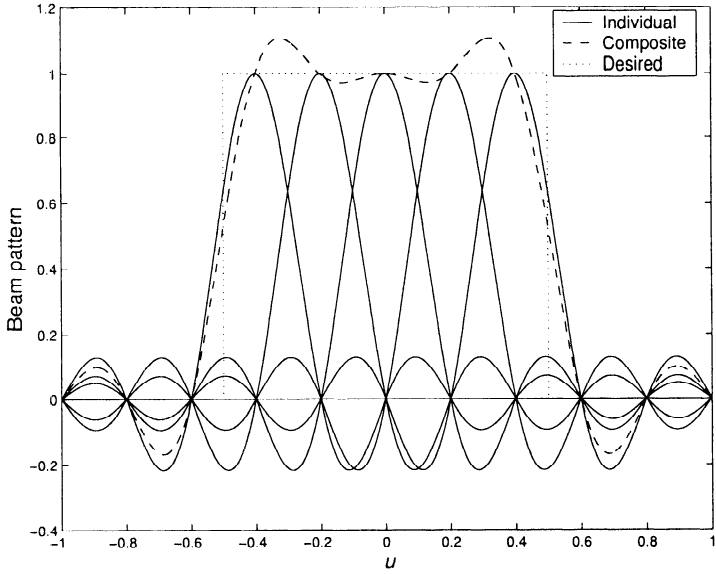


Figure 3.18 Desired and synthesized patterns using the Woodward synthesis procedure.

Because $d = \lambda/2$, the number of pattern samples in the visible region ($|u| \leq 1$) is equal to the number of elements. We consider the case when $d < \lambda/2$ in the next section.

Using (3.76), the component beam pattern can be written as

$$B_{u_m}(u) = B_{du}(u_m) \frac{\sin \left[\frac{N}{2} \pi (u - u_m) \right]}{N \sin \left[\frac{\pi}{2} (u - u_m) \right]}, \quad m = 0, 1, \dots, N-1, \quad (3.82)$$

and the total beam pattern is

$$B_u(u) = \sum_{m=0}^{N-1} B_{du}(u_m) \frac{\sin \left[\frac{N}{2} \pi (u - u_m) \right]}{N \sin \left[\frac{\pi}{2} (u - u_m) \right]}. \quad (3.83)$$

In order to find the weight vector, we use (2.91) and (2.92) to rewrite (3.83) as

$$\begin{aligned} B_u(u) &= \sum_{m=0}^{N-1} B_{du}(u_m) \cdot \frac{1}{N} \sum_{k=0}^{N-1} e^{j(k-\frac{N-1}{2})\pi(u-u_m)} \\ &= \sum_{k=0}^{N-1} e^{j(k-\frac{N-1}{2})\pi u} \left(\sum_{m=0}^{N-1} B_{du}(u_m) \cdot \frac{1}{N} e^{-j(k-\frac{N-1}{2})\pi u_m} \right). \end{aligned} \quad (3.84)$$

The term in parentheses is $w^*(k)$. Thus,

$$w_n^* = \frac{1}{N} \sum_{m=0}^{N-1} B_{du}(u_m) e^{-j(n-\frac{N-1}{2})\pi u_m}, \quad n = 0, \dots, N-1. \quad (3.85)$$

If $B_{du}(u)$ is a real symmetric beam pattern, then the weights will be real if

$$u_m = u_{N-1-m}, \quad (3.86)$$

which corresponds to symmetric spacing. Two comments are necessary:

(i) The case in which

$$B_d(u) = 0, \quad -1 \leq u \leq \frac{2}{N},$$

is an exception to (3.86) and any initial sampling point gives symmetric weights.

(ii) In many applications, the desired beam pattern is not symmetric, so we will have complex weights.

We also want to interpret these results in the context of the discrete Fourier transform.

3.3.3 Discrete Fourier Transform

In Section 3.2, we represented the beam pattern as the z -transform of the array weighting function. From (3.40),

$$B_\psi(\psi) = \left[z^{-\frac{N-1}{2}} B_z^*(z) \right]_{z=e^{j\psi}}, \quad (3.87)$$

and

$$B_z(z) = \sum_{n=0}^{N-1} w_n z^{-n}, \quad (3.88)$$

or

$$B_z(z)|_{z=e^{j\psi}} = B_\psi^*(\psi) e^{-j\frac{N-1}{2}\psi}. \quad (3.89)$$

We sample at

$$z_k = e^{j(k-\frac{N-1}{2})\frac{2\pi}{N}}, \quad k = 0, 1, \dots, N-1. \quad (3.90)$$

This corresponds to N samples symmetric about the origin and ψ ranges from $-\pi \leq \psi \leq \pi$.

$$\begin{aligned} B_\psi^*(\psi_k) e^{-j\frac{N-1}{2}\psi_k} &= \sum_{n=0}^{N-1} w_n z_k^{-n} \\ &= \sum_{n=0}^{N-1} w_n e^{-j(k - \frac{N-1}{2}) \frac{2\pi}{N} n} \\ &= \sum_{n=0}^{N-1} \left(w_n e^{jn\pi(\frac{N-1}{N})} \right) e^{-jkn\frac{2\pi}{N}}, \end{aligned} \quad (3.91)$$

where

$$\psi_k = \left(k - \frac{N-1}{2} \right) \frac{2\pi}{N}, \quad k = 0, 1, \dots, N-1. \quad (3.92)$$

Now define,

$$b_n \triangleq w_n e^{jn\pi(\frac{N-1}{N})}, \quad (3.93)$$

and

$$B(k) = B_\psi^*(\psi_k) e^{-j\psi_k(\frac{N-1}{2})}. \quad (3.94)$$

Then,

$$B(k) = \sum_{n=0}^{N-1} b_n e^{-jkn\frac{2\pi}{N}}, \quad k = 0, 1, \dots, N-1, \quad (3.95)$$

which is called the **discrete Fourier transform**.

The relation in (3.91) is a linear transformation from the N -dimensional vector \mathbf{b} to the N -dimensional vector \mathbf{B} ,

$$\boxed{\mathbf{B} = \mathbf{F}\mathbf{b}}, \quad (3.96)$$

where \mathbf{F} is an $N \times N$ matrix, whose kl element is

$$[\mathbf{F}]_{kl} = (F_N)^{kl} = \left(e^{-j\frac{2\pi}{N}} \right)^{kl}, \quad (3.97)$$

where

$$F_N \triangleq e^{-j\frac{2\pi}{N}}. \quad (3.98)$$

To obtain the inverse, we multiply $B(k)$ by $e^{jkm\frac{2\pi}{N}}$, sum on k , and divide by N ,

$$\frac{1}{N} \sum_{k=0}^{N-1} B(k) e^{jkm\frac{2\pi}{N}} = \frac{1}{N} \sum_{n=0}^{N-1} b_n \left(\sum_{k=0}^{N-1} e^{jk(m-n)\frac{2\pi}{N}} \right). \quad (3.99)$$

The sum in parentheses is N , if $m = n$, and 0 if $m \neq n$. Thus,

$$b_n = \frac{1}{N} \sum_{k=0}^{N-1} B(k) e^{jkn\frac{2\pi}{N}}, \quad (3.100)$$

which is the **inverse discrete Fourier transform (IDFT)**, and

$$w_n = b_n e^{-jn\pi(\frac{N-1}{N})}. \quad (3.101)$$

In order to write (3.100) in vector notation, we first observe that

$$\mathbf{F}^H = \frac{1}{N} \mathbf{F}^{-1}. \quad (3.102)$$

Thus,

$$\mathbf{b} = \frac{1}{N} \mathbf{F}^{-1} \mathbf{B}. \quad (3.103)$$

We observe from (3.103) that, if we know \mathbf{B} , which is the vector of samples $B(k)$, $k = 0, 1, \dots, N - 1$, then we can find \mathbf{b} and \mathbf{w} . However, knowing \mathbf{w} enables us to find the complete beam pattern $B_\psi(\psi)$. Therefore the pattern samples at $2\pi/N$ intervals completely determine the beam pattern.

We use this result in two different ways. In the first case, we have a beam pattern that we know was generated by a standard linear array. We encounter this case frequently in subsequent sections so we denote it as the **IDFT Weight Vector Determination** algorithm. The steps in the algorithm are:

(i) Sample the beam pattern at

$$\psi_k = \left(k - \frac{N-1}{2} \right) \frac{2\pi}{N}, \quad k = 0, 1, \dots, N-1$$

to obtain $B_\psi(\psi_k)$.

(ii) Use (3.94) to find $B(k)$.

(iii) Find \mathbf{b} as the IDFT of $B(k)$ using (3.100).

(iv) Use (3.101) to find \mathbf{w} .

In this case, the result will not depend on the initial sample point.

In the second case, we have a desired beam pattern that is not necessarily realizable by a standard linear array. We repeat steps (i)–(iv). We then use (2.65) to find the resulting beam pattern.

We consider two simple examples to illustrate the procedure.

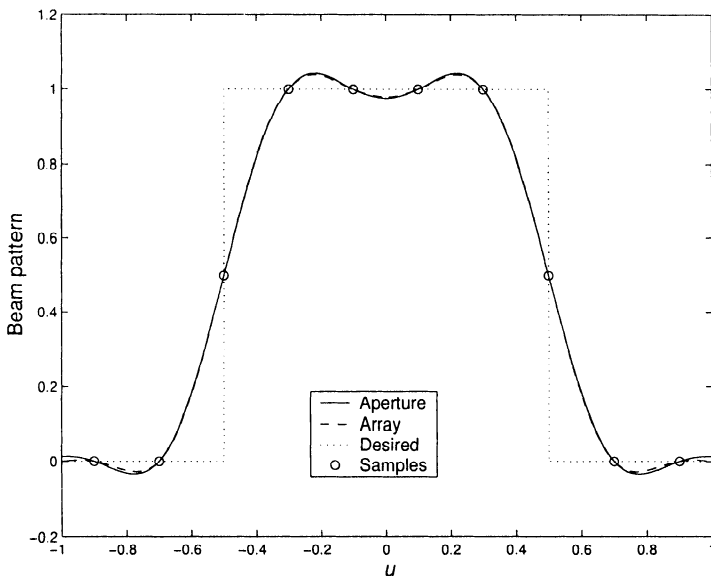


Figure 3.19 Array and aperture beam patterns using wavenumber sampling technique, symmetric sampling: $L = 5.0\lambda$, $d = \lambda/2$, $N = 10$.

Example 3.3.2 (continuation)

The array corresponding to the aperture in the previous example contains ten elements with spacing $d = \lambda/2$. The samples are taken symmetrically about $u = 0$. At the discontinuity ($u=0.5$) we use the value at the mid-point. The resulting pattern is shown in Figure 3.19. We see that the aperture and the array give essentially the same beam pattern.

Example 3.3.3 (continuation)

Consider the case when $N = 11$ and $d = \lambda/2$. The samples are taken symmetrically. The result is shown in Figure 3.20. The different sample separation causes a difference in the two beam patterns.

The discussion up to this point assumed a standard linear array so that $d = \lambda/2$. For the case when $d < \lambda/2$ a similar procedure can be utilized but there are some important changes. To illustrate the technique, we consider the case where

$$d = \frac{\lambda}{4}. \quad (3.104)$$

The DFT relations in (3.91) and (3.100) are still valid and we still sample at $2\pi/N$ intervals in ψ -space. However, we need to sample over a complete period of $\Upsilon_u(u)$, which in this case corresponds to $-2 \leq u \leq 2$ (recall Figure 2.20(a)). Thus, if we use a $2/N$ sampling interval, we use pattern samples

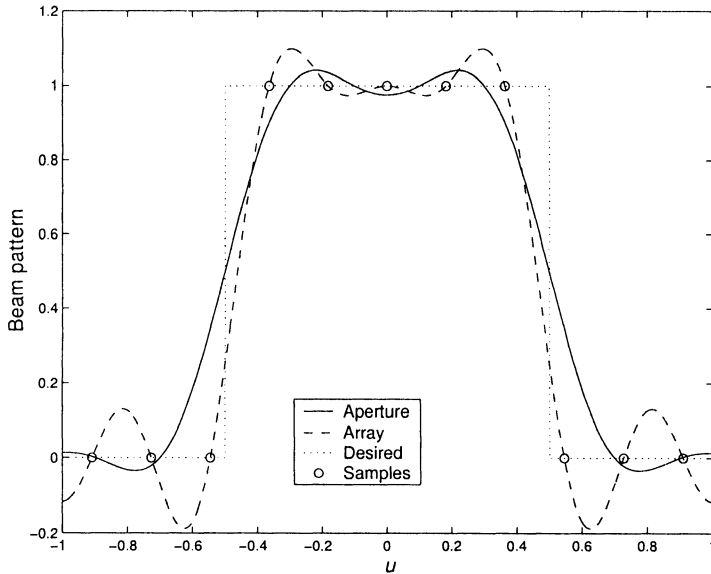


Figure 3.20 Array and aperture beam patterns using wavenumber sampling technique, symmetric sampling: $L = 5.0\lambda$, $d = \lambda/2$, $N = 11$.

outside the visible region to determine the weight vector and to find $B_\psi(\psi)$.

Example 3.3.4 (continuation)

Consider the same desired pattern with an array where $d = \lambda/4$ and $N = 20$. The result using symmetric sampling is shown in Figure 3.21.

3.3.4 Norms

In Section 2.6.4, we indicated the importance of the norm of the weight vector, $\|\mathbf{w}\|^2$. We want to relate the weight vector norm to the norm of the vector of beam pattern samples. From (3.96),

$$\mathbf{B}^H \mathbf{B} = \mathbf{b}^H \mathbf{F}^H \mathbf{F} \mathbf{b}. \quad (3.105)$$

Using (3.102), we obtain

$$\frac{1}{N} \mathbf{B}^H \mathbf{B} = \mathbf{b}^H \mathbf{b}. \quad (3.106)$$

Both \mathbf{B} and \mathbf{b} contain exponential factors that are not necessary in the norm relationship. From (3.93),

$$\mathbf{b} = \text{diag} \left[e^{jn\pi \left(\frac{N-1}{N} \right)} \right] \mathbf{w}. \quad (3.107)$$

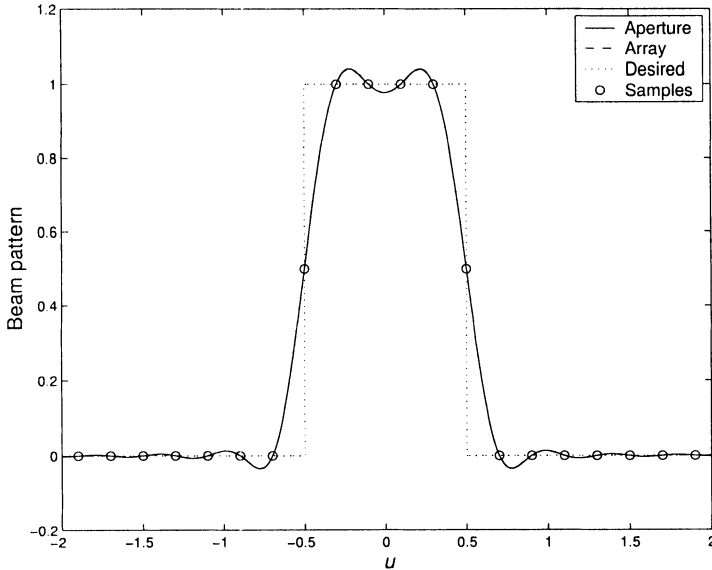


Figure 3.21 Array and aperture beam patterns using wavenumber sampling technique, symmetric samples from $-2.0 \leq u \leq 2.0$: $L = 5.0\lambda$, $d = \lambda/4$, $N = 20$.

Thus,

$$\mathbf{b}^H \mathbf{b} = \mathbf{w}^H \mathbf{w}. \quad (3.108)$$

Now define

$$[\mathbf{B}_\psi]_k = \mathbf{B}_\psi(\psi_k), \quad k = 0, 1, \dots, N-1, \quad (3.109)$$

where ψ_k is given by (3.92). Then, from (3.94),

$$\mathbf{B} = \text{diag} \left\{ e^{-j\psi_k \left(\frac{N-1}{2} \right)} \right\} \mathbf{B}_\psi^*. \quad (3.110)$$

Thus,

$$\mathbf{B}^H \mathbf{B} = \mathbf{B}_\psi^T \mathbf{B}_\psi = \mathbf{B}_\psi^H \mathbf{B}_\psi. \quad (3.111)$$

Using (3.108) and (3.111) in (3.106) gives

$$\mathbf{w}^H \mathbf{w} = \frac{1}{N} \mathbf{B}_\psi^H \mathbf{B}_\psi,$$

(3.112)

which is the desired result. Therefore, to find the directivity D , the white noise array gain A_w , or the sensitivity function T_{se} , we sample the beam pattern at the ψ_k given by (3.92), sum the magnitudes squared, and divide by N .

3.3.5 Summary

In this section, we introduced the Woodward sampling technique as a method to approximate a desired beam pattern. For linear arrays this leads us to the DFT and the inverse DFT. The examples focused on the approximation technique. The other usage of the IDFT that is described in the paragraphs following (3.103) is equally important. In this case we know that the desired beam pattern can be generated by a standard linear array and we use the IDFT to find the weights. We give further examples of these techniques in subsequent sections.

The relationships between the beam pattern, the weight vector, and the z -transform are summarized in Table 3.3.

Table 3.3 Relationships

1	$B_\psi(\psi) = e^{-j(\frac{N-1}{2})\psi} \sum_{n=0}^{N-1} w_n^* e^{jn\psi}$	$w_n^* = \frac{1}{2\pi} \int_{-\pi}^{\pi} B_\psi(\psi) e^{j[(\frac{N-1}{2})-n]\psi} d\psi$
2	z -Transform $B_\psi(\psi) = \left[z^{-\frac{N-1}{2}} B_z^*(z) \right]_{z=e^{j\psi}}$ (3.87)	
3	DFT $b_n = w_n e^{jn\pi(\frac{N-1}{N})}$ (3.93) $B(k) = \sum_{n=0}^{N-1} b_n e^{-jk\pi\frac{2\pi}{N}}$ (3.95)	IDFT $b_n = \frac{1}{N} \sum_{k=0}^{N-1} B(k) e^{jk\pi\frac{2\pi}{N}}$ (3.100) $w_n = b_n e^{-jn\pi(\frac{N-1}{N})}$ (3.101)

3.4 Minimum Beamwidth for Specified Sidelobe Level

3.4.1 Introduction

In this section, we consider the problem of minimizing the beamwidth for a given maximum sidelobe level.

The major focus of the section is on the Dolph-Chebychev weighting. It results in constant sidelobes and a beamwidth that is the minimum possible for the given sidelobe level. We first describe the classical Dolph-Chebychev

synthesis technique and then show how it can be simplified by using the IDFT.

In many cases, a constant sidelobe behavior is not desirable. We develop a weighting due to Taylor that gives decreasing sidelobes.

We consider the case of linear uniformly spaced array pointed at broadside. The desired beam pattern is a real symmetric function, so the weights will be real and symmetric.

In this case it is useful to index the weights in a symmetric manner. For N odd, we define the weights as

$$a_m = w_n|_{n=m+\frac{N-1}{2}}, \quad m = -(N-1)/2, \dots, (N-1)/2. \quad (3.113)$$

The assumption that $B(\psi)$ is a real symmetric function results in real symmetric weights,

$$\cdot a_m = a_{-m}, \quad (3.114)$$

and we can write $B(\psi)$ in a trigonometric form,

$$B(\psi) = a_0 + 2 \sum_{m=1}^{\frac{N-1}{2}} a_m \cos(m\psi), \quad N \text{ odd.}$$

(3.115)

Similarly, for N even, we define

$$a_m = w_n|_{n=m-1+\frac{N}{2}}, \quad m = 1, 2, \dots, \frac{N}{2}, \quad (3.116)$$

and

$$a_{-m} = a_m, \quad m = 1, 2, \dots, \frac{N}{2}. \quad (3.117)$$

Then,

$$B(\psi) = \sum_{m=-\frac{N}{2}}^{-1} a_m e^{j[(m+\frac{1}{2})\psi]} + \sum_{m=1}^{\frac{N}{2}} a_m e^{j[(m-\frac{1}{2})\psi]}, \quad N \text{ even,} \quad (3.118)$$

which can be written as

$$B(\psi) = 2 \sum_{m=1}^{\frac{N}{2}} a_m \cos \left(\left(m - \frac{1}{2} \right) \psi \right), \quad N \text{ even.}$$

(3.119)

The indexing for the cases of N odd and N even are shown in Figure 3.22.

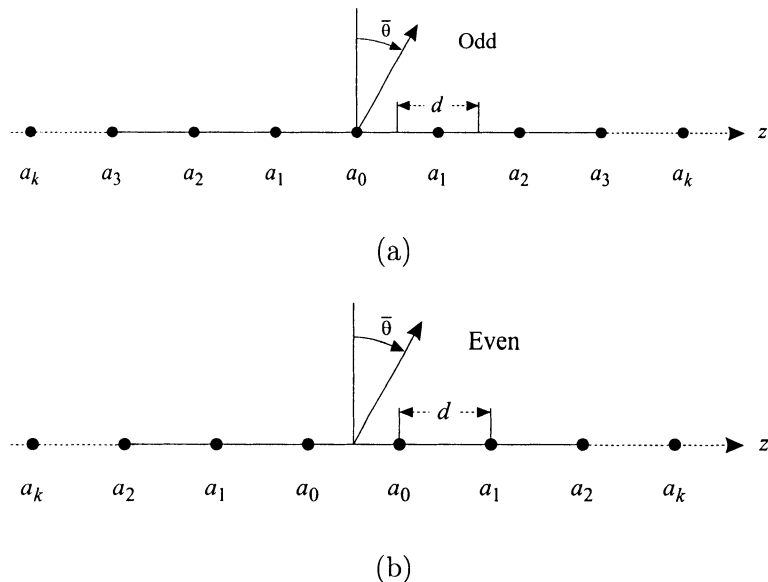


Figure 3.22 Linear broadside arrays of n isotropic sources with uniform spacing: (a) N odd; (b) N even.

3.4.2 Dolph-Chebychev Arrays

The spectral weightings control sidelobes by exploiting Fourier transform properties. However, they do not explicitly control the height of the sidelobes. For linear, equally spaced arrays there are methods to design weights that control sidelobes and beamwidths explicitly. The method that is discussed in this section was introduced by Dolph [Dol46], [Rib47] and is based upon the properties of Chebychev¹³ polynomials. Our development follows that in Section 4.11 of Kraus [Kra88].

Consider the linear arrays shown in Figure 3.22. First, assume that there are an odd number of elements as shown in Figure 3.22(b), and that the main response axis is broadside. The weights are symmetric about the origin. In addition, we can use real weights because we want to design a real symmetric pattern.

Because the weights are real, the beam pattern can be written as (from (3.115))

$$B(\psi) = \alpha_0 + \alpha_1 \cos \psi + \alpha_2 \cos 2\psi$$

¹³There are various spellings of Chebychev in the literature (e.g., Tchebyscheff).

$$+ \cdots + \alpha_{\frac{N-1}{2}} \cos \left[\left(\frac{N-1}{2} \right) \psi \right], \quad N \text{ odd}, \quad (3.120)$$

where

$$\psi = \frac{2\pi d}{\lambda} \cos \theta, \quad (3.121)$$

and α_n is defined as,

$$\alpha_n = \begin{cases} a_0, & n = 0, \\ 2a_n, & n = 1, \dots, \frac{N-1}{2}, \end{cases} \quad \text{for } N \text{ odd}. \quad (3.122)$$

We have deleted the ψ subscript on $B_\psi(\psi)$. This is the Fourier series expansion of the beam pattern. We can rewrite (3.120) as

$$B(\psi) = \sum_{k=0}^{\frac{N-1}{2}} \alpha_k \cos \left(2k \frac{\psi}{2} \right), \quad N \text{ odd}. \quad (3.123)$$

If N is even, the array is shown in Figure 3.22(a). Now, from (3.119),

$$B(\psi) = \alpha_1 \cos \left(\frac{\psi}{2} \right) + \cdots + \alpha_{\frac{N}{2}} \cos \left[\left(\frac{N-1}{2} \right) \psi \right], \quad (3.124)$$

where

$$\alpha_n = 2a_n, \quad n = 1, \dots, \frac{N}{2}, \quad N \text{ even}. \quad (3.125)$$

Then, (3.124) can be written as

$$B(\psi) = \sum_{k=1}^{\frac{N}{2}} \alpha_k \cos \left[\left(\frac{2k-1}{2} \right) \psi \right], \quad N \text{ even}. \quad (3.126)$$

In this section, we want to derive an amplitude distribution that will produce a beam pattern with the minimum null-to-null beamwidth for a specified sidelobe level. The amplitude distribution is called the Dolph-Chebychev distribution.¹⁴

The first step is to show that $B(\psi)$ can be represented as a polynomial of order $N - 1$. We represent the $\cos \left(m \frac{\psi}{2} \right)$ terms as a sum of $\cos^m \left(\frac{\psi}{2} \right)$ terms. We write

$$\begin{aligned} \exp \left[jm \frac{\psi}{2} \right] &= \cos \left(m \frac{\psi}{2} \right) + j \sin \left(m \frac{\psi}{2} \right) \\ &= \left[\cos \left(\frac{\psi}{2} \right) + j \sin \left(\frac{\psi}{2} \right) \right]^m. \end{aligned} \quad (3.127)$$

¹⁴The relationships in (3.123) and (3.126) were first given by Wolf [Wol37].

Expanding in a binomial series and taking the real part gives

$$\begin{aligned}\cos m \frac{\psi}{2} &= \cos^m \frac{\psi}{2} - \frac{m(m-1)}{2!} \cos^{m-2} \frac{\psi}{2} \sin^2 \frac{\psi}{2} \\ &\quad + \frac{m(m-1)(m-2)(m-3)}{4!} \cos^{m-4} \frac{\psi}{2} \sin^4 \frac{\psi}{2} - \dots.\end{aligned}\tag{3.128}$$

Putting $\sin^2(\psi/2) = 1 - \cos^2(\psi/2)$, and substituting particular values of m ,¹⁵ (3.128) reduces to the following:

$$\left. \begin{array}{l} m = 0, \quad \cos m \frac{\psi}{2} = 1 \\ m = 1, \quad \cos m \frac{\psi}{2} = \cos \frac{\psi}{2} \\ m = 2, \quad \cos m \frac{\psi}{2} = 2\cos^2 \frac{\psi}{2} - 1 \\ m = 3, \quad \cos m \frac{\psi}{2} = 4\cos^3 \frac{\psi}{2} - 3\cos \frac{\psi}{2} \\ m = 4, \quad \cos m \frac{\psi}{2} = 8\cos^4 \frac{\psi}{2} - 8\cos^2 \frac{\psi}{2} + 1 \end{array} \right\} .\tag{3.129}$$

Define

$$x = \cos \frac{\psi}{2},\tag{3.130}$$

then (3.128) becomes

$$\left. \begin{array}{ll} \cos m \frac{\psi}{2} = 1, & \text{when } m = 0 \\ \cos m \frac{\psi}{2} = x, & \text{when } m = 1 \\ \cos m \frac{\psi}{2} = 2x^2 - 1, & \text{when } m = 2 \end{array} \right\} .\tag{3.131}$$

The polynomials of (3.131) are Chebychev polynomials, which may be designated in general by

$$T_m(x) = \cos \left(m \frac{\psi}{2} \right) \Big|_{\cos(\frac{\psi}{2})=x}.\tag{3.132}$$

For particular values of m , the first eight Chebychev polynomials are

$$\left. \begin{array}{l} T_0(x) = 1 \\ T_1(x) = x \\ T_2(x) = 2x^2 - 1 \\ T_3(x) = 4x^3 - 3x \\ T_4(x) = 8x^4 - 8x^2 + 1 \\ T_5(x) = 16x^5 - 20x^3 + 5x \\ T_6(x) = 32x^6 - 48x^4 + 18x^2 - 1 \\ T_7(x) = 64x^7 - 112x^5 + 56x^3 - 7x \end{array} \right\} .\tag{3.133}$$

¹⁵ m will equal $2k$ or $2k+1$ depending on whether N is odd or even.

We note that the degree of the polynomial in (3.133) is the same as the value of m .

The m th-degree Chebychev polynomial is defined as

$$T_m(x) = \begin{cases} \cos(m \cos^{-1} x), & |x| \leq 1, \\ \cosh(m \cosh^{-1} x), & x > 1, \\ (-1)^m \cosh(m \cosh^{-1} x), & x < -1. \end{cases} \quad (3.134)$$

The Chebychev polynomials are a set of functions that are orthogonal over the interval $-1 \leq x \leq 1$ with respect to the weighting function $w(x) = 1/\sqrt{1-x^2}$ (e.g., [AS65]),

$$\begin{aligned} \int_{-1}^1 \frac{1}{\sqrt{1-x^2}} T_m(x) T_n(x) dx &= \\ \int_0^\pi T_m(\cos \theta) T_n(\cos \theta) d\theta &= c_m \delta_{mn}. \end{aligned} \quad (3.135)$$

The orthogonality constant c_m is

$$c_m = \begin{cases} \pi, & m = 0, \\ \frac{\pi}{2}, & m \neq 0. \end{cases} \quad (3.136)$$

The polynomials can be extended beyond the region $|x| \leq 1$ as defined in (3.134). The Chebychev polynomials of order $m = 2$ through $m = 4$ are shown in Figure 3.23. The following properties of Chebychev polynomials are useful for our development.

1. For $m \geq 2$,

$$T_m(x) = 2xT_{m-1}(x) - T_{m-2}(x), \quad (3.137)$$

where $T_0(x)$ and $T_1(x)$ are given in (3.133).

2. $T_m(x)$ has m real roots in the interval $|x| < 1$. The roots of the polynomials occur when $\cos(m(\psi/2)) = 0$ or when

$$m \frac{\psi}{2} = (2p-1) \frac{\pi}{2}, \quad p = 1, \dots, m. \quad (3.138)$$

Thus, they are evenly spaced in ψ -space. The roots of x , designated x_p , are

$$x_p = \cos \left[(2p-1) \frac{\pi}{2m} \right]. \quad (3.139)$$

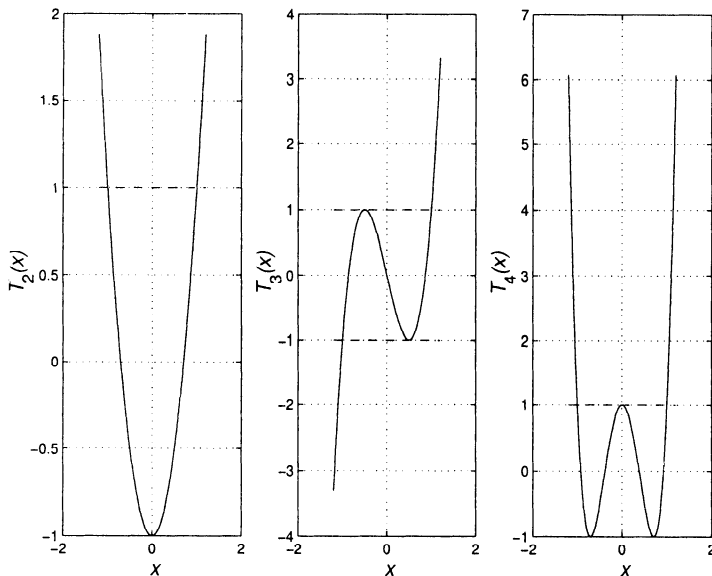


Figure 3.23 Chebychev polynomials: (a) $m = 2$; (b) $m = 3$; (c) $m = 4$.

3. $T_m(x)$ has alternating maxima and minima in the interval $-1 < x < 1$ that occur at

$$x_k = \cos\left(\frac{k\pi}{m}\right), \quad k = 1, 2, \dots, m-1. \quad (3.140)$$

The magnitude of every maxima and minima is unity,

$$|T_m(x_k)| = 1. \quad (3.141)$$

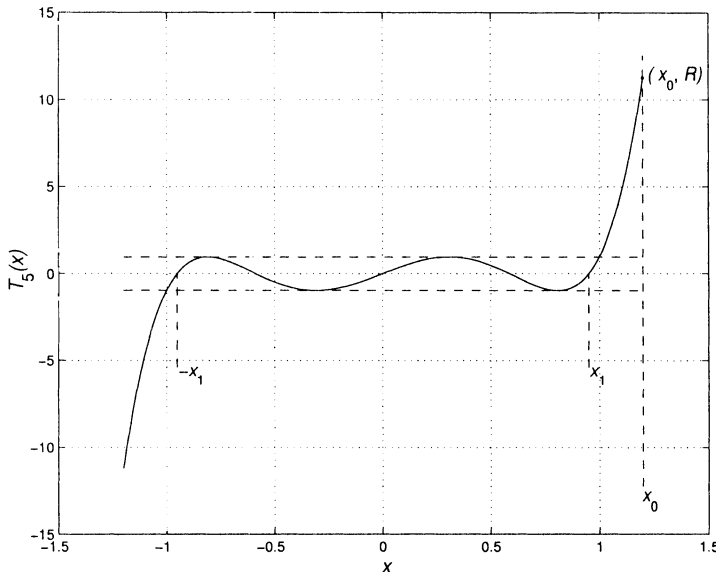
Thus, the polynomials have an equal ripple characteristic in the interval $-1 < x < 1$.

4. All of the polynomials pass through the point $(1, 1)$ and at $x = \pm 1, |T_m(\pm 1)| = 1$. For $x > 1$,

$$|T_m(x)| > 1. \quad (3.142)$$

From (3.129), the beam pattern, $B(\psi)$, for a symmetric, equally spaced array aimed at broadside (isotropic sources) is a polynomial of degree $N - 1$ in the variable $\cos(\psi/2)$.

If we set this array polynomial equal to the Chebychev polynomial of the same degree $N - 1$ and equate the array coefficients to the Chebychev

Figure 3.24 $T_5(x)$ with coordinate axes.

polynomial coefficients, then the beam pattern of the array will correspond to a Chebychev polynomial of degree $N - 1$.

Dolph [Dol46] developed a procedure to utilize the properties of the Chebychev polynomials to develop an optimum pattern.

In the Dolph-Chebychev method the magnitude of the main lobe corresponds to the value of $T_m(x_0)$ where $x_0 > 1$ and the magnitude of the sidelobes is unity. We define the ratio of the main-lobe maximum to the sidelobe level as R ,

$$R = \frac{\text{main-lobe maximum}}{\text{sidelobe level}}. \quad (3.143)$$

To illustrate this, consider the $T_5(x)$ curve in Figure 3.24. The point (x_0, R) on the $T_5(x)$ polynomial curve corresponds to the main-lobe maximum. From (3.134),

$$T_{N-1}(x_0) = \cosh((N-1)\cosh^{-1}x_0) = R, \quad |x_0| > 1, \quad (3.144)$$

or

$$x_0 = \cosh\left(\frac{1}{N-1}\cosh^{-1}R\right), \quad |x_0| > 1. \quad (3.145)$$

For example, if $R = 20$, the sidelobes will be 26 dB below the main-lobe maximum. The value $R = 31.62$ would lead to -30-dB sidelobes.

The synthesis procedure consists of five steps:

1. For an N -element array, select the Chebychev polynomial $T_m(x)$ of the same degree as the array polynomial. Thus,

$$m = N - 1. \quad (3.146)$$

2. Choose R and solve for x_0 . Since $R > 1$, $x_0 > 1$. However, to use (3.130) we require $|x| < 1$.
3. Change the scale by defining a new abscissa w ,

$$w = \frac{x}{x_0}, \quad (3.147)$$

and let

$$w = \cos\left(\frac{\psi}{2}\right), \quad (3.148)$$

and

$$x = x_0 \cos\left(\frac{\psi}{2}\right). \quad (3.149)$$

4. The beam pattern is

$$B(\psi) = \frac{1}{R} T_{N-1}(x_0 \cos(\frac{\psi}{2})). \quad (3.150)$$

The $1/R$ factor normalizes the beam pattern so that $B(0) = 1$.

5. The last step is to find the array weights to produce the beam pattern in (3.150).

The easiest way to find the weight vector is to find the zeros of the beam pattern and then use (2.88). The original zeros are given by (3.138),

$$\frac{\psi_{po}}{2} = \frac{(2p-1)\pi}{(N-1)2}, \quad p = 1, \dots, N-1, \quad (3.151)$$

or in x -space,

$$x_p = \cos\left(\frac{(2p-1)\pi}{(N-1)2}\right), \quad p = 1, \dots, N-1. \quad (3.152)$$

Changing the scale into w -space gives

$$w_p = \frac{1}{x_0} \cos\left(\frac{(2p-1)\pi}{(N-1)2}\right), \quad p = 1, \dots, N-1. \quad (3.153)$$

Using (3.148) gives the zeros in ψ -space,

$$\psi_p = 2 \cos^{-1} \left(\frac{1}{x_0} \cos \left(\frac{(2p-1)\pi}{(N-1)2} \right) \right), \quad p = 1, \dots, N-1. \quad (3.154)$$

We then construct a $N \times N$ array manifold matrix, $\mathbf{V}(\psi)$, (2.81),

$$\mathbf{V}(\psi) = \begin{bmatrix} \mathbf{v}(0) & \mathbf{v}(\psi_1) & \cdots & \mathbf{v}(\psi_p) & \cdots & \mathbf{v}(\psi_{N-1}) \end{bmatrix}, \quad (3.155)$$

and use (2.88)

$$\mathbf{w} = [\mathbf{V}^H(\psi)]^{-1} \mathbf{e}_1, \quad (3.156)$$

which specifies the weight vector. We can translate from w_n to a_n , if desired, but it is not necessary.¹⁶

The results in (3.151)–(3.153) complete the Dolph-Chebychev synthesis process.

We now consider a typical example and then discuss the optimality of the result.

Example 3.4.1¹⁷

Consider an array of eight isotropic sources spaced at $d = \lambda/2$. Design a Dolph-Chebychev weighting with the sidelobes at -26 dB.

In this case, $R = 20$, so we set

$$T_7(x_0) = 20. \quad (3.157)$$

From (3.145),

$$x_0 = \cosh \left(\frac{1}{7} \cosh^{-1}(20) \right) = 1.142. \quad (3.158)$$

Then,

$$B(\psi) = \frac{1}{20} T_7 \left(x_0 \cos \frac{\psi}{2} \right). \quad (3.159)$$

We use (3.156) to find the weights

$$\left. \begin{aligned} w_0 &= a_4 = 0.0633 \\ w_1 &= a_3 = 0.1035 \\ w_2 &= a_2 = 0.1517 \\ w_3 &= a_1 = 0.1815 \end{aligned} \right\}. \quad (3.160)$$

A plot of $T_7(x)$ and the mapping in (3.159) is shown in Figure 3.25. As ψ moves from 0 to π , $B(\psi)$ moves from R through three zero crossings to 0 at $\psi = \pi$. Since the beam pattern is symmetric, this gives us a complete description.

The movement described in Figure 3.25 is summarized in Table 3.4.

¹⁶Stegen [Ste53] developed a procedure for finding an explicit formula for the coefficients. It corresponds to the IDFT approach in Section 3.3.3. We discuss this approach in Problem 3.4.18.

¹⁷This example is contained in [Kra88], but we use a simpler technique.

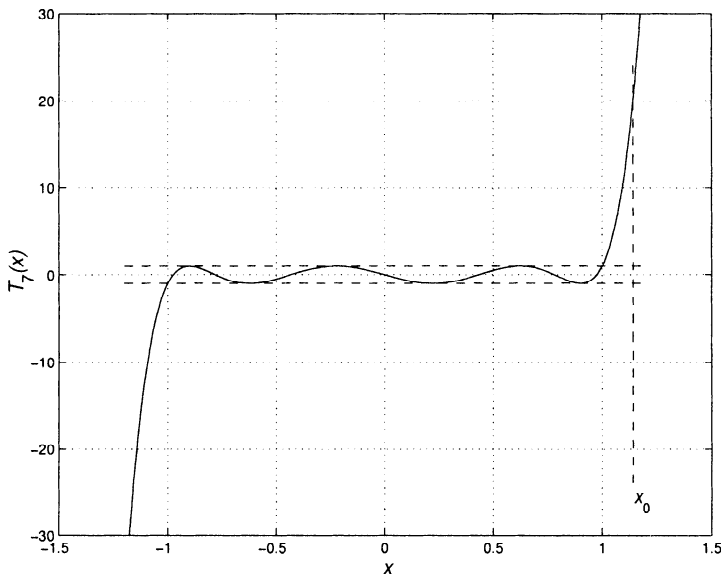


Figure 3.25 Chebychev polynomial of the seventh degree.

Table 3.4 Beam Pattern Movement

θ	0	$\frac{\pi}{2}$	π
$\psi = \pi \cos \theta$	π	0	$-\pi$
$x = x_0 \cos \left(\frac{\psi}{2} \right)$	0	x_0	0

We see that we have mapped the visible region in θ -space $(0, \pi)$ into a region in x -space $(0, x_0)$. We have not utilized the Chebychev polynomial in the region $(-1, 0)$. This is because we used an expression in $\psi/2$ and that the array spacing is $d = \lambda/2$.

For other values of d , the mapping is shown in Table 3.5.

Table 3.5 Mapping as a Function of d

θ	0	$\frac{\pi}{2}$	π
$\psi = \frac{2\pi}{\lambda} d \cos \theta$	$\frac{2\pi}{\lambda} d$	0	$-\frac{2\pi}{\lambda} d$
$x = x_0 \cos \left(\frac{\psi}{2} \right)$	$x_0 \cos \left(\frac{\pi d}{\lambda} \right)$	x_0	$x_0 \cos \left(\frac{\pi d}{\lambda} \right)$

For some representative values of d , the ranges on the x -axis are:

- (i) $d = \frac{\lambda}{4}$, $0.707x_0 \leq x \leq x_0$,

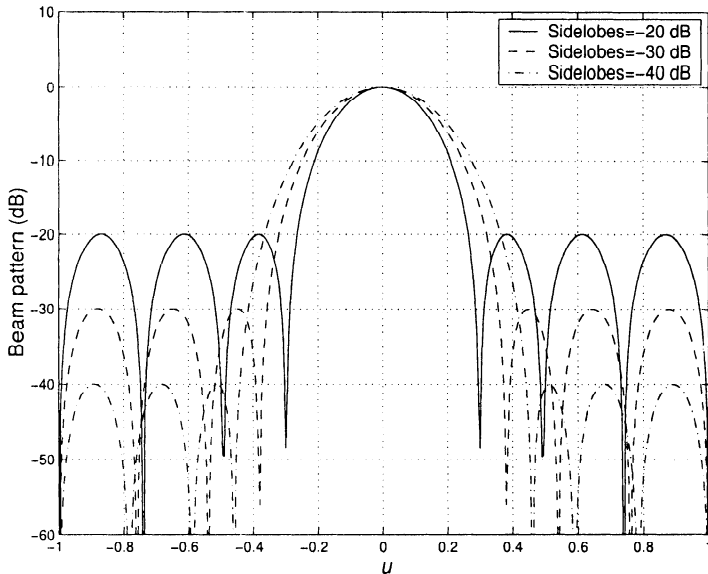


Figure 3.26 Beam patterns, Dolph-Chebychev weights: $N = 8$ (-20 -, -30 -, -40 -dB sidelobes).

$$(ii) \quad d = \frac{\lambda}{2}, \quad 0 \leq x \leq x_0,$$

$$(iii) \quad d = \frac{3\lambda}{4}, \quad -0.707x_0 \leq x \leq x_0.$$

The maximum d that we can use corresponds to the point where the left end of the range is -1 :

$$d = \frac{\lambda}{\pi} \cos^{-1} \left(-\frac{1}{x_0} \right). \quad (3.161)$$

In Figure 3.26, we show the beam patterns for an 8-element standard linear array for various sidelobe levels. As expected, the beamwidth increases as the sidelobe level decreases. In Figure 3.27, we show a z -plane plot of the zeros of the Dolph-Chebychev weighting for -20 -dB, -30 -dB, and -40 -dB sidelobes.

In his original work, Dolph [Dol46] showed the optimality of the Dolph-Chebychev polynomials. In this case, the optimum beam pattern is defined to be the beam pattern with the smallest null-null beamwidth for a given sidelobe level. We discuss it in the context of $T_5(x)$ in Figure 3.24.¹⁸ Consider another polynomial $P(x)$ of degree 5 that passes through (x_0, R) and

¹⁸This discussion follows p.170 of [Kra88]

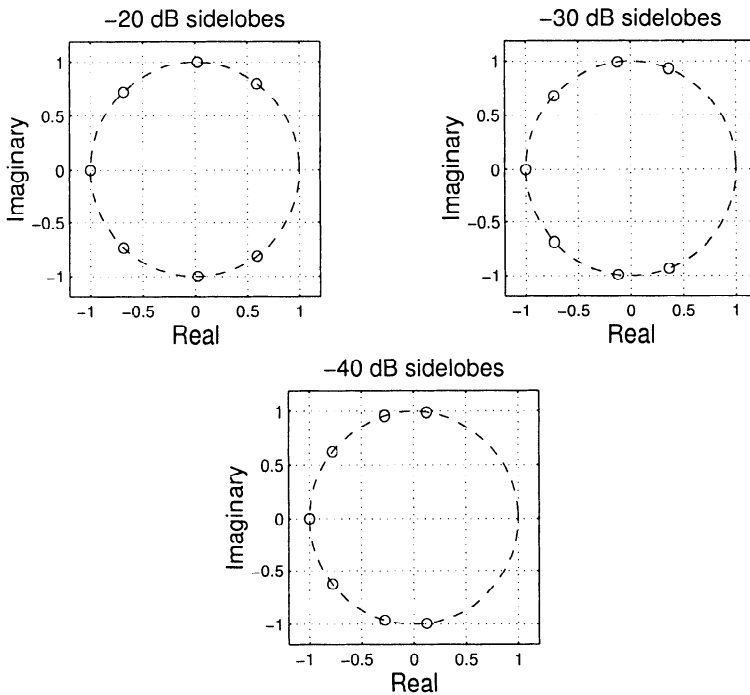


Figure 3.27 Zero plots of the Dolph-Chebychev weighting: (a) -20-dB sidelobes, (b) -30-dB sidelobes, (c) -40-dB sidelobes.

x'_1 (the largest root) and, for $x < x'_1$, it lies between +1 and -1. The null-null beamwidth is determined by x'_1 . We want to try and find a $P(x)$ whose values lies between $(1 - \epsilon)$ and $-(1 - \epsilon)$ for some positive ϵ . However, since $P(x)$ lies between ± 1 in the range $[-x'_1, x'_1]$, it must intersect $T_5(x)$ in at least $m+1 = 6$ points, including (x_0, R) . But two polynomials of the same degree that intersect at $m+1$ points must be the same polynomial, so $P(x) = T_5(x)$. Thus, the Chebychev polynomial is optimum. Riblet [Rib47] subsequently showed that the procedure was only optimum for $d \geq \lambda/2$ and proposed an improved procedure for $d < \lambda/2$. The non-optimality for $d < \lambda/2$ is because of the mapping in Table 3.5. For $d < \lambda/2$, the range on the x -axis is not adequate to constrain the beam pattern everywhere in the visible region.

We describe the Riblet-Chebychev technique briefly. For $d = \lambda/2$, the two techniques give the same result.

Riblet-Chebychev weighting

In this case we use an expansion of $\cos \psi$ rather than $\cos(\psi/2)$. Assuming N is odd, we then match the array polynomial to a Chebychev polynomial of

order $(N - 1)/2$. In addition, we choose a mapping such that θ moves from 0 to π , so we use the entire range $(-1, x_0)$ of the Chebychev polynomial.

Thus, the mapping is

$$x = c_1 \cos \psi + c_2, \quad (3.162)$$

where

$$\psi = \frac{2\pi}{\lambda} d \cos \theta, \quad (3.163)$$

and, from (3.134),

$$x_0 = \cosh \left(\frac{2}{N-1} \cosh^{-1} R \right). \quad (3.164)$$

The required mapping is shown in Table 3.6.

Table 3.6 Mapping Requirement

θ	0	$\frac{\pi}{2}$	π
$\psi = \frac{2\pi}{\lambda} d \cos \theta$	$\frac{2\pi}{\lambda} d$	0	$-\frac{2\pi}{\lambda} d$
$x = c_1 \cos \psi + c_2$	-1	x_0	-1

To find the constants, we require

$$c_1 + c_2 = x_0, \quad (3.165)$$

$$c_1 \cos \left(\frac{2\pi}{\lambda} d \right) + c_2 = -1. \quad (3.166)$$

Solving for c_1 and c_2 and substituting into (3.162), we have

$$x = \frac{1}{1 - \cos \left(\frac{2\pi}{\lambda} d \right)} \left\{ (x_0 + 1) \cos \psi - \left[1 + x_0 \cos \left(\frac{2\pi}{\lambda} d \right) \right] \right\}. \quad (3.167)$$

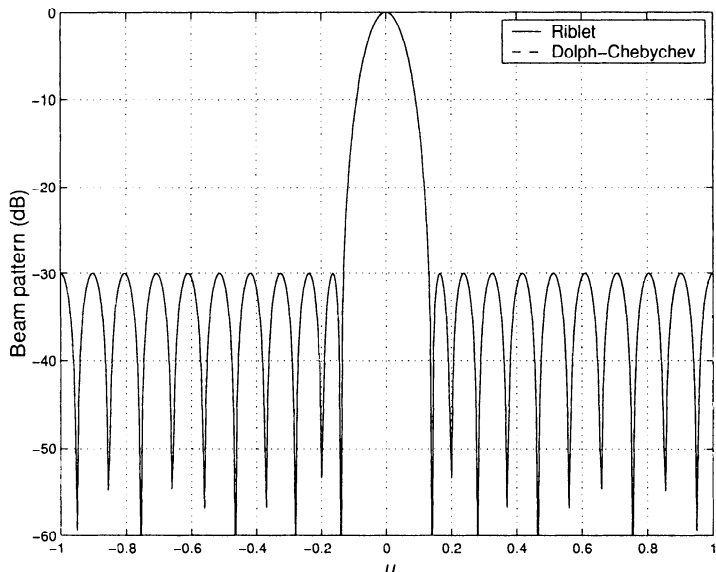
For $d = \lambda/2$, (3.167) reduces to

$$x = \frac{1}{2} \{ (x_0 + 1) \cos \psi + (x_0 - 1) \}. \quad (3.168)$$

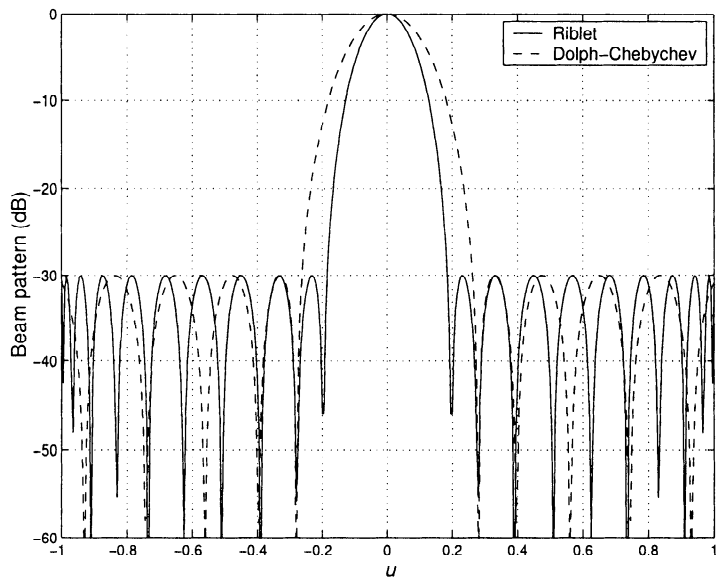
One can show that the two approaches lead to identical arrays for $d = \lambda/2$. For $d < \lambda/2$, Riblet's approach leads to arrays with smaller beamwidth for a given sidelobe level. We consider an example to illustrate the behavior.

Example 3.4.2

Consider a 21-element linear array. We require -30-dB sidelobes and design the array using both the Dolph-Chebychev and Riblet-Chebychev procedures. We consider element



(a)



(b)

Figure 3.28 Beam patterns for Dolph-Chebychev and Riblet weighting: $N = 21$, -30-dB sidelobes: (a) $d = \lambda/2$, (b) $d = \lambda/4$.

spacings of $d = \lambda/2$ and $\lambda/4$. The results are shown in Figure 3.28. We see that there is significant difference in the main-lobe width.

Riblets' procedure is only applicable to the case when N is odd and $N \geq 7$.

Subsequent to Dolph's original work in 1946 [Dol46] and Riblet's discussion in 1947 [Rib47], work has been done to simplify the synthesis procedure and derive the beamwidth and directivity characteristics of Dolph-Chebychev arrays.

The Dolph-Chebychev weighting is used in a number of array applications because of its constant sidelobe behavior. In many applications, we would prefer that the sidelobes decay rather than remain constant. The motivation for decaying sidelobes is to reduce the effect of interferers that are located at angles that are significantly different from the MRA. In the next section, we discuss a weighting developed by Taylor [Tay53] to achieve this behavior.

3.4.3 Taylor Distribution

In [Tay53] and [Tay55], Taylor developed a technique that constrains the maximum sidelobe height and gives decaying outer sidelobes. The development is for a linear aperture. It can be applied to linear arrays by sampling the aperture weighting or by root-matching.¹⁹ We can also solve for the array weighting directly (see Section 3.4.4).

Taylor starts with the uniform aperture weighting that we used in Section 2.7. The resulting beam pattern was derived and plotted in Figure 2.29. We define

$$v = \frac{L}{\lambda} u, \quad (3.169)$$

so that

$$B_v(v) = \frac{\sin(\pi v)}{\pi v} = \text{sinc}(\pi v). \quad (3.170)$$

With this change of variables, all of the zeros of the pattern are located on the integers,

$$v = \pm 1, \pm 2, \dots \quad (3.171)$$

Taylor approaches the synthesis problem by moving the “inner” zeros to new locations on the unit circle in order to lower the inner sidelobes and leaving the outer zeros in the same location as the uniform distribution in order to maintain the $|v|^{-1}$ decay.

¹⁹This discussion follows Elliott [Ell81].

We first write (3.170) as an infinite product,

$$B_v(v) = \prod_{n=1}^{\infty} \left(1 - \frac{v^2}{n^2}\right). \quad (3.172)$$

We then define a new pattern,

$$B_T(v) = \frac{\sin(\pi v)}{\pi v} \frac{\prod_{n=1}^{\bar{n}-1} \left(1 - \frac{v^2}{v_n^2}\right)}{\prod_{n=1}^{\bar{n}-1} \left(1 - \frac{v^2}{n^2}\right)}. \quad (3.173)$$

The denominator removes the first $\bar{n} - 1$ pairs of zeros and the numerator replaces them with $\bar{n} - 1$ new pairs of zeros located at v_n , $n = 1, 2, \dots, \bar{n} - 1$.

Taylor showed that the new zeros should be located at

$$v_n = \bar{n} \left[\frac{A^2 + (n - \frac{1}{2})^2}{A^2 + (\bar{n} - \frac{1}{2})^2} \right]^{\frac{1}{2}}, \quad (3.174)$$

where

$$\cosh(\pi A) = R, \quad (3.175)$$

and R is the same as in the Dolph-Chebychev derivation. Thus, the maximum sidelobe height is $-20 \log_{10} R$.

To find the corresponding aperture weighting, we recall from (2.215) that

$$B_T(v) = \int_{-\frac{L}{2}}^{\frac{L}{2}} w^*(z) e^{j\frac{2\pi}{L} vz} dz. \quad (3.176)$$

Since the weighting will be symmetric we can expand $w^*(z)$ in a Fourier cosine series:

$$w^*(z) = \sum_{m=0}^{\infty} c_m \cos\left(\frac{2m\pi z}{L}\right), \quad (3.177)$$

where c_m is a real constant. Using (3.177) in (3.176) gives,

$$B_T(v) = \int_{-\frac{L}{2}}^{\frac{L}{2}} \sum_{m=0}^{\infty} c_m \cos\left(\frac{2\pi m z}{L}\right) \cos\left(\frac{2\pi v z}{L}\right) dz. \quad (3.178)$$

We now choose integer values of the pattern $v = 0, 1, 2, \dots$. Then, the integral will be zero unless $v = m$. Therefore,

$$L B_T(0) = c_0, \quad (3.179)$$

$$\frac{L}{2}B_T(m) = c_m, \quad m \leq \bar{n} - 1, \quad (3.180)$$

and, from (3.173), $B_T(m) = 0$ for $m \geq \bar{n}$. Thus,

$$w^*(z) = \frac{1}{L} \left\{ B_T(0) + 2 \sum_{m=1}^{\bar{n}-1} B_T(m) \cos \left(\frac{2m\pi z}{L} \right) \right\}, \quad (3.181)$$

which is the desired result.

To find the corresponding weighting for an array, we can either sample $w^*(z)$ in (3.181) or we can match the zeros in (3.174).

To carry out the latter procedure, we define the zeros in u -space as,

$$u_n = \frac{\lambda}{Nd} \left\{ \bar{n} \left[\frac{A^2 + (n - \frac{1}{2})^2}{A^2 + (\bar{n} - \frac{1}{2})^2} \right]^{\frac{1}{2}} \right\}. \quad (3.182)$$

The weight vector for a standard linear array is obtained by using (2.88) with

$$\psi_n = \frac{2\pi}{N} \left\{ \bar{n} \left[\frac{A^2 + (n - \frac{1}{2})^2}{A^2 + (\bar{n} - \frac{1}{2})^2} \right]^{\frac{1}{2}} \right\}. \quad (3.183)$$

We now consider a simple example to illustrate the result.

Example 3.4.3

Consider a linear aperture of length $L = 10.5\lambda$ and a corresponding linear array with $d = \lambda/2$ so that $N = 21$. We require -30 -dB sidelobes and utilize $\bar{n} = 6$. In Figure 3.29(a), we show the beam pattern for the aperture obtained from (3.173) and the beam pattern for the array obtained by sampling $w^*(z)$ given in (3.181). In Figure 3.29(b), we show the Dolph-Chebychev pattern from Figure 3.28(a) and the Taylor pattern.

The Taylor distribution is widely used in practice. After the desired sidelobe level is chosen, \bar{n} has to be selected. If \bar{n} is too large, the aperture weighting function will increase as z approaches L . Usually, \bar{n} is chosen to have the largest value that does not cause $w^*(z)$ to increase as z increases (e.g., [Han98]).

There are several modifications to the Taylor pattern that are discussed in the antenna literature. For example, Elliott ([Ell75], [Ell81]) has developed techniques for designing modified Taylor patterns in which sidelobe heights can be individually specified. In Section 3.9, we develop techniques for controlling the sidelobe heights in specified regions.

The technique of assuming a continuous aperture and then finding a discretized weighting works well for large N . We can also solve the array problem directly using a technique invented by Villeneuve that is described in the next section.

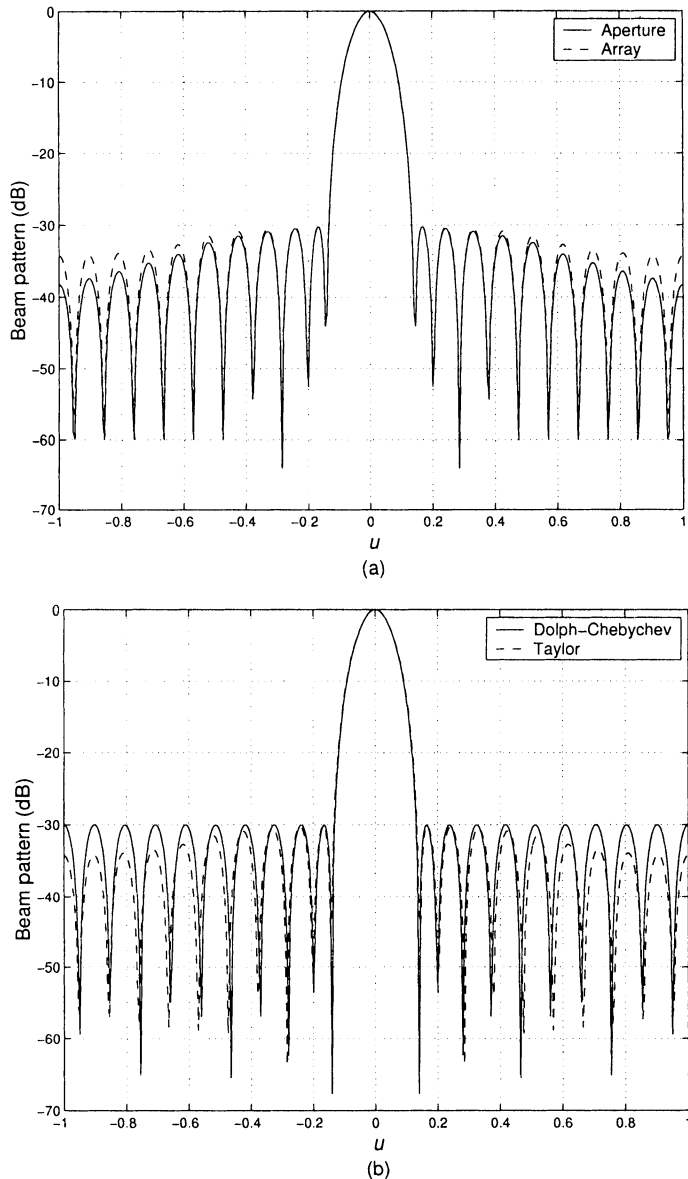


Figure 3.29 Beam pattern for Taylor weighting: $N = 21, \bar{n} = 6, \text{SLL} = -30$ dB (a) aperture and array; (b) array with Taylor weighting and Dolph-Chebychev weighting.

3.4.4 Villeneuve \bar{n} Distribution

The Chebychev distribution for an array with $N = 2M + 1$ elements can be written as,

$$T_{2M} \left(x_0 \cos \frac{\psi}{2} \right) = cB(e^{j\psi}) = \prod_{p=1}^{2M} (z - z_p), \quad (3.184)$$

where

$$z = e^{j\psi}, \quad (3.185)$$

$$z_p = e^{j\psi_p}, \quad (3.186)$$

and c is a normalizing constant. We consider N odd in the text; the derivation for N even is similar.

The roots are given by (3.154),

$$\psi_p = 2\cos^{-1} \left(\frac{1}{x_0} \cos \left[(2p-1) \frac{\pi}{4M} \right] \right), \quad p = 1, 2, \dots, 2M. \quad (3.187)$$

The beam pattern can be written as

$$B_\psi(\psi) = e^{jM\psi} 4^M \prod_{p=1}^M \sin \left(\frac{\psi - \psi_p}{2} \right) \sin \left(\frac{\psi + \psi_p}{2} \right), \quad (3.188)$$

which is the Chebychev pattern for $N = 2M + 1$ elements.

Villeneuve [Vil84] (e.g., [Kum92]) developed a technique for discrete arrays. He combines the better features of the uniform and Chebychev weightings. We start with the beam pattern for uniform weighting and replace the first $\bar{n} - 1$ roots with modified Dolph-Chebychev roots. The resulting beam pattern is

$$B_\psi(\psi) = \frac{\sin \left(\frac{N}{2} \psi \right)}{\sin \left(\frac{\psi}{2} \right)} \cdot \left[\frac{\prod_{n=1}^{\bar{n}-1} \sin \left(\frac{\psi - \psi'_n}{2} \right) \sin \left(\frac{\psi + \psi'_n}{2} \right)}{\prod_{n=1}^{\bar{n}-1} \sin \left(\frac{\psi - \psi_{un}}{2} \right) \sin \left(\frac{\psi + \psi_{un}}{2} \right)} \right]. \quad (3.189)$$

The term in brackets modifies the beam pattern of the uniform weighting. In the numerator are the modified Chebychev roots corresponding to the first $\bar{n} - 1$ interior sidelobes. In the denominator are the corresponding roots of the uniform weighting,

$$\psi_{un} = \frac{2\pi n}{N}, \quad n = 1, 2, \dots, \bar{n} - 1. \quad (3.190)$$

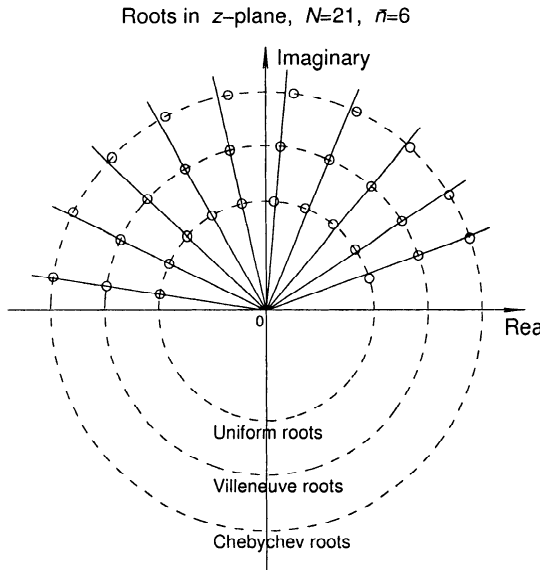


Figure 3.30 Roots of the three beam patterns. The three unit circles are shown with different radii. Only upper half-plane roots are shown.

The Chebychev roots are modified so there is not a jump at $n = \bar{n}$. This modification is accomplished by a progressive shift such that the \bar{n} th root of uniform weighting is unchanged.

The Chebychev zeros are given in (3.187). Each Chebychev zero is multiplied by

$$\sigma = \frac{2\pi\bar{n}}{N\psi_{\bar{n}}}, \quad (3.191)$$

where $\psi_{\bar{n}}$ is the \bar{n} th Chebychev root. Therefore,

$$\sigma = \frac{\pi\bar{n}}{N\cos^{-1}\left(\frac{1}{x_0} \cos\left[(2\bar{n}-1)\frac{\pi}{4M}\right]\right)}. \quad (3.192)$$

Then,

$$\psi'_n = \sigma\psi_n, \quad n = 1, \dots, \bar{n}-1. \quad (3.193)$$

The remaining roots are uniform,

$$\psi_{un} = \frac{2\pi}{N}n, \quad n = \bar{n}, \dots, \frac{N-1}{2}. \quad (3.194)$$

The resulting root patterns are shown in Figure 3.30 for $N = 21$. For clarity,

we have shown three unit circles. We only show the roots in the upper half. The remaining roots are complex conjugates. The inner six (plus their six complex conjugates) Chebychev roots are moved outward. The amount of movement increases until, at $\bar{n} = 6$, the Villeneuve root corresponds to the uniform root. The remaining roots are the uniform roots. The shift in roots is reasonably small, but it results in a significant pattern change. A beam pattern for a 21-element and 41-element array with -20-dB sidelobes are shown in Figure 3.31. It is essentially the same as the discretized Taylor beam pattern. For $N \leq 11$, there is some difference in the beam patterns and the Villeneuve technique is preferable.

The weight vector is obtained by using (3.193), (3.194) and their symmetrical values in either (2.88) or (3.188).

Villeneuve [Vil84] also derives the results for N even and provides further comparisons with the Taylor distribution. Hansen ([Han85], [Han92]) has studied the properties of the distribution. [Han98] has tables with detailed comparisons of Taylor and Villeneuve \bar{n} beam patterns.

3.5 Least Squares Error Pattern Synthesis

In this section, we develop techniques for finding the least squares error approximation to a desired beam pattern. The technique is valid for an arbitrary array geometry. For notational simplicity, the 1-D case is discussed in the text.

The desired beam pattern is $B_d(\psi)$. The square error is defined as

$$\xi = \int_{-\pi}^{\pi} |B_d(\psi) - \mathbf{w}^H \mathbf{v}(\psi)|^2 d\psi. \quad (3.195)$$

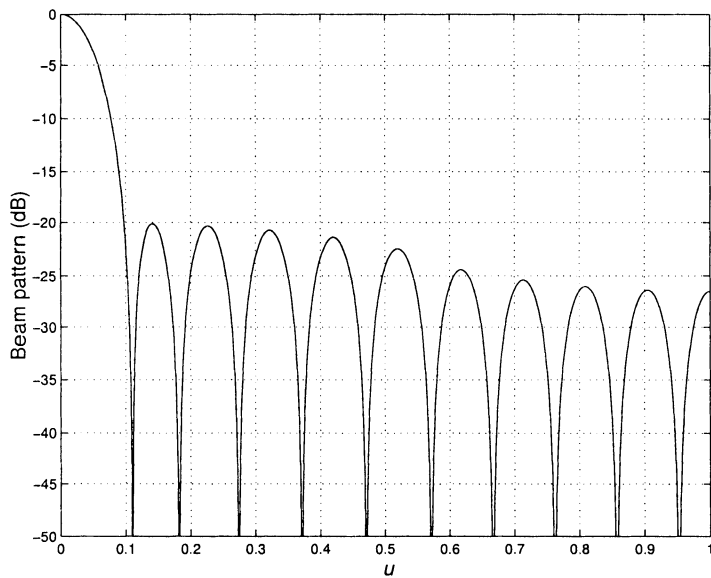
A more general error expression includes a weighting function inside the integral. The expression in (3.195) is adequate for the present discussion. Taking the complex gradient with respect to \mathbf{w}^H and setting the result equal to zero gives²⁰

$$-\int_{-\pi}^{\pi} \mathbf{v}(\psi) B_d^*(\psi) + \left\{ \int_{-\pi}^{\pi} \mathbf{v}(\psi) \mathbf{v}^H(\psi) d\psi \right\} \mathbf{w}_o = \mathbf{0}. \quad (3.196)$$

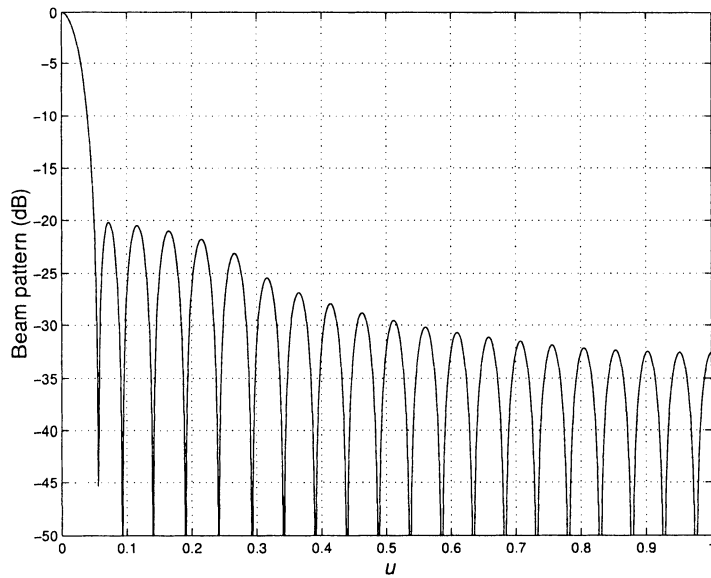
Defining

$$\mathbf{A} = \int_{-\pi}^{\pi} \mathbf{v}(\psi) \mathbf{v}^H(\psi) d\psi, \quad (3.197)$$

²⁰See Appendix A (Section A.7.4) for a discussion of complex gradients.



(a)



(b)

Figure 3.31 Beam pattern with Villeneuve weighting: $\bar{n} = 6$, SLL = -20 dB; (a) $N = 21$; (b) $N = 41$.

(3.196) can be written as

$$\mathbf{w}_o = \mathbf{A}^{-1} \int_{-\pi}^{\pi} \mathbf{v}(\psi) B_d^*(\psi) d\psi. \quad (3.198)$$

The result in (3.198) is an explicit expression for the least squares approximation to $B_d(\psi)$ and can be evaluated for a specific array manifold vector.

For the special case of a standard linear array, the array manifold vector is given by (2.70) and the nk element of \mathbf{A} is

$$\begin{aligned} [\mathbf{A}]_{nk} &= \int_{-\pi}^{\pi} \exp \left\{ \left[j \left(n - \frac{N-1}{2} \right) - j \left(k - \frac{N-1}{2} \right) \right] \psi \right\} d\psi \\ &= \int_{-\pi}^{\pi} \exp [j(n-k)\psi] d\psi = 2\pi \delta_{nk}. \end{aligned} \quad (3.199)$$

Using (2.70) and (3.199) in (3.198) gives

$$\mathbf{w}_{no} = \frac{1}{2\pi} \int_{-\pi}^{\pi} \exp \left(j \left(n - \frac{N-1}{2} \right) \psi \right) B_d^*(\psi) d\psi. \quad (3.200)$$

The weight vector is \mathbf{w}^H , whose components are

$$\mathbf{w}_{no}^* = \frac{1}{2\pi} \int_{-\pi}^{\pi} \exp \left\{ -j \left(n - \frac{N-1}{2} \right) \psi \right\} B_d(\psi) d\psi. \quad (3.201)$$

For the special case of a real symmetric $B_d(\psi)$, it is convenient to use the symmetric indexing. For N odd,

$$a_{mo} = \frac{1}{2\pi} \int_{-\pi}^{\pi} B_d(\psi) e^{-jm\psi} d\psi. \quad (3.202)$$

For N even,

$$a_{mo} = \frac{1}{2\pi} \int_{-\pi}^{\pi} B_d(\psi) e^{-j(m-\frac{1}{2})\psi} d\psi. \quad (3.203)$$

In both cases,

$$a_{-mo} = a_{mo}. \quad (3.204)$$

The results in (3.202) and (3.203) are familiar as the Fourier series expansion of the desired beam pattern. The resulting beam pattern is

$$\hat{B}_d(\psi) = \sum_{m=-\frac{N-1}{2}}^{\frac{N-1}{2}} a_{mo} e^{jm\psi} \quad (3.205)$$

for N odd and a similar expression for N even.

In some cases the desired pattern $B_d(\psi)$ is constant from $-\psi_0 \leq \psi \leq \psi_0$ and zero elsewhere in ψ -space. In this case,

$$a_m = \frac{1}{2\pi} \int_{-\psi_0}^{\psi_0} e^{-jm\psi} d\psi = \frac{\sin m\psi_0}{m\pi}, \quad N \text{ odd}, \quad (3.206)$$

and

$$a_m = \frac{1}{2\pi} \int_{-\psi_0}^{\psi_0} e^{-j(m-\frac{1}{2})\psi} d\psi = \frac{\sin((m-\frac{1}{2})\psi_0)}{((m-\frac{1}{2})\psi_0)}, \quad N \text{ even}. \quad (3.207)$$

We consider a simple example to illustrate the technique.

Example 3.5.1

The desired $B_d(\psi)$ is shown in Figure 3.32. It is uniform from $60^\circ \leq \theta \leq 120^\circ$ or, since $\psi = \pi \cos \theta$,

$$-0.5\pi \leq \psi \leq 0.5\pi. \quad (3.208)$$

The results for $N = 10$ and 20 are shown in Figure 3.32. We also show the beam pattern using Woodward sampling.

We observe that the pattern has oscillatory overshoots at the discontinuities. This behavior is known as Gibbs phenomenon and is familiar from Fourier theory. We can use windows to decrease the overshoots.

To introduce the concept of windows, we write (3.205) as

$$\hat{B}_d(\psi) = \sum_{m=-\infty}^{\infty} a_{mo} R[m] e^{jm\psi}, \quad (3.209)$$

where $R[m]$ is a discrete rectangular window. We denote its Fourier transform by $B_R(\psi)$ and normalize it so $B_R(0)$ equals one. For N odd,

$$R[m] = \begin{cases} \frac{1}{N}, & m = -\frac{N-1}{2}, \dots, 0, \dots, \frac{N-1}{2} \\ 0, & \text{elsewhere.} \end{cases} \quad (3.210)$$

From Fourier transform properties, (3.209) corresponds to convolving $B_d(\psi)$ and $B_R(\psi)$ in ψ -space,

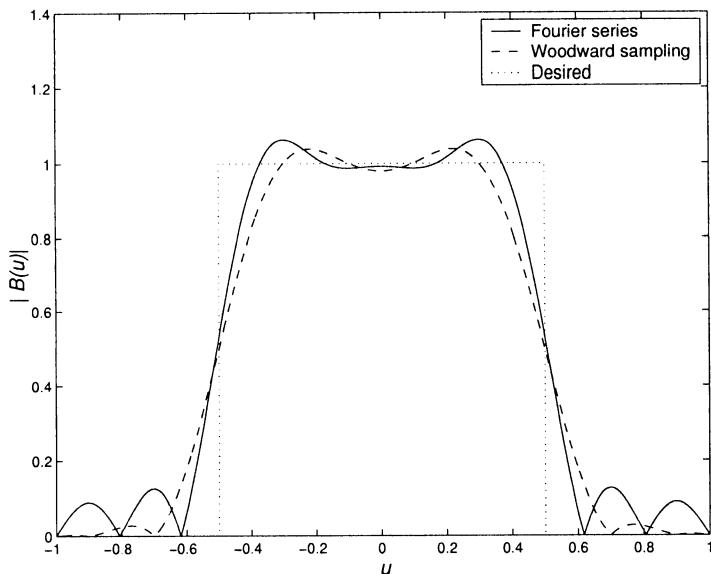
$$\hat{B}_d(\psi) = B_d(\psi) * B_R(\psi), \quad (3.211)$$

or

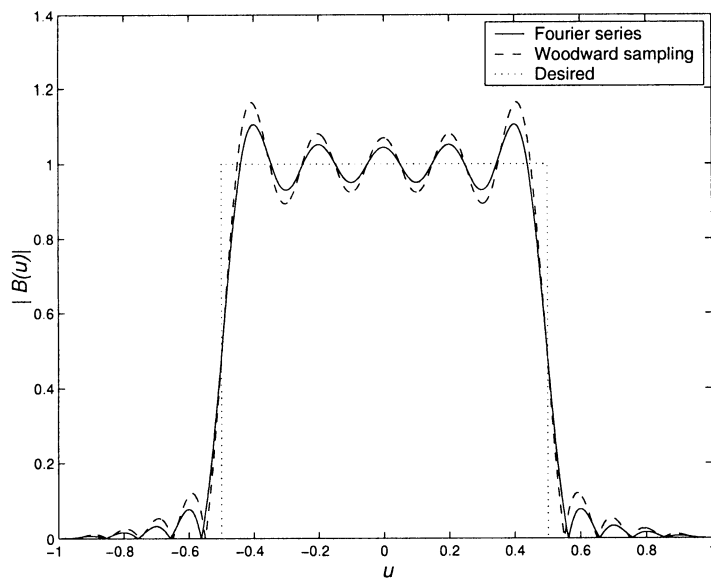
$$\hat{B}_d(\psi) = \frac{1}{2\pi} \int_{-\pi}^{\pi} B_d(\psi_x) B_R(\psi - \psi_x) d\psi_x, \quad (3.212)$$

where

$$B_R(\psi) = \frac{1}{N} \sum_{m=-\frac{N-1}{2}}^{\frac{N-1}{2}} e^{jm\psi} = \frac{1}{N} \frac{\sin\left(\frac{N}{2}\psi\right)}{\sin\left(\frac{\psi}{2}\right)}. \quad (3.213)$$



(a)



(b)

Figure 3.32 Desired beam pattern and synthesized patterns for linear array of 10 and 20 elements using the Fourier series method and the Woodward sampling technique: (a) $N=10$; (b) $N=20$.

This amplitude of $B_R(\psi)$ was plotted in Figure 2.15. The convolution process consists of sliding $B_R(\psi)$ by $B_d(\psi)$. The integral will oscillate as each sidelobe moves past the discontinuity.

We can alleviate the oscillation problem by tapering the weighting of $R[m]$ so as to decrease the area of the sidelobes. This is similar to the problem that we solved in Section 3.1 (in Section 3.1, we were concerned about the height of the sidelobes). Thus, all of the weightings that we developed there can be used as “windows” to truncate our Fourier series. We recall that as we shape the weighting, the width of the main lobe increases. Thus, the cost of using a shaped window will be a wider transition region.

We consider the same desired $B_d(\psi)$ as in Example 3.5.1 and look at the effect of different windows.

Example 3.5.2 (continuation)

The desired beam pattern $B_d(\psi)$ is shown in Figure 3.32. It is uniform in u -space from $-0.5 \leq u \leq 0.5$. The a_{mo} are calculated using (3.202). The synthesized $\hat{B}_d(\psi)$ is given by

$$\hat{B}_d(\psi) = \sum_{m=-\infty}^{\infty} a_{mo} R_w(m) e^{j m \psi}, \quad (3.214)$$

where $R_w(m)$ is the window corresponding to one of the weightings in Section 3.1. We consider the standard 11-element linear array used in Example 3.5.1.

We consider three windows from Section 3.1: Hann, Hamming, and Kaiser. For the Hann window the beam pattern is obtained by using $R_w(m)$ from Section 3.1 and a_{mo} from (3.202) to obtain,

$$B_{HANN}(\psi) = c_1 \sum_{m=-\frac{N-1}{2}}^{\frac{N-1}{2}} \left[\frac{\sin(0.5m\pi)}{m\pi} \right] \left[0.5 + 0.5 \cos \left(2\pi \frac{m}{N} \right) \right] e^{j m \psi}, \quad (3.215)$$

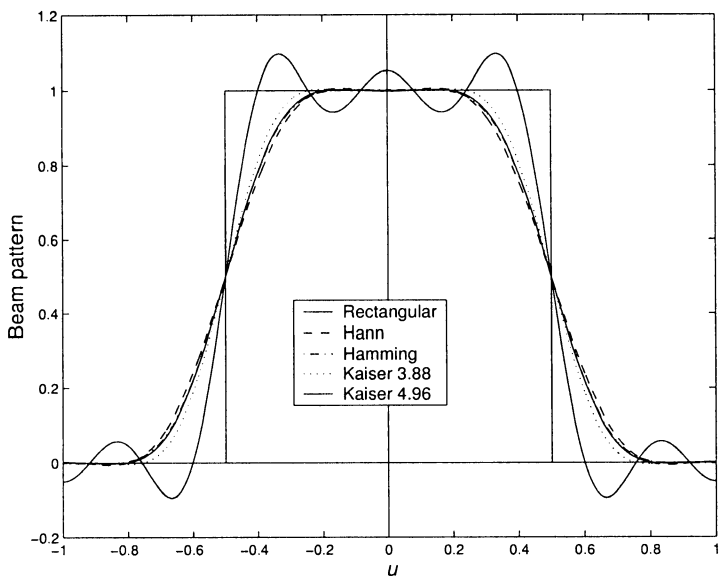
$$B_{HAMMING}(\psi) = c_2 \sum_{m=-\frac{N-1}{2}}^{\frac{N-1}{2}} \left[\frac{\sin(0.5m\pi)}{m\pi} \right] \left[0.54 + 0.46 \cos \left(2\pi \frac{m}{N} \right) \right] e^{j m \psi}, \quad (3.216)$$

$$B_{KAISER}(\psi) = c_3 \sum_{n=-\frac{N-1}{2}}^{\frac{N-1}{2}} \left[\frac{\sin(0.5m\pi)}{m\pi} \right] \left[I_0 \left(\beta \sqrt{1 - \left(\frac{2m}{N} \right)^2} \right) \right] e^{j m \psi}, \quad (3.217)$$

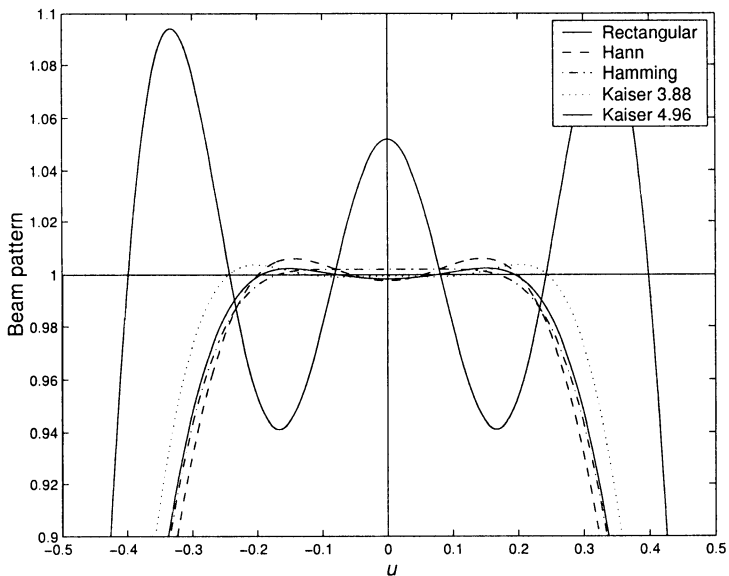
where the constant normalizes the window. For the Kaiser window, we use $\beta = 3.88$ to match the Hann overshoot and $\beta = 4.96$ to match the Hamming overshoot.

The resulting patterns are plotted in Figure 3.33(a). In Figure 3.33(b), we show an expanded view of the plateau of the beam pattern. The effect of the windows is to reduce the overshoot and to widen the main lobe (which causes the transition region to widen).

If we use the Kaiser window, we must choose a suitable value of β . Kaiser [KK66], [Kai74] developed a procedure to design FIR filters that can



(a)



(b)

Figure 3.33 Beam patterns for various windows: $N = 11$.

be applied directly to the array problem.²¹

$$\Delta\psi = \psi_s - \psi_p, \quad (3.218)$$

and

$$A = -20 \log \delta, \quad (3.219)$$

where δ is the overshoot shown in Figure 3.34 in Section 3.6 with $\delta_p = \delta_s$. Kaiser determined empirically that the required β is given by

$$\beta = \begin{cases} 0.1102(A - 8.7), & A > 50, \\ 0.5842(A - 21)^{0.4} + 0.07886(A - 21), & 21 \leq A \leq 50, \\ 0.0, & A < 21, \end{cases} \quad (3.220)$$

where $A = 21$ corresponds to a rectangular window. The number of elements to achieve the desired A and $\Delta\psi$ is

$$N - 1 = \frac{A - 8}{2.285 \Delta\psi}. \quad (3.221)$$

If N is fixed, the required value of δ will determine the transition region $\Delta\psi$. We used (3.220) and (3.221) to determine the β used in Figure 3.33(a). Other examples are developed in the problems.

In this section, we introduced least squares error approximations to a desired beam pattern. For standard linear arrays, this approach led to a Fourier series representation. When the desired beam pattern has discontinuities, there are overshoots that can be reduced by using the weighting functions developed in Section 3.2 as windows. The use of windows reduced the overshoot at the expense of widening the transition region between the main lobe and the sidelobes.

3.6 Minimax Design

In this section we consider the problem shown in Figure 3.34. In the main-lobe region, we would like the pattern to be unity. Thus, we use a design constraint that $B(e^{j\psi})$ must lie between $1 - \delta_p$ and $1 + \delta_p$ in the range $[0, \psi_p]$ and between $+\delta_s$ and $-\delta_s$ in the range $[\psi_s, \pi]$. This problem is the spatial filter analog to optimum minimax error design problems for FIR filters.

There are tutorial discussions of the optimum techniques in Section 7.6 of Oppenheim [OS89], Chapter 8 of Proakis [PRLN92], Chapter 3 of Rabiner

²¹Our discussion follows pp. 452–455 of [OS89]

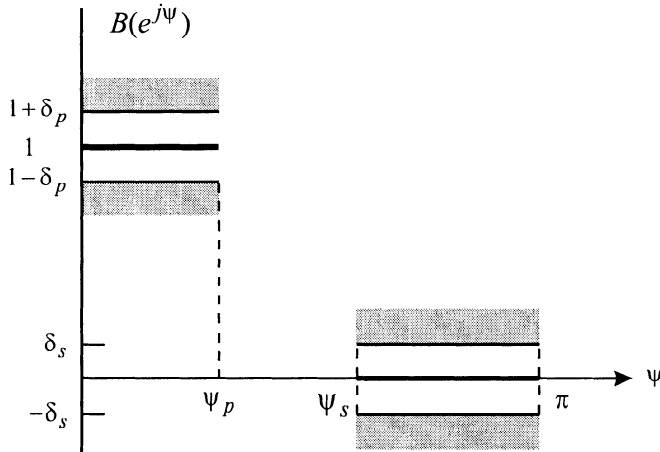


Figure 3.34 Tolerance scheme. [Adapted from [OS89]]

and Gold [RG75], and Chapter 4 of [MK93]. These discussions are based on the work of Parks and McClellan [PM72a], [PM72b] with subsequent contributions (e.g., McClellan et al. [MPR73], [MP73], [MR79], [RMP75]). Our discussion is similar to the above presentations.

At the same time that Parks and McClellan published [PM72a] and [PM72b], Hersey et al. [HTL72] published a paper on minimax design of digital filters that was more general because arbitrary upper and lower constraining functions can be used. The results were applied to linear arrays by Mucci et al. [MTL75]. Discussion of the history of these techniques is contained in Rabiner et al. [RMP75] and Tufts [Tuf75] (see also Farden and Scharf [FS74]).

We define a weighted error as

$$e_{pm}(\psi) = W_{pm}(\psi) [B_d(e^{j\psi}) - B(e^{j\psi})]. \quad (3.222)$$

We assume that $B_d(e^{j\psi})$ is a real symmetric function. The functions $e_{pm}(\psi)$, $W_{pm}(\psi)$, and $B_d(e^{j\psi})$ are defined only over closed sub-intervals of $0 \leq \psi \leq \pi$. For the N -odd case, they are defined over $[0, \psi_p]$ and $[\psi_s, \pi]$. We assume N , ψ_p , and ψ_s are fixed design parameters. Then, for the model in Figure 3.34,

$$B_d(e^{j\psi}) = \begin{cases} 1, & 0 \leq \psi \leq \psi_p, \\ 0, & \psi_s \leq \psi \leq \pi, \end{cases} \quad (3.223)$$

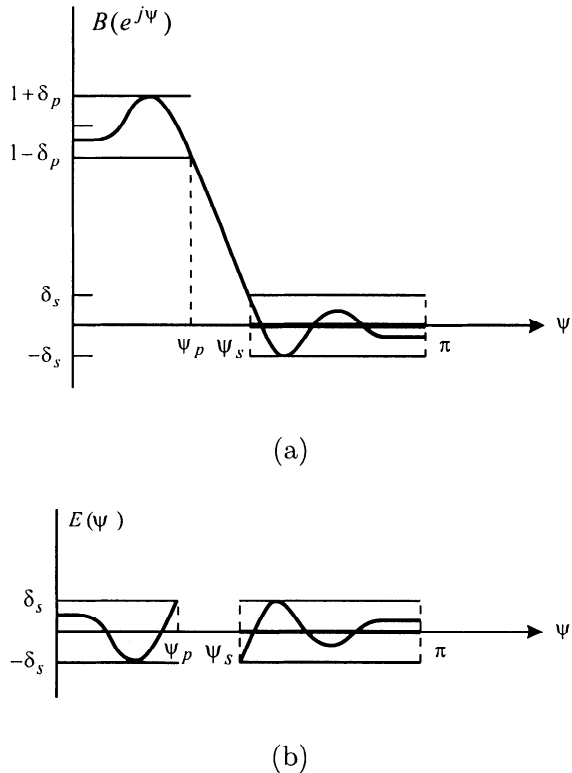


Figure 3.35 (a) Possible beam pattern meeting the specifications of Figure 3.34; (b) weighted error for the approximation in (a). [Adapted from [OS89]]

and the weighting function is

$$W_{pm}(\psi) = \begin{cases} \frac{1}{K}, & 0 \leq \psi \leq \psi_p, \\ 1, & \psi_s \leq \psi \leq \pi, \end{cases} \quad (3.224)$$

where $K = \delta_p/\delta_s$ and is a fixed parameter. The value of δ_p (or δ_s) is variable. A possible $B(e^{j\psi})$ that meets the desired criteria is shown in Figure 3.35(a). The corresponding error function is shown in Figure 3.35(b). We see that the maximum weighted approximation error is δ_s in both bands.

The criterion of interest is the minimax (or Chebychev) criterion. We seek a beam pattern that **minimizes** the maximum weighted approximation error.

$$\min_{\{w_n, n=0, 1, \dots, N-1\}} \left(\max_{\psi \in F} |e_{pm}(\psi)| \right), \quad (3.225)$$

where F is closed subset of $0 \leq \psi \leq \pi$:

$$[0 \leq \psi \leq \psi_p] \cup [\psi_s \leq \psi \leq \pi]. \quad (3.226)$$

Parks and McClellan [PM72a] formulate the problem as a polynomial approximation problem. Recall from Section 3.4.2, that we can write²²

$$\cos(n\psi) = T_n(\cos \psi), \quad (3.227)$$

where $T_n(x)$ is the n th order Chebychev polynomial, and therefore

$$B(e^{j\psi}) = \sum_{k=0}^L c_k (\cos \psi)^k, \quad (3.228)$$

where the c_k are constants related to the original weights w_n and $L = (N - 1)/2$. Letting

$$x = \cos \psi, \quad (3.229)$$

we have

$$B(e^{j\psi}) = P(x) |_{x=\cos \psi}, \quad (3.230)$$

where

$$P(x) = \sum_{k=0}^L c_k x^k. \quad (3.231)$$

There are several useful theorems [Che66] available to solve the approximation problem.²³ Parks and McClellan utilized the following theorem.

3.6.1 Alternation Theorem

Alternation Theorem²⁴ Let F_p denote the closed subset consisting of the disjoint union of closed subsets of the real axis x . $P(x)$ denotes an L th-order polynomial

$$P(x) = \sum_{k=0}^L c_k x^k. \quad (3.232)$$

Also, $D_p(x)$ denotes a given desired function of x that is continuous on F_p ; $W_{pm}(x)$ is a positive function, continuous on F_p , and $e_{pm}(x)$ denotes the weighted error

$$e_{pm}(x) = W_{pm}(x) [D_p(x) - P(x)]. \quad (3.233)$$

²²Note that we are using a polynomial in $\cos \psi$ instead of $\cos \psi/2$.

²³Other discussions of the approximation problem are contained in Rice [Ric64], Taylor [Tay69], and Taylor and Winter [TW70].

²⁴This version of the alternation theorem follows [OS89] but is due to [PM72a].

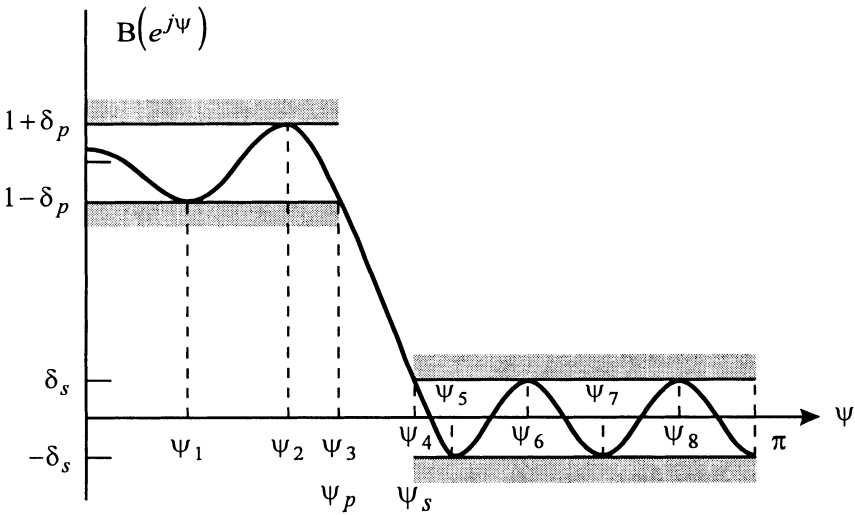


Figure 3.36 Typical example of a beam pattern approximation that is optimal according to the alternation theorem for $L = 7$. [Adapted from [OS89]]

The maximum error $\|E\|$ is defined as

$$\|E\| = \max_{x \in F_p} |e_{pm}(x)|. \quad (3.234)$$

A necessary and sufficient condition that $P(x)$ is the unique L th-order polynomial that minimizes $\|E\|$ is that $e_{pm}(x)$ exhibit *at least* $(L + 2)$ alternations, that is, there must exist at least $(L + 2)$ values x_i in F_p such that $x_1 < x_2 < \dots < x_{L+2}$ and such that $e_{pm}(x_i) = -e_{pm}(x_{i+1}) = \pm \|E\|$ for $i = 1, 2, \dots, (L + 2)$.

We now apply the alternation theorem to the array design. We let $x = \cos \psi$ and plot the polynomial versus ψ . A function that satisfies the Alternation Theorem for $L = 7$ is shown in Figure 3.36. We see that there are nine alternations of the error, occurring at $\psi_1, \psi_2, \dots, \psi_8$ and π .

There are other possible functions that satisfy the Alternation Theorem (e.g., p. 472 of [OS89]).

3.6.2 Parks-McClellan-Rabiner Algorithm

From the alternation theorem, the optimum pattern $B_o(e^{j\psi})$ will satisfy the following set of equations,

$$W_{pm}(\psi_i) \left[B_d(e^{j\psi_i}) - B_o(e^{j\psi_i}) \right] = (-1)^{i+1} \delta, \quad i = 1, 2, \dots, L + 2, \quad (3.235)$$

where δ is the optimum error and $B_o(e^{j\psi})$ is given by (3.228).

These equations lead to an iterative algorithm called the *Remez Multiple Exchange Algorithm* for finding the $B_o(e^{j\psi})$.

Step 1: Select an initial set of $\psi_i, i = 1, 2, \dots, L+2$. ψ_p and ψ_s are included in the set.

Step 2: The set of equations (3.235) could be solved for c_k and δ . However, Parks and McClellan found a more efficient approach using a polynomial approximation.

(a) For a given set of ψ_i , δ is given by

$$\delta = \frac{\sum_{k=1}^{L+2} b_k B_d(e^{j\psi_k})}{\sum_{k=1}^{L+2} \frac{b_k (-1)^{k+1}}{W_{pm}(\psi_k)}}, \quad (3.236)$$

where

$$b_k = \prod_{\substack{i=1 \\ i \neq k}}^{L+2} \frac{1}{x_k - x_i}, \quad (3.237)$$

and

$$x_i = \cos \psi_i. \quad (3.238)$$

(b) Since $B_o(e^{j\psi})$ is an L th-order trigonometric polynomial, we can interpolate it through $L+1$ of the known $L+2$ values. Parks and McClellan used a Lagrange interpolation formula to obtain

$$B_o(e^{j\psi}) = P(\cos \psi) = \frac{\sum_{k=1}^{L+1} \left[\frac{d_k}{x - x_k} \right] f_k}{\sum_{k=1}^{L+1} \left[\frac{d_k}{x - x_k} \right]}, \quad (3.239)$$

where $x = \cos \psi$ and $x_k = \cos \psi_k$,

$$f_k = B_d(e^{j\psi_k}) - \frac{(-1)^{k+1} \delta}{W_{pm}(\psi_k)}, \quad (3.240)$$

and

$$d_k = \prod_{\substack{i=1 \\ i \neq k}}^{L+1} \frac{1}{x_k - x_i} = \frac{b_k}{x_k - x_{L+2}}, \quad (3.241)$$

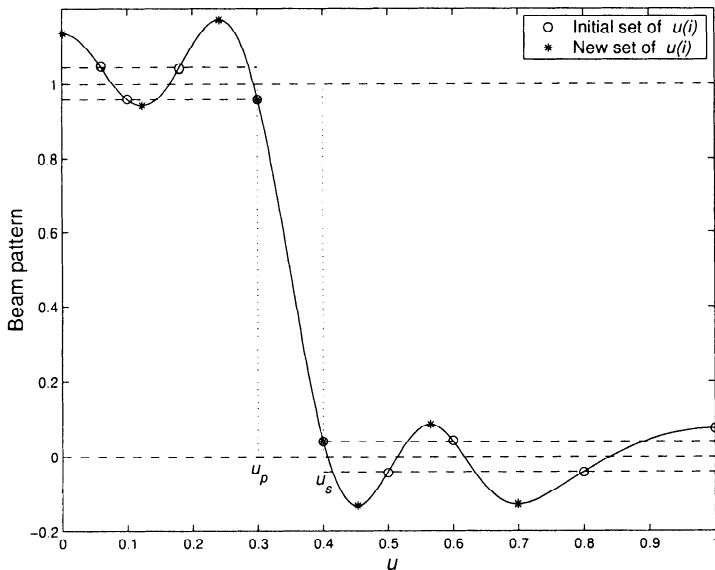


Figure 3.37 Illustration of the Parks-McClellan algorithm for equiripple approximation. [Adapted from [OS89]]

where we use $\psi_1, \psi_2, \dots, \psi_{L+1}$ to find the polynomial, the value at ψ_{L+2} will be correct because $B_o(e^{j\psi})$ in (3.239) satisfies (3.235). A typical result is shown in Figure 3.37 after the first iteration.

Step 3: The original set $\psi_1, \psi_2, \dots, \psi_{L+1}$ is exchanged for a completely new set $\psi'_1, \psi'_2, \dots, \psi'_{L+1}$ (ψ_p and ψ_s are still included). The new ψ_i are defined by the $(L+2)$ largest peaks of the plotted curve. There are at most $L-1$ local minima and maxima in the open intervals $(0 < \psi < \psi_p)$ and $(\psi_s < \psi < \pi)$. If there are $L-1$, then the remaining point can be either 0 or π ; one chooses the largest error point for the next iteration.

Step 4: The iteration is continued in this manner until the change in δ between iterations falls below some small pre-selected amount. The result is $B_o(e^{j\psi})$.

Notice that the array weightings were not computed as part of the design process. The calculation of the weightings is straightforward using the IDFT developed in Section 3.3.

We consider an example to illustrate the technique.

Example 3.6.1

Consider a standard 11-element linear array. The desired beam pattern is shown in Figure 3.17. In Figure 3.38, we show the resulting beam patterns using the Parks-McClellan, Woodward, and Fourier algorithms. We see that the Parks-McClellan algorithm gives uniform ripples with a slight increase in the transition region.

3.6.3 Summary

In this section, we have given a brief discussion of the Parks-McClellan (PM) algorithm for minimax optimization. The references at the beginning of the section give more comprehensive discussions and should be utilized if the algorithm is going to be used in practice. Lewis et al. [LMT76] developed a technique that mixes least squares and minimax techniques that may be useful in some applications.

In sections 3.1 through 3.6, we developed three major topics:

- (i) Synthesis of single MRA arrays
- (ii) Synthesis of desired beam patterns
- (iii) Relationships between beam patterns, weight vectors, and zeros of the array polynomial

In the single MRA problem, we assume that the signal of interest is a plane wave arriving from a specific direction (expressed in either angle space or wavenumber space). We want to design a beam pattern with good directivity (corresponding to a narrow main lobe) and low sidelobes. Our design procedures trades-off main-lobe width and sidelobe level. In Section 3.1, we used a cosine building block and developed several useful weight vectors. The Hamming weighting provided a good compromise between main-lobe expansion and sidelobe height. We then considered the case in which there was a region of interest around the main lobe. The DPSS and Kaiser weightings were effective for this application. In Section 3.4, we developed Dolph-Chebychev and Riblet-Chebychev weightings to provide uniform-height sidelobes and a main lobe whose width was the minimum possible for the given sidelobe height. We also developed Taylor and Villenueve weightings that had decreasing sidelobes. This collection of weightings is the most widely used for the deterministic synthesis of uniform linear arrays.

In Sections 3.3, 3.5, and 3.6, we studied the problem of synthesizing a desired beam pattern. We developed three approaches; the Woodward sampling approach, the least squares error approach, and the minimax algorithm. Each approach has advantages and disadvantages, and the appropriate technique will depend on the specific desired beam pattern. We revisit

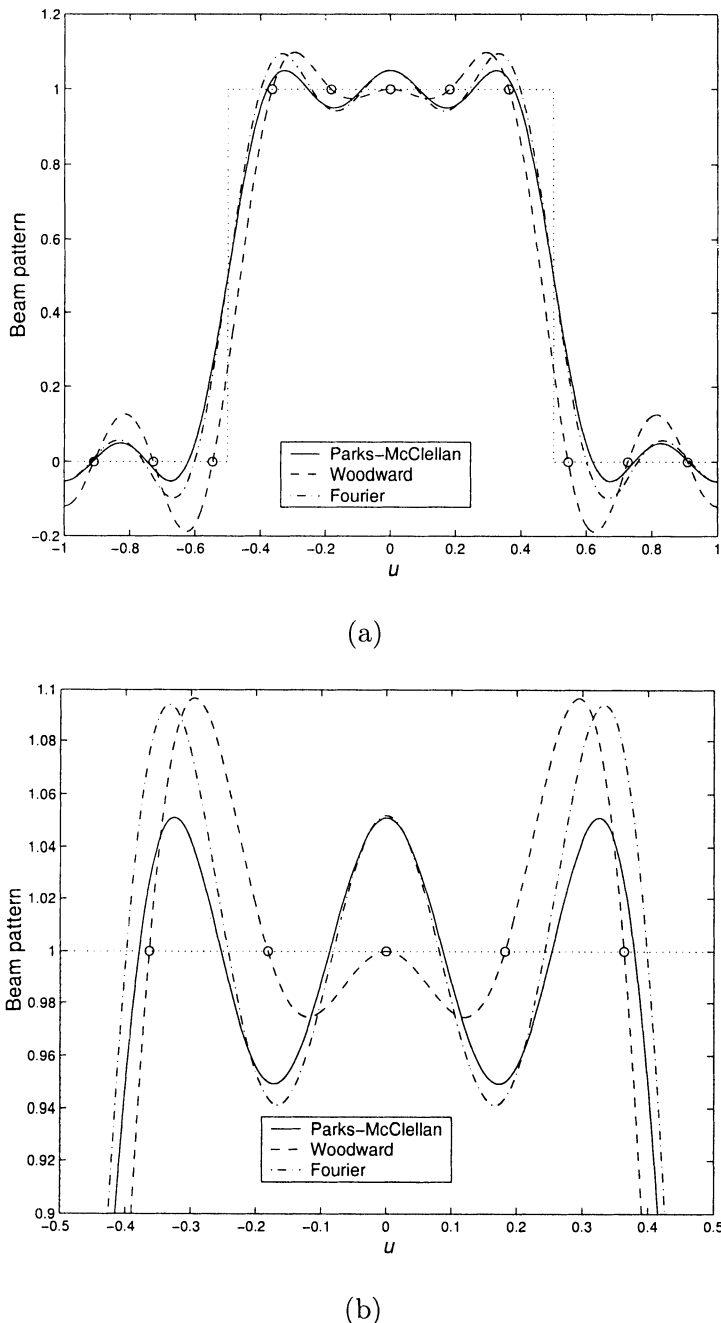


Figure 3.38 Comparison of various beam pattern synthesis techniques.

the synthesis problem in Sections 3.7 and 3.9.3. In Section 3.7, we generalize the least squares error solution to include linear constraints. In Section 3.9.3, we solve the minimax problem for arbitrary arrays.

In the course of the discussion we introduced various tools, such as the array polynomial and its zeros, the DFT, and the IDFT. All of these tools are used in many subsequent discussions.

All of the discussion up to this point did not assume any detailed knowledge of the interference environment. Using a beam pattern with constant sidelobe levels tacitly assumes that the interference is equally likely to arrive anywhere in the sidelobe region. In the next section we consider a model in which we have some knowledge of the location of the interference.

3.7 Null Steering

In our discussion of array design, we have seen the importance of pattern nulls. In many applications, we want to guarantee that the pattern will have a null in a given direction. In radar or communications applications, a jamming signal may be located at a specific wavenumber and we want to eliminate its effect.

3.7.1 Null Constraints

For an arbitrary array, to put a null at a given wavenumber \mathbf{k}_J , we require

$$B(\mathbf{k}_J) = \mathbf{w}^H \mathbf{v}_k(\mathbf{k}_J) = 0, \quad (3.242)$$

where

$$\mathbf{v}_k(\mathbf{k}_J) = \begin{bmatrix} e^{-j\mathbf{k}_J^T \mathbf{p}_1} \\ e^{-j\mathbf{k}_J^T \mathbf{p}_2} \\ \vdots \\ e^{-j\mathbf{k}_J^T \mathbf{p}_N} \end{bmatrix}. \quad (3.243)$$

For a uniformly spaced linear array with N odd, this reduces to

$$0 = \sum_{n=-\frac{N-1}{2}}^{\frac{N-1}{2}} w_n^* e^{jn\psi_J}. \quad (3.244)$$

Symmetric indexing is more convenient for this problem. We denote these weights as $w_n, n = -\frac{N-1}{2}, \dots, \frac{N-1}{2}$.

We can then choose the w_i to synthesize a desired pattern subject to the constraint in (3.244). We now consider several ways to implement null constraints.

3.7.2 Least Squares Error Pattern Synthesis with Nulls

In this section we consider the problem of finding the best least squares error approximation to a desired pattern subject to a set of null constraints.²⁵ We develop the solution for an arbitrary array geometry and then consider some examples of linear arrays.

We assume that there is some desired beam pattern that can be synthesized by a discrete array.

$$B_d(\mathbf{k}) = \mathbf{w}_d^H \mathbf{v}_k(\mathbf{k}). \quad (3.245)$$

We approximate it by a second pattern that has a set of constraints imposed on it. This pattern is denoted by

$$B(\mathbf{k}) = \mathbf{w}^H \mathbf{v}_k(\mathbf{k}). \quad (3.246)$$

We minimize the squared error between the desired pattern $B_d(\mathbf{k})$ and the constrained pattern,

$$\varepsilon = \iint |B_d(\mathbf{k}) - B(\mathbf{k})|^2 d\mathbf{k}. \quad (3.247)$$

Substituting (3.245) and (3.246) into (3.247) and performing the integration gives,

$$\varepsilon = \| \mathbf{w}_d - \mathbf{w} \|^2. \quad (3.248)$$

The restriction that $B_d(\mathbf{k})$ be synthesizable by a discrete array is for convenience. If the actual desired pattern is not synthesizable in this form, we let $B_d(\mathbf{k})$ be the least squares error approximation to it. For a linear equally spaced array, $B_d(\mathbf{k})$ would be obtained by the Fourier series approach of Section 3.4.

We consider constraints on the beam pattern and its derivatives at various values of \mathbf{k} . Normally we would include a constraint on the array response along the MRA. If the array is pointed at \mathbf{k}_T , then the constraint

$$\mathbf{w}^H \mathbf{v}_k(\mathbf{k}_T) = 1 \quad (3.249)$$

is referred to as a distortionless constraint. Any plane-wave signal arriving along \mathbf{k}_T will pass through the array processing undistorted. We use this

²⁵This general formulation appeared in the adaptive array context in Applebaum [AC76]. The specific approach used here was done by Steyskal [Ste82] for linear arrays. The generalization to arbitrary arrays is straightforward. This problem is a special case of the problem of finding a weighted least squares error approximation to a desired beam pattern subject to a set of constraints (not necessarily zero). A solution to this problem is given in Mucci et al. [MTL76].

constraint extensively starting in Chapter 6. In this section, we focus on null constraints. If we only consider null constraints in the sidelobe region, we can omit (3.249) and get a slightly simpler derivation.

The first type of constraint is a null constraint. From (3.246)

$$\mathbf{w}^H \mathbf{v}_k(k_i) = 0, \quad i = 1, 2, \dots, M_0. \quad (3.250)$$

We refer to this as a zero-order constraint (or zero-order null) and define an $N \times M_0$ constraint matrix, \mathbf{C}_0

$$\mathbf{C}_0 = [\mathbf{v}_k(k_1) \mid \mathbf{v}_k(k_2) \mid \dots \mid \mathbf{v}_k(k_{M_0})]. \quad (3.251)$$

The second type of constraint is the first derivative of the beam pattern with respect to \mathbf{k} . For a linear array, this corresponds to

$$\frac{d}{dk} B(k) \Big|_{k=k_i} = \mathbf{w}^H \left[\frac{d}{dk} \mathbf{v}_k(k) \right]_{k=k_i} \triangleq \mathbf{w}^H \mathbf{d}_1(k) \Big|_{k=k_i}, \quad i \in \Omega_1, \quad (3.252)$$

where Ω_1 is a subset of the M_0 locations where we want the derivative to equal zero and contains M_1 points.²⁶

We assume that some of the nulls have derivatives set to zero while others do not. Thus, for a linear array, we define an $N \times M_1$ constraint matrix, \mathbf{C}_1 :

$$\mathbf{C}_1 = [\mathbf{d}_1(k_1) \mid \mathbf{d}_1(k_2) \mid \dots \mid \mathbf{d}_1(k_{M_1})]. \quad (3.253)$$

If we have a 2-D array, there will be a derivative with respect to two components of the wavenumber so \mathbf{C}_1 will be $2M_1$ -dimensional.

The n th type of constraint is the n th derivative of the beam pattern with respect to \mathbf{k} . For a linear array, this corresponds to

$$\frac{d^n}{dk^n} B(k) \Big|_{k=k_i} = \mathbf{w}^H \left[\frac{d^n}{dk^n} \mathbf{v}_k(k) \right]_{k=k_i} \triangleq \mathbf{w}^H \mathbf{d}_n(k) \Big|_{k=k_i}, \quad i \in \Omega_n \quad (3.254)$$

where the set Ω_n is a subset of Ω_{n-1} and contains M_n points. For $n = 2$,

$$\mathbf{C}_2 = [\mathbf{d}_2(k_1) \mid \mathbf{d}_2(k_2) \mid \dots \mid \mathbf{d}_2(k_{M_2})]. \quad (3.255)$$

For a 2-D array, \mathbf{C}_2 will be $3M_2$ -dimensional. In practice, constraints beyond \mathbf{C}_2 are seldom used.

²⁶A derivative with respect to a scalar wavenumber \mathbf{k} is indicated. In many cases, a derivative with respect to ψ or u will be used.

Then, the total \mathbf{C} matrix is an $N \times M_c$ matrix,

$$\mathbf{C} = \left[\begin{array}{c|c|c} \mathbf{C}_0 & \mathbf{C}_1 & \mathbf{C}_2 \end{array} \right], \quad (3.256)$$

where M_c is the total number of constraints and $M_c < N$. We assume that the columns of \mathbf{C} are linearly independent. The solution to the optimization problem requires the inversion of $\mathbf{C}^H \mathbf{C}$. If the columns of \mathbf{C} are linearly independent, then $\mathbf{C}^H \mathbf{C}$ will not be singular. If the M_n are not selected carefully, there is no guarantee that the columns will be independent. In some cases, the columns may be independent, but several columns may be highly correlated, which will cause $\mathbf{C}^H \mathbf{C}$ to have a poor condition number. One approach to alleviate this problem is to use a singular value decomposition on the right-hand side of (3.256) and retain only the dominant singular value terms to form \mathbf{C} . This guarantees that $\mathbf{C}^H \mathbf{C}$ is not singular.²⁷

Before solving the optimization problem, we develop the explicit form of the constraint matrices for a standard linear array with N elements (N odd).

The array manifold vector is

$$\mathbf{v}_u(u) = \mathbf{v}_k(k)|_{k=\pi u} = \begin{bmatrix} e^{-j(\frac{N-1}{2})\pi u} \\ \vdots \\ e^{j(\frac{N-1}{2})\pi u} \end{bmatrix}. \quad (3.257)$$

Thus,

$$B_u(u) = \sum_{n=-\frac{N-1}{2}}^{\frac{N-1}{2}} w_n^* e^{jn\pi u} = \mathbf{w}^H \mathbf{v}_u(u), \quad (3.258)$$

and

$$\begin{aligned} \frac{d^n}{du^n} B_u(u) &= \sum_{m=-\frac{N-1}{2}}^{\frac{N-1}{2}} w_m^* (jm\pi)^n e^{jm\pi u} \\ &= \mathbf{w}^H \mathbf{d}_n(u), \end{aligned} \quad (3.259)$$

where $\mathbf{d}_n(u)$ is a $N \times 1$ matrix whose m th element is

$$[\mathbf{d}_n(u)]_m = (jm\pi)^n e^{jm\pi u}. \quad (3.260)$$

Note that $\mathbf{v}_u(u)$ and the even-numbered derivatives are conjugate symmetric and the odd-numbered derivatives are conjugate asymmetric.

We now solve the optimization problem.

²⁷N. Owsley (private communication).

Optimization

We want to optimize the squared weighting error subject to the constraint that

$$\mathbf{w}^H \mathbf{C} = \mathbf{0}, \quad (3.261)$$

where \mathbf{C} is the constraint matrix in (3.256). We require the columns of \mathbf{C} to be linearly independent. Using Lagrange multipliers we want to minimize G , where²⁸

$$G = [\mathbf{w}_d^H - \mathbf{w}^H] [\mathbf{w}_d - \mathbf{w}] + \mathbf{w}^H \mathbf{C} \boldsymbol{\lambda} + \boldsymbol{\lambda}^H \mathbf{C}^H \mathbf{w}, \quad (3.262)$$

where $\boldsymbol{\lambda}$ is a $M \times 1$ Lagrange multiplier vector. Taking the gradient with respect to \mathbf{w} gives

$$-\mathbf{w}_d^H + \mathbf{w}_o^H + \boldsymbol{\lambda}^H \mathbf{C}^H = \mathbf{0}, \quad (3.263)$$

or

$$\mathbf{w}_o^H = \mathbf{w}_d^H - \boldsymbol{\lambda}^H \mathbf{C}^H. \quad (3.264)$$

We solve for the Lagrange multiplier vector by using the constraint,

$$\mathbf{w}_o^H \mathbf{C} = \mathbf{0}. \quad (3.265)$$

Thus,

$$\mathbf{w}_d^H \mathbf{C} - \boldsymbol{\lambda}^H \mathbf{C}^H \mathbf{C} = \mathbf{0}. \quad (3.266)$$

The matrix $\mathbf{C}^H \mathbf{C}$ is not singular due to the assumption of linearly independent columns. Then, we can write

$$\boldsymbol{\lambda}^H = \mathbf{w}_d^H \mathbf{C} [\mathbf{C}^H \mathbf{C}]^{-1}. \quad (3.267)$$

Although the inverse of $[\mathbf{C}^H \mathbf{C}]$ exists, the condition number of the matrix may be poor if the columns of \mathbf{C} approach dependency (e.g., null directions too close to each other).

The optimum weighting is

$$\mathbf{w}_o^H = \mathbf{w}_d^H \left(\mathbf{I}_N - \mathbf{C} [\mathbf{C}^H \mathbf{C}]^{-1} \mathbf{C}^H \right). \quad (3.268)$$

The matrix

$$\mathbf{P}_C = \mathbf{C} [\mathbf{C}^H \mathbf{C}]^{-1} \mathbf{C}^H \quad (3.269)$$

²⁸See Appendix A (Section A.7.4) for a discussion of complex gradients.

is the projection matrix onto the constraint subspace. Thus \mathbf{w}_o^H is the component of \mathbf{w}_d^H in the subspace orthogonal to the constraint subspace. Thus (3.268) can be written as

$$\mathbf{w}_o^H = \mathbf{w}_d^H \mathbf{P}_{\mathbf{C}}^\perp, \quad (3.270)$$

and

$$\mathbf{w}_e^H = \mathbf{w}_d^H - \mathbf{w}_o^H = \mathbf{w}_d^H \mathbf{P}_{\mathbf{C}}. \quad (3.271)$$

The orthogonal behavior of \mathbf{w}_e^H is familiar from other optimization problems.

A second interpretation of (3.270) is also of interest. We can write (3.268) as

$$\begin{aligned} \mathbf{w}_o^H &= \mathbf{w}_d^H - \left(\mathbf{w}_d^H \mathbf{C} [\mathbf{C}^H \mathbf{C}]^{-1} \right) \mathbf{C}^H \\ &= \mathbf{w}_d^H - \mathbf{a} \mathbf{C}^H, \end{aligned} \quad (3.272)$$

where \mathbf{a} is a $1 \times M$ weighting vector. Thus, the optimum weight vector consists of the desired weight vector minus a weighted sum of the constraint vectors. The resulting beam pattern is

$$\begin{aligned} B_o(u) &= [\mathbf{w}_d^H - \mathbf{a} \mathbf{C}^H] \mathbf{v}(u) \\ &= B_d(u) - \mathbf{a} \mathbf{C}^H \mathbf{v}(u). \end{aligned} \quad (3.273)$$

For the zero-order constraints (i.e., null-only), the second term in (3.273) is a sum of conventional beam patterns steered at the wavenumber of the interferer. Thus,

$$B_o(u) = B_d(u) - \sum_{m=1}^{M_0} a_m B_c(u - u_m). \quad (3.274)$$

Note that, since $B_o(u_k) = 0$ and $B_c(u - u_k) = 1$,

$$B_d(u_k) = \sum_{m=1}^{M_0} a_m B_c(u_k - u_m), \quad k = 1, \dots, M_0. \quad (3.275)$$

For the linear array,

$$B_c(u - u_m) = \frac{\sin \left[N\pi \frac{(u - u_m)}{2} \right]}{\sin \left[\pi \frac{(u - u_m)}{2} \right]}. \quad (3.276)$$

Similarly, for an n th-order derivative constraint, the cancellation beam patterns are derivatives of the conventional beam pattern,

$$B_c^{(n)}(u - u_m) = \frac{d^n}{du^n} \frac{\sin \left[N\pi \frac{(u-u_m)}{2} \right]}{\sin \left[\pi \frac{(u-u_m)}{2} \right]}. \quad (3.277)$$

Thus the beam pattern of the optimum processor is just the desired beam pattern $B_d(u)$ minus a weighted sum of conventional beam patterns and derivatives of conventional beam patterns centered at the null locations.

We observe that the same result holds for arbitrary arrays. For example, for zero-order nulls, from (3.251),

$$\mathbf{C}_0 = \left[\mathbf{v}_k(\mathbf{k}_1) \mid \mathbf{v}_k(\mathbf{k}_2) \mid \cdots \mid \mathbf{v}_k(\mathbf{k}_{M_0}) \right]. \quad (3.278)$$

and (3.246) and (3.272) becomes

$$\begin{aligned} B_o(\mathbf{k}) &= \mathbf{w}_o^H \mathbf{v}_k(\mathbf{k}) \\ &= B_d(\mathbf{k}) - \mathbf{a} \mathbf{C}_0^H \mathbf{v}_k(\mathbf{k}) \\ &= B_d(\mathbf{k}) - \sum_{m=1}^{M_0} a_m B_c(\mathbf{k} - \mathbf{k}_m), \end{aligned} \quad (3.279)$$

where a_m is the m^{th} element of the $1 \times M_0$ matrix,

$$\mathbf{a} = \mathbf{w}_d^H \mathbf{C}_0 \left[\mathbf{C}_0^H \mathbf{C}_0 \right]^{-1}. \quad (3.280)$$

Note that the discussion in (3.270)–(3.280) is useful in interpreting the result. We use (3.268) to find \mathbf{w}_o^H .

The resulting pattern error is

$$\varepsilon_0 = \mathbf{w}_e^H \mathbf{w}_e, \quad (3.281)$$

where \mathbf{w}_e was defined in (3.271). Using (3.271) in (3.281) and recalling that $P_c P_c = P_c$, we obtain

$$\varepsilon_0 = \mathbf{w}_d^H \mathbf{C} \left[\mathbf{C}^H \mathbf{C} \right]^{-1} \mathbf{C}^H \mathbf{w}_d = \mathbf{w}_d^H \mathbf{P}_c \mathbf{w}_d. \quad (3.282)$$

We now consider several examples to illustrate the application of these results.

Example 3.7.1²⁹

We consider a 21-element linear array spaced at $\lambda/2$. The desired pattern corresponds to uniform weighting ($w_n = 1/N$). We put a zero-order, first-order, and second-order null

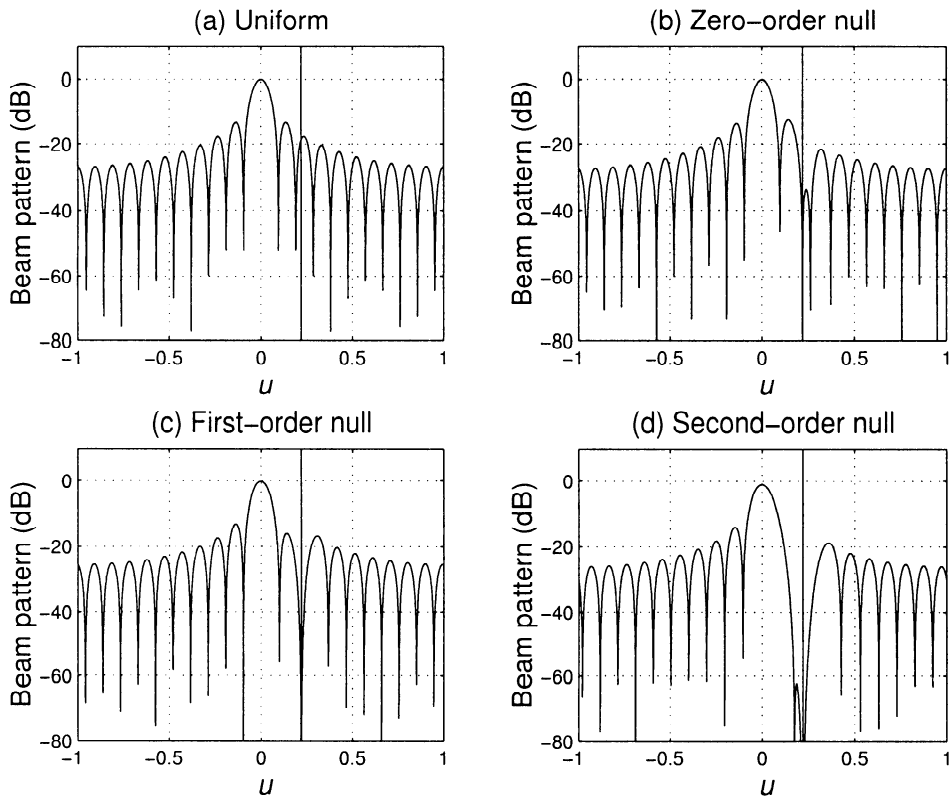


Figure 3.39 (a) Initial sinc-pattern; (b) pattern with a null of zero order imposed at $u = 0.22$; (c) with null of first order; (d) with null of second order.

at $u = 0.22$. The only important aspect of this location is that it is outside the main lobe. The results are shown in Figure 3.39.

Example 3.7.2 (continuation)

We consider the same array as in the preceding example. We now place three zero-order nulls at $u_1 = 0.21$, $u_2 = 0.22$, and $u_3 = 0.23$. Note that the nulls in the conventional pattern are spaced at $2/21 = 0.095$ so that the constraint vectors are not orthogonal.

The resulting pattern is shown in Figure 3.40. We have reduced the highest sidelobe in the sector $0.18 \leq u \leq 0.26$ to -63 dB.

Example 3.7.3

In this example, we consider a 41-element linear array spaced at $\lambda/2$. In these first two cases, the desired pattern is a Chebychev pattern with -40 -dB sidelobes.

²⁹This sequence of examples (3.7.1–3.7.3) is due to Steyskal [Ste82].

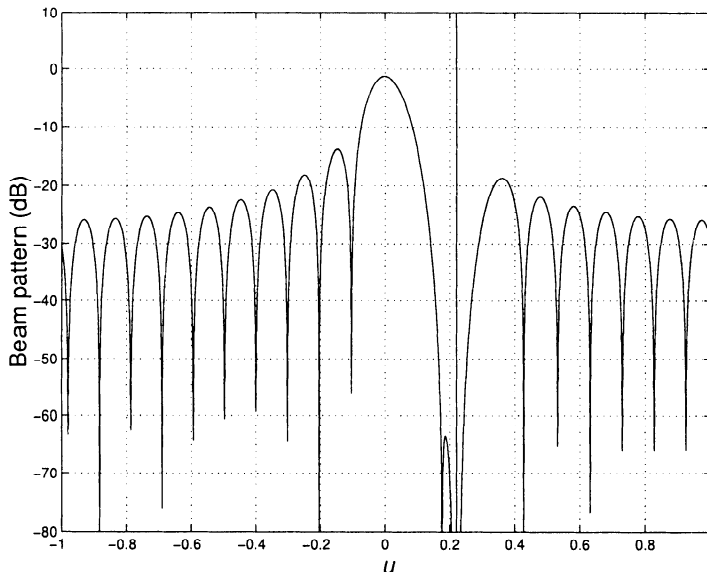


Figure 3.40 Sinc-pattern with three nulls equispaced over the sector $(0.18, 0.26)$.

In case 1, we place four zero-order nulls at $0.22, 0.24, 0.26$, and 0.28 . The resulting pattern is shown in Figure 3.41.

In case 2, we place eight zero-order nulls spaced at $\Delta u = 0.02$ in the sector $(0.22, 0.36)$. The result is shown in Figure 3.42.

We revisit the problem of constrained optimization several times in the text. In Chapter 6, we derive similar results for different constraints. In Chapter 7, we study adaptive arrays to achieve constrained optimization.

3.8 Asymmetric Beams

In many array applications, we want to measure the direction of arrival of an incoming plane wave. One method for doing this is to utilize an asymmetric beam that has a slope at the steering angle that can be used in a closed loop system to point the steering angle in the direction of the plane wave. This technique is the basis of many monopulse radars (e.g., [Sko80]). The beam pattern design problem consists of finding the maximum (or acceptable) slope of the beam pattern at the origin subject to a suitable constraint on

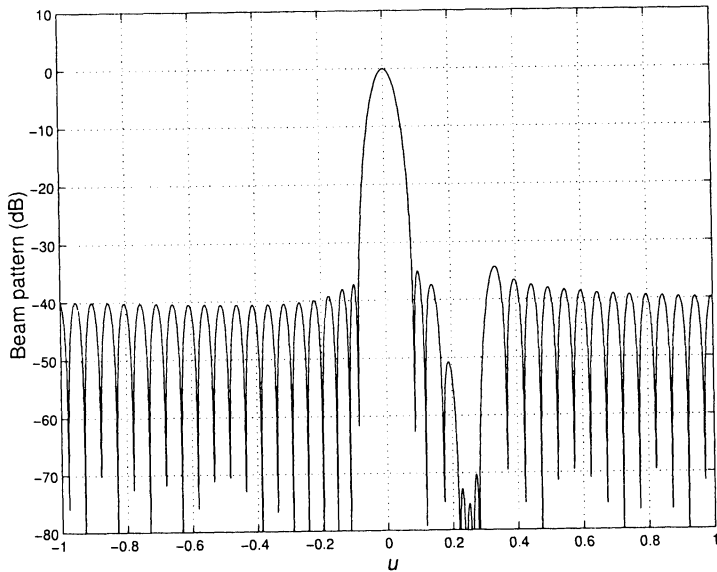


Figure 3.41 Initial 40-dB Chebychev pattern with four nulls equispaced over the sector $(0.22, 0.28)$.

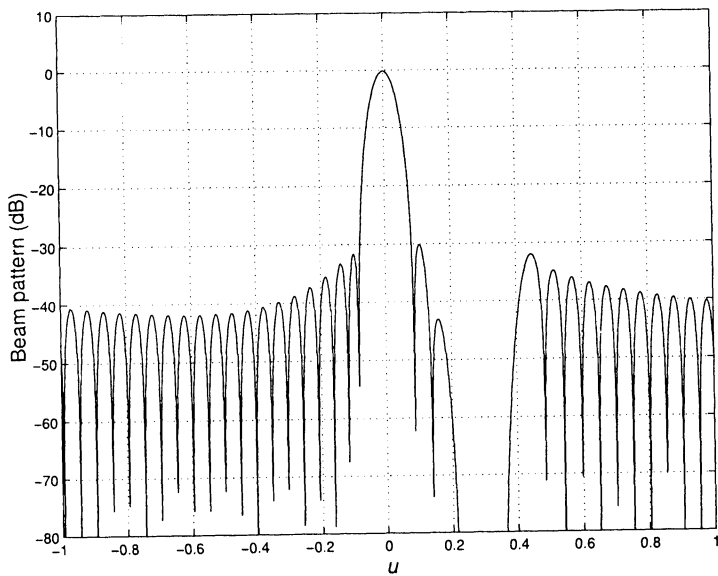


Figure 3.42 Initial 40-dB Chebychev pattern with eight nulls equispaced over the sector $(0.22, 0.36)$.

the sidelobes. We define an asymmetric³⁰ array weighting as one in which

$$w(-n) = \begin{cases} -w(n), & n = -\frac{N-1}{2}, \dots, -1, 1, \dots, \frac{N-1}{2} : N \text{ odd}, \\ 0, & n = 0 : N \text{ odd}, \end{cases} \quad (3.283)$$

and

$$w(-n) = -w(n), \quad n = -\frac{N}{2}, \dots, -1, 1, \dots, \frac{N}{2} : N \text{ even}, \quad (3.284)$$

where we have used a symmetric indexing and assume that the weights are real.

In this section, we look at several examples of difference beams. The beam pattern is

$$B_a(\psi) = \sum_{n=-\frac{N}{2}}^{\frac{N}{2}-1} w_n e^{j(n+\frac{1}{2})\psi}, \quad (3.285)$$

for N even. Using (3.284) in (3.285) gives

$$\begin{aligned} B_a(\psi) &= \sum_{m=1}^{\frac{N}{2}} w_m e^{j(m-\frac{1}{2})\psi} + \sum_{m=1}^{\frac{N}{2}} (-w_m) e^{-j(m-\frac{1}{2})\psi} \\ &= 2j \sum_{m=1}^{\frac{N}{2}} w_m \sin(m - \frac{1}{2})\psi. \end{aligned} \quad (3.286)$$

The simplest case is uniform asymmetric weighting

$$w_n = \frac{1}{N}, \quad n \geq 1. \quad (3.287)$$

Then (3.286) becomes

$$B_a(\psi) = \frac{e^{-j\frac{\psi}{2}}}{N} \sum_{m=1}^{\frac{N}{2}} e^{jm\psi} - \frac{e^{j\frac{\psi}{2}}}{N} \sum_{m=1}^{\frac{N}{2}} e^{-jm\psi}. \quad (3.288)$$

The beam pattern in (3.288) is the difference between two shifted conventional beams so we refer to it as a difference beam. The corresponding beam with a plus sign is referred to a sum beam. For uniform weighting, the sum

³⁰The dictionary definition of asymmetric is “non-symmetric.” Our definition is in (3.283) and (3.284).

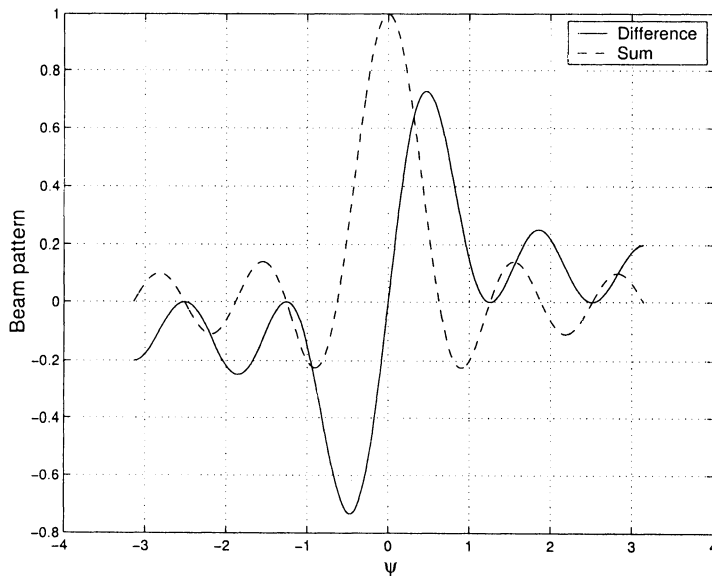


Figure 3.43 Beam pattern versus ψ : Difference beam with uniform weighting, $N = 10$.

beam is the familiar conventional beam pattern. The expression in (3.288) can be written as

$$B_a(\psi) = \frac{2j}{N} \frac{\sin^2\left(\frac{N}{4}\psi\right)}{\sin\left(\frac{\psi}{2}\right)}, \quad (3.289)$$

for N even. Proceeding in a similar manner, we obtain

$$B_a(\psi) = \frac{2j}{N} \frac{\sin\left(\frac{N+1}{4}\psi\right) \sin\left(\frac{N-1}{4}\psi\right)}{\sin\left(\frac{\psi}{2}\right)}, \quad (3.290)$$

for N odd.

The beam pattern of the difference beam is a purely imaginary function. We write

$$B_a(\psi) = j B_{aI}(\psi), \quad (3.291)$$

and plot $B_{aI}(\psi)$ in Figure 3.43 for a standard linear array with $N = 10$. The corresponding sum beam pattern is also plotted.

Several observations are useful:

- (a) The sum and difference beams are orthogonal (this follows from the Fourier transform relationship).

- (b) The difference beam is a weighted sum of two shifted conventional beams (see (3.288)).
- (c) The first zero of the difference beam is at

$$\psi = \begin{cases} \frac{4\pi}{N+1}, & N \text{ odd}, \\ \frac{4\pi}{N}, & N \text{ even}. \end{cases} \quad (3.292)$$

- (d) The first sidelobe of the difference beam is 10 dB below the main lobe.
- (e) The slope at the origin is

$$\left. \frac{dB_{aI}(\psi)}{d\psi} \right|_{\psi=0} = \frac{N}{4}. \quad (3.293)$$

The usage of difference beams for angle estimation (and tracking) is common. They are implemented in monopulse radars and phased array radars (e.g., [Sko80], [Sko90], [Bro88], [Bar89]).

Many useful difference beam patterns can be constructed as linear combinations of shifted conventional beam patterns. We can also use linear combinations of shifted beams designed using the techniques developed in sections 3.1 and 3.5.

In the sum beam case we discussed design procedures due to Dolph and Taylor that allowed us to control the sidelobe behavior while maintaining the beamwidth of the main lobe. Zolotarev, a student of Chebychev, developed a class of odd polynomials that give an equal-ripple approximation over a given interval.³¹ McNamara [McN93] used these polynomials to produce difference patterns with constant sidelobes. A discrete \bar{n} difference pattern analogous to the discrete \bar{n} Villenueve sum pattern was also developed by McNamara [McN94]. The Taylor distribution for sum beams was developed for a continuous aperture. Analogous procedures have been developed for difference beams by Bayliss [Bay68], in which he controls the sidelobe height. Discussions of his technique are available in Elliott [Ell81] and Mailloux [Mai94]. The reader is referred to these references.

Other properties of difference beams and their applications are discussed in the problems and at various points in the text.

³¹This discussion follows Hansen [Han98].

3.9 Spatially Non-uniform Linear Arrays

3.9.1 Introduction

The discussion of arrays up to this point has focused on linear arrays with uniform spacing. In many applications, the arrays are linear but have non-uniform spacing.

One application in which we encounter non-uniform arrays is the thinned or sparse array problem. In this case, we start with an N -element uniform linear array or linear aperture of length L that has a desired weighting and associated beam pattern. We then construct a linear array with fewer elements that retains the desirable features of the beam pattern. In some cases, we allow the elements to be in any location on the line. In other cases, we restrict their positions to a uniform grid. The motivation is to reduce the cost and complexity of the array by having fewer sensors. There are a large number of references in this area (e.g., [LL59], [KPT60], [San60], [Unz60], [Maf62], [Ish62], [Wil62], [Sko69], [IC65], [Har61], [Lo63], and [Ste76]).

A second application is the case in which the array locations are random along a segment of the axis (or, more generally, in an area in a plane or a volume in three dimensions). In this case, there are two categories. In the first category, the nominal locations are deterministic but the actual locations vary in a random manner. This is a generalization of our discussion of sensitivity and tolerance factors in Section 2.3.3. An example of this model is the dropping of sonobouys in the ocean to locate submarines. It also includes such problems as random removal or failure of elements. There is a large amount of literature in this area (e.g., [All61], [MC63], [Ruz52] and [GM55]).

In the second category there are arrays in which the elements are placed at random over some segment of the axis according to some probability density as part of the design procedure. This is known as statistical density tapering. There is a large amount of literature in this area (e.g., [Lo64a], [Lo64b], [Lo68], [PL69], [AL69], [Ste72] and [Ste76]).

There are a number of other references that discuss various issues concerning non-uniform arrays. We will limit our discussion to two topics that we will use later in the text.

In Section 3.9.2, we discuss a class of non-uniform linear arrays called minimum redundancy arrays. The reason for the name will be clear when we discuss these arrays.

In Section 3.9.3, we assume that the element locations are given and derive an algorithm for designing a desired beam pattern. In essence, this

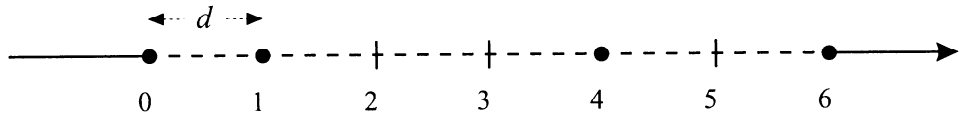


Figure 3.44 “Ideal” MRLA.

algorithm generalizes the minimax algorithms of Section 3.6 to the arbitrary array case.

3.9.2 Minimum Redundancy Arrays

In this section, we consider a class of non-uniformly spaced linear arrays referred to as minimum redundancy linear arrays (MRLA). We restrict our attention to the case in which the arrays are constructed on an underlying grid structure with grid spacing d .

MRLAs are designed so that the number of sensor pairs that have the same spatial correlation lag is made as small as possible. An example of an “ideal” MRLA is shown in Figure 3.44. This is a 4-element array whose aperture length is equivalent to a 7-element standard linear array.

We see that this configuration allows us to estimate

$$E[x(t, id)x^*(t, jd)] \triangleq R_x((i - j)d) \quad (3.294)$$

for at least one $(i - j)$ combination from 0 to 6. For example,

SENSOR LOCATIONS	LAG
0-1	d
4-6	$2d$
1-4	$3d$
0-4	$4d$
1-6	$5d$
0-6	$6d$

For the moment, we will assume that our estimate of $R_x((i - j)d)$ is correct.³² If we denote the sensor outputs of the 7-element standard linear array by the 7×1 vector $\mathbf{x}(t)$, then the correlation matrix is a 7×7 matrix,

$$\mathbf{R}_x = E[\mathbf{x}(t)\mathbf{x}^H(t)], \quad (3.295)$$

³²Our discussion at this point is heuristic because we have not developed the appropriate statistical model. We revisit the issue in Chapter 5.

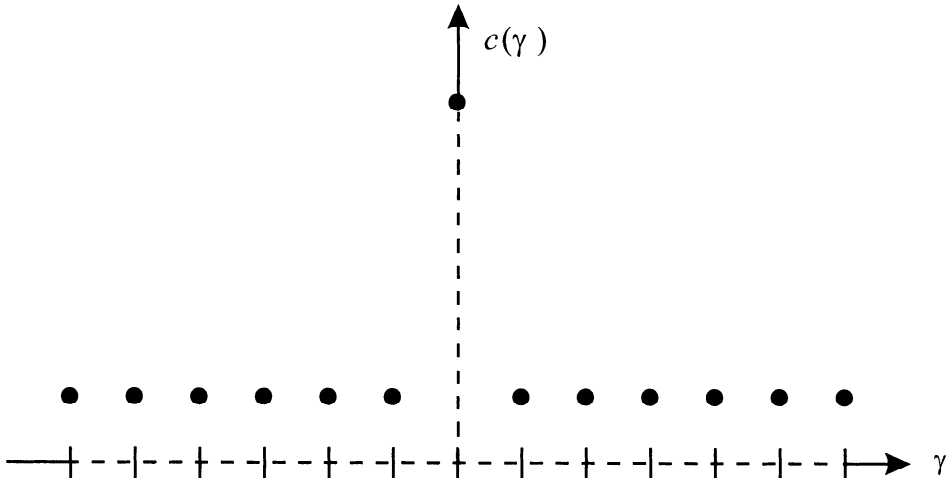


Figure 3.45 Co-array for the array in Figure 3.44.

whose elements are all of the form

$$R_x((i-j)d), \quad i = 0, \dots, 6; j = 0, \dots, 6. \quad (3.296)$$

Thus, the 4-element array allows us to measure all of the elements in the correlation matrix of a 7-element standard array. We find that many of our optimum processing algorithms are based on \mathbf{R}_x . Thus, there is a possibility that the 4-element MRLA might have similar performance to a 7-element standard linear array.

We explore the statistical significance of this conjecture in Chapters 5 and 7. In our present discussion, we consider the beam pattern behavior.

We denote the aperture length as N_a and it is measured in terms of number of grid intervals. For example, in Figure 3.44, $N_a = 6$ and $N = 4$.

In order to compute the number of times each spatial correlation lag is contained in an array, we assume the elements are uniformly weighted and compute the correlation of \mathbf{w} with itself.

$$c(\gamma) \triangleq \sum_{|m-n|=\gamma} w_m w_n^*. \quad (3.297)$$

The resulting function is called the **co-array** (e.g., [Hau68], [Kre71], or [Bag76]) and is a symmetric function. The co-array for the array in Figure 3.44 is shown in Figure 3.45.

In Chapter 5, we argue that, from the standpoint of efficient spatial sampling, we would like the co-array to equal one except at the origin. If we

could find an array with this property then

$$N_a = \frac{N(N - 1)}{2}. \quad (3.298)$$

This is the number of different off-diagonal elements in the $N \times N$ correlation matrix \mathbf{R}_x . Unfortunately, such arrays (sometimes called perfect arrays) do not exist for $N > 4$. For larger arrays, we consider two options. In the first option, we construct the array so that $c(\gamma)$ is either zero or one except at the origin. These are called non-redundant arrays and a representative set is shown in Table 3.7.³³

Table 3.7 Non-redundant Arrays

N	Sensor Separation	D
2	.1.	1
3	.1 · 2.	1
4	.1 · 3 · 2.	1
5	.1 · 3 · 5 · 2.	1.10
6	.1 · 3 · 6 · 2 · 5.	1.13
7	.1 · 3 · 6 · 8 · 5 · 2.	1.19
8	.1 · 3 · 5 · 6 · 7 · 10 · 2.	1.21
9	.1 · 4 · 7 · 13 · 2 · 8 · 6 · 3.	1.22
10	.1 · 5 · 4 · 13 · 3 · 8 · 7 · 12 · 2.	1.22

The corresponding co-arrays for $N > 4$ have “gaps” or “holes” in their values. The number D is the ratio of the aperture length N_a to aperture length of a hypothetical perfect array ($N(N - 1)/2$). We look at the significance of these “gaps” later.

In this second option, we construct arrays that have no gaps and have the largest possible aperture. These are referred to as minimum redundancy arrays. We choose the sensor positions to make N_a as large as possible without having any gaps. We can write N_a as

$$N_a = \frac{N(N - 1)}{2} - N_R + N_H, \quad (3.299)$$

where N_R is the number of redundancies and N_H is the number of holes. We require $N_H = 0$ in a minimum redundant array.

There has been a significant amount of research on element spacing to achieve as low a redundancy as possible. For $N \leq 17$, minimum redun-

³³From [JD93].

dancy arrays have been found through exhaustive search routines. These configurations are shown in Table 3.8.³⁴

Table 3.8 Minimum Redundancy Linear Arrays

N	N_R	N_a	$\frac{N^2}{N_a}$	$\frac{N(N-1)}{2N_a}$	Array(s)
3	0	3	3.0	1.0	12
4	0	6	2.67	1.0	132
5	1	9	2.78	1.11	1332 & 3411
6	2	13	2.77	1.15	13162 & 15322 & 11443
7	4	17	2.88	1.24	136232 & 114443 & 111554 116423 & 173222
8	5	23	2.78	1.22	1366232 & 1194332
9	7	29	2.79	1.24	136 ³ 232 & 12377441 & 11(12)43332
10	9	36	2.78	1.25	1237 ³ 441
11	12	43	2.81	1.28	1237 ⁴ 441
12	16	50	2.88	1.32	1237 ⁵ 441 & 111(20)54 ⁴ 33
13	20	58	2.91	1.34	111(24)54 ⁵ 33 & 11671(10) ³ 3423 143499995122
14	23	68	2.88	1.34	11671(10) ⁴ 3423 & 11355(11) ³ 66611
15	26	79	2.85	1.33	11355(11) ⁴ 66611
16	30	90	2.84	1.33	11355(11) ⁵ 66611
17	35	101	2.86	1.35	11355(11) ⁶ 66611

Notation n^m means m repetitions of the spacing n .

Several authors have developed techniques for generating low redundancy arrays. Pearson et al. [PPL90] develop an efficient constructive procedure for near-optimal placement of sensors. Ruf [Ruf93] uses simulated annealing to obtain low redundancy arrays and gives results for $N \leq 30$ ($N_a \leq 287$). Linebarger et al. [LST93] provide algorithms for constructing sparse arrays and develop bounds. Linebarger [Lin92] presents a fast method for computing co-arrays. (See also Abramovich et al. [AGGS98], [ASG99a], [ASG99b].)

We consider two examples to illustrate the behavior of the beam patterns.

Example 3.9.1

Consider the MRLA in Figure 3.44 with $d = \lambda/2$. The beam pattern for uniform weighting is shown in Figure 3.46. The HPBW is 0.666 and the BW_{NOT} is 1.385 in ψ -space. Note that the beam pattern does not have a perfect null so we use BW notch-notch. This compares to 1.429 and 3.1416, respectively, for a standard 4-element array and to 0.801 and 1.795, respectively, for a standard 7-element linear array. Thus, in terms of main-lobe characteristics, the MRLA offers improvement over the standard 4-element array.

³⁴This table was taken from Linebarger et al. [LST93], but the result is due to a sequence of earlier papers.

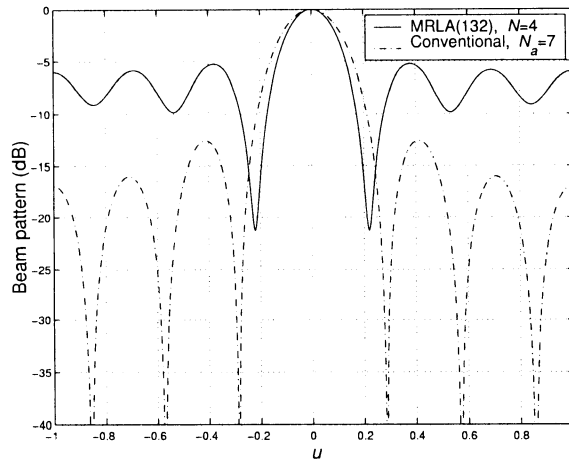


Figure 3.46 Beam pattern for 4-element MRLA with uniform weighting.

The problem with the MRLA is that the sidelobes are significantly higher than the uniform array.

Example 3.9.2 (continuation)

Consider the two 5-element minimum redundancy arrays from Table 3.8. In these cases, $N_a = 9$. The beam patterns are shown in Figure 3.47. For the case 1 (1,3,3,2), the HPBW is 0.464 and the BW_{NOT} is 0.98. For the case 2 (3,4,1,1), the HPBW is 0.473 and the BW_{NOT} is 0.94. This compares to 0.559 and 1.25, respectively, for a standard 10-element linear array.

Just as in the uniform linear case, we can improve the sidelobe behavior by using a non-uniform weighting.

We revisit minimum redundancy arrays at several points in the text and see how their performance compares to standard arrays.

3.9.3 Beam Pattern Design Algorithm

In this section, we derive an algorithm that provides a simple iterative technique for designing desired beam patterns for arbitrary arrays.³⁵ The algorithm is due to Bell et al. [BVG00] and is based on the techniques developed previously by Olen and Compton [OC90] and Zhou and Ingram [ZI98], [ZI99]. Earlier work using this type of algorithm is contained in Sureau and Keeping [SK82] and Dufort [Duf89]. An alternative approach that uses least squares constraints on sidelobe levels is given in Er [Er92]. Tseng and Griffiths [TG92] also developed an alternative approach to designing beam patterns.

³⁵This section is due to Professor Kristine Bell (private communication).

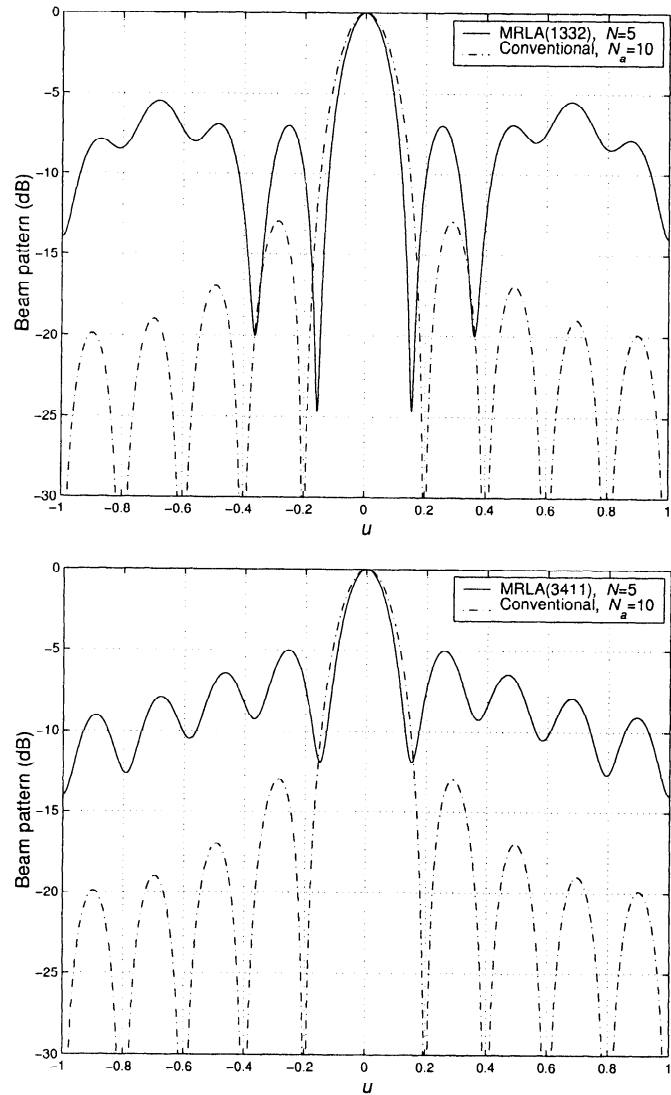


Figure 3.47 Beam pattern for 5-element MRLAs.

The objective is to find weights that maximize the directivity of the array subject to a set of constraints on the beam pattern, which limit the sidelobe levels. We develop the algorithm in the context of linear arrays of isotropic elements, although it applies to arrays of arbitrary geometry, and with non-isotropic elements.

We assume a linear array of isotropic elements on the z -axis with $N \times 1$ array response vector $\mathbf{v}(u)$. When the pattern response at the main response axis or pointing direction is equal to one, the directivity is given by (2.148),

$$\begin{aligned} D &= \left\{ \frac{1}{2} \int_{-1}^1 |B(u)|^2 du \right\}^{-1} \\ &= \left\{ \frac{1}{2} \int_{-1}^1 |\mathbf{w}^H \mathbf{v}(u)|^2 du \right\}^{-1} \\ &= \left\{ \mathbf{w}^H \mathbf{A} \mathbf{w} \right\}^{-1}, \end{aligned} \quad (3.300)$$

where

$$\mathbf{A} = \frac{1}{2} \int_{-1}^1 \mathbf{v}(u) \mathbf{v}^H(u) du. \quad (3.301)$$

The entries in \mathbf{A} are:

$$[\mathbf{A}]_{mn} = \text{sinc}\left(\frac{2\pi}{\lambda} |p_m - p_n|\right), \quad (3.302)$$

where p_n is the position of the n th element.

Let $\mathbf{v}_T = \mathbf{v}(u_T)$ be the array response vector for the steering direction. The basic problem is to maximize the directivity (or equivalently minimize the inverse of the directivity), subject to the unity response constraint at the main response axis, that is,

$$\min \mathbf{w}^H \mathbf{A} \mathbf{w} \quad \text{s.t. } \mathbf{w}^H \mathbf{v}_T = 1. \quad (3.303)$$

The solution is

$$\mathbf{w} = \mathbf{A}^{-1} \mathbf{v}_T \left(\mathbf{v}_T^H \mathbf{A}^{-1} \mathbf{v}_T \right)^{-1}. \quad (3.304)$$

In the special case of a uniform linear array, $\mathbf{A} = \mathbf{I}$, and the maximum directivity weight vector is the uniform weight vector steered to the desired direction, $\mathbf{w} = \frac{1}{N} \mathbf{v}_T$. For both uniformly and non-uniformly spaced arrays, we wish to obtain lower sidelobes by sacrificing some directivity. This can be done by partitioning u -space into r sectors, $\Omega_1, \dots, \Omega_r$ and defining a desired (although not necessarily realizable) beam pattern in each sector,

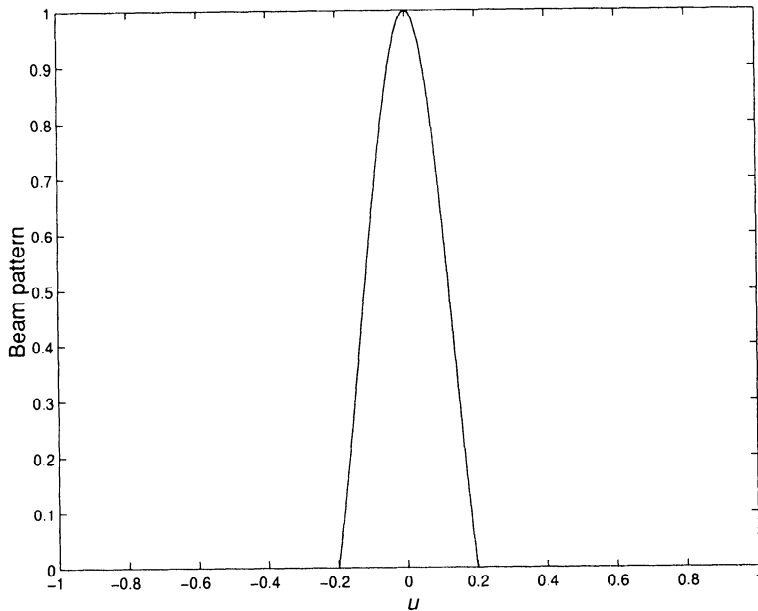


Figure 3.48 Desired three-sector beam pattern.

then limiting deviations between the synthesized and desired beam pattern. A typical desired beam pattern defined in three sectors is shown in Figure 3.48, in which the main beam sector has a beam pattern with some desired main beam shape, and the sidelobe sectors are ideally zero. We assume there is a weight vector $\mathbf{w}_{d,i}$ that generates the desired beam pattern in the i th sector. Let $B_{d,i}(u) = \mathbf{w}_{d,i}^H \mathbf{v}(u)$ be the corresponding beam pattern. The square error between the beam pattern generated by the synthesized weight vector \mathbf{w} and the desired beam pattern over the region Ω_i is given by

$$\begin{aligned}
\epsilon_i^2 &= \int_{\Omega_i} |B(u) - B_{d,i}(u)|^2 du \\
&= \int_{\Omega_i} \left| \mathbf{w}^H \mathbf{v}(u) - \mathbf{w}_{d,i}^H \mathbf{v}(u) \right|^2 du \\
&= (\mathbf{w} - \mathbf{w}_{d,i})^H \mathbf{Q}_i (\mathbf{w} - \mathbf{w}_{d,i}),
\end{aligned} \tag{3.305}$$

where

$$\mathbf{Q}_i = \int_{\Omega_i} \mathbf{v}(u) \mathbf{v}(u)^H du. \tag{3.306}$$

Let Ω_i be the region $(u_i - \Delta_i, u_i + \Delta_i)$. The entries in \mathbf{Q}_i are:

$$[\mathbf{Q}_i]_{mn} = e^{j\frac{2\pi}{\lambda}(p_m - p_n)u_i} 2\Delta_i \operatorname{sinc}\left(\frac{2\pi\Delta_i}{\lambda}|p_m - p_n|\right). \quad (3.307)$$

Now we can maximize directivity subject to constraints on the pattern error as follows:

$$\begin{aligned} \min \quad & \mathbf{w}^H \mathbf{A} \mathbf{w} \quad \text{s.t. } \mathbf{w}^H \mathbf{v}_T = 1 \\ \text{s.t.} \quad & (\mathbf{w} - \mathbf{w}_{d,i})^H \mathbf{Q}_i (\mathbf{w} - \mathbf{w}_{d,i}) \leq L_i \quad i = 1 \dots r. \end{aligned} \quad (3.308)$$

We define

$$\begin{aligned} F = \quad & \mathbf{w}^H \mathbf{A} \mathbf{w} + \lambda_0 (\mathbf{w}^H \mathbf{v}_T - 1) + \lambda_0^* (\mathbf{v}_T^H \mathbf{w} - 1) \\ & + \sum_{i=1}^r \lambda_i (\mathbf{w} - \mathbf{w}_{d,i})^H \mathbf{Q}_i (\mathbf{w} - \mathbf{w}_{d,i}). \end{aligned} \quad (3.309)$$

Differentiating with respect to \mathbf{w}^H and setting the result equal to zero gives

$$\mathbf{A} \mathbf{w} + \lambda_0 \mathbf{v}_T^H + \sum_{i=1}^r \lambda_i [\mathbf{Q}_i (\mathbf{w} - \mathbf{w}_{d,i})] = \mathbf{0}. \quad (3.310)$$

Defining

$$\mathbf{A}_Q = \mathbf{A} + \sum_{i=1}^r \lambda_i \mathbf{Q}_i, \quad (3.311)$$

and

$$\mathbf{w}_Q = \sum_{i=1}^r \lambda_i \mathbf{Q}_i \mathbf{w}_{d,i}, \quad (3.312)$$

we can write (3.310) as

$$\mathbf{w} = -\lambda_0 \mathbf{A}_Q^{-1} \mathbf{v}_T + \mathbf{A}_Q^{-1} \mathbf{w}_Q. \quad (3.313)$$

Solving for λ_0 and substituting the result into 3.313 gives:

$$\begin{aligned} \mathbf{w} = \quad & \mathbf{A}_Q^{-1} \mathbf{v}_T \left(\mathbf{v}_T^H \mathbf{A}_Q^{-1} \mathbf{v}_T \right)^{-1} \\ & + \left[\mathbf{A}_Q^{-1} - \mathbf{A}_Q^{-1} \mathbf{v}_T \left(\mathbf{v}_T^H \mathbf{A}_Q^{-1} \mathbf{v}_T \right)^{-1} \mathbf{v}_T^H \mathbf{A}_Q^{-1} \right] \mathbf{w}_Q. \end{aligned} \quad (3.314)$$

We can obtain tight sidelobe control by defining a set of small sectors in the sidelobe region, as shown in Figure 3.49, and setting the desired beam pattern to zero in these regions. The desired weight vector in each sector

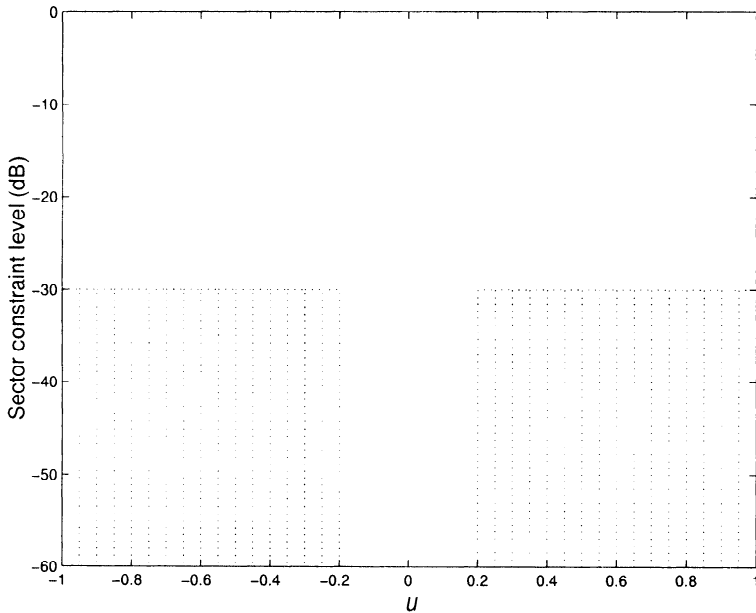


Figure 3.49 Sidelobe sectors.

is just the all-zero vector. In the limit of infinitesimally small sectors, the pattern error constraints become constraints on the magnitude squared of the beam pattern at every point in the sidelobe region. The allowed deviation can be set to the maximum allowable sidelobe level, and the sidelobe levels can be controlled directly. By choosing wider but relatively small sectors, we can still control sidelobe levels fairly accurately. Furthermore, if we choose to constrain pattern “error” only in the sidelobe region and not in the main beam, the desired weight vector in each constrained sector will be zero, and the second term in (3.314) drops out, so the weight vector becomes

$$\mathbf{w} = \mathbf{A}_Q^{-1} \mathbf{v}_T \left(\mathbf{v}_T^H \mathbf{A}_Q^{-1} \mathbf{v}_T \right)^{-1}. \quad (3.315)$$

In this expression, a weighted sum of loading matrices $\mathbf{Q}_i, i = 1 \dots r$ are added to \mathbf{A} . The loading factors balance the maximum directivity pattern with the desired low sidelobe level pattern. There is generally a set of optimum loading levels $\lambda_i, i = 1 \dots r$ that satisfy the constraints; however, there is no closed-form solution for the loading levels, even when $r = 1$. It can be shown that the mean-square pattern error decreases with increasing λ_i , but at the expense of decreased directivity. An iterative procedure can be used to adjust the loading levels to achieve the sidelobe level constraints. At

each iteration, the pattern errors are computed and checked against the constraints. If a constraint is exceeded, the loading for that sector is increased, and the weights are updated.

One way to achieve fast convergence is to let the loading increment at the p th iteration, $\delta_i^{(p)}$, be a fraction of the current loading value, that is, $\delta_i^{(p)} = \alpha \lambda_i^{(p-1)}$. This requires that the initial loading level be non-zero. One possibility is to initialize all of the loading levels to some small value, such as, $\lambda_i^{(0)} = \lambda_0, i = 1 \dots r$. If the initial loading is small enough, the initial weight vector is essentially the maximum directivity weight vector. The update procedure is:

$$\begin{aligned} & \text{if } \mathbf{w}^{(p-1)H} \mathbf{Q}_i \mathbf{w}^{(p-1)} > L_i, \\ & \text{then } \delta_i^{(p)} = \alpha \lambda_i^{(p-1)}, \end{aligned} \quad (3.316)$$

$$\text{else } \delta_i^{(p)} = 0.$$

$$\lambda_i^{(p)} = \lambda_i^{(p)} + \delta_i^{(p)}. \quad (3.317)$$

$$\mathbf{A}_Q^{(p)} = \mathbf{A}_Q^{(p-1)} + \sum_{i=1}^r \delta_i^{(p)} \mathbf{Q}_i. \quad (3.318)$$

$$\mathbf{w}^{(p)} = \left(\mathbf{A}_Q^{(p)} \right)^{-1} \mathbf{v}_T \left\{ \mathbf{v}_T^H \left(\mathbf{A}_Q^{(p)} \right)^{-1} \mathbf{v}_T \right\}^{-1}. \quad (3.319)$$

The iteration is repeated until a convergence criterion is satisfied.

It is usually necessary to adjust the sectors included in the sidelobe region at each iteration. As the sidelobes are pushed down, the main beam widens, and some sectors previously in the sidelobe region fall in the main beam. The constraints on these sectors must then be dropped.

Example 3.9.3

Consider a standard 10-element linear array. The desired look direction is $u_T = 0$ and the desired sidelobe level is -30 dB. Initially, 80 sidelobe regions are defined as sectors of width $2\Delta_i = 0.02$ in the regions $0 \leq u \leq -0.2$ and $0.2 \leq u \leq 1$. The constraint levels are all set to the sidelobe level times the width of each sector $L_i = 2 \times 10^{-5}$. The initial loading level is set to $\lambda_0 = 1$, and $\alpha = 0.3$. In Figure 3.50, we show the beam pattern and sidelobe region evolution. The final beam pattern is obtained after 14 iterations. The final beam pattern is essentially the same as the Dolph Chebychev pattern in Section 3.4.2.

Example 3.9.4

In this example, 10 elements were located along the z -axis. The elements were spaced at a distance of $\lambda/2$ with a random perturbation between $\pm\lambda/4$. Specifically,

$$p_n = \left(-\frac{N-1}{2} + n \right) \frac{\lambda}{2} + \left(d_i - \frac{1}{2} \right) \frac{\lambda}{2}, \quad (3.320)$$

where d_i is a uniform random variable $[0, 1]$. The desired look direction is broadside. An equal-ripple beam pattern was designed with -25 dB sidelobes.

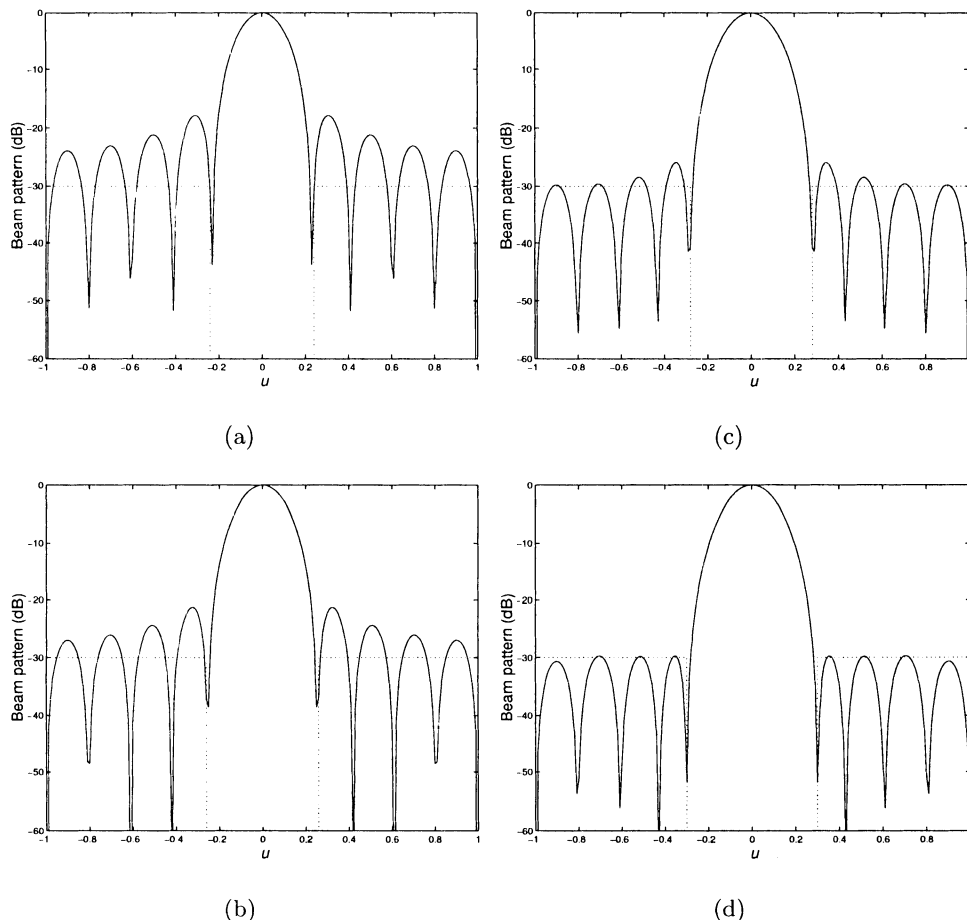


Figure 3.50 Beam pattern evolution for 10-element uniform linear array and -30 -dB sidelobes. (a) First iteration; (b) fifth iteration; (c) 10th iteration; (d) 14th iteration.

Table 3.9 Element Locations Used for the Isotropic Linear Random Array

Element No.	Relative Position
0	-2.2509λ
1	-1.6501λ
2	-1.1696λ
3	-0.7138λ
4	-0.1705λ
5	0.2901λ
6	0.7105λ
7	1.1974λ
8	1.7103λ
9	2.2585λ

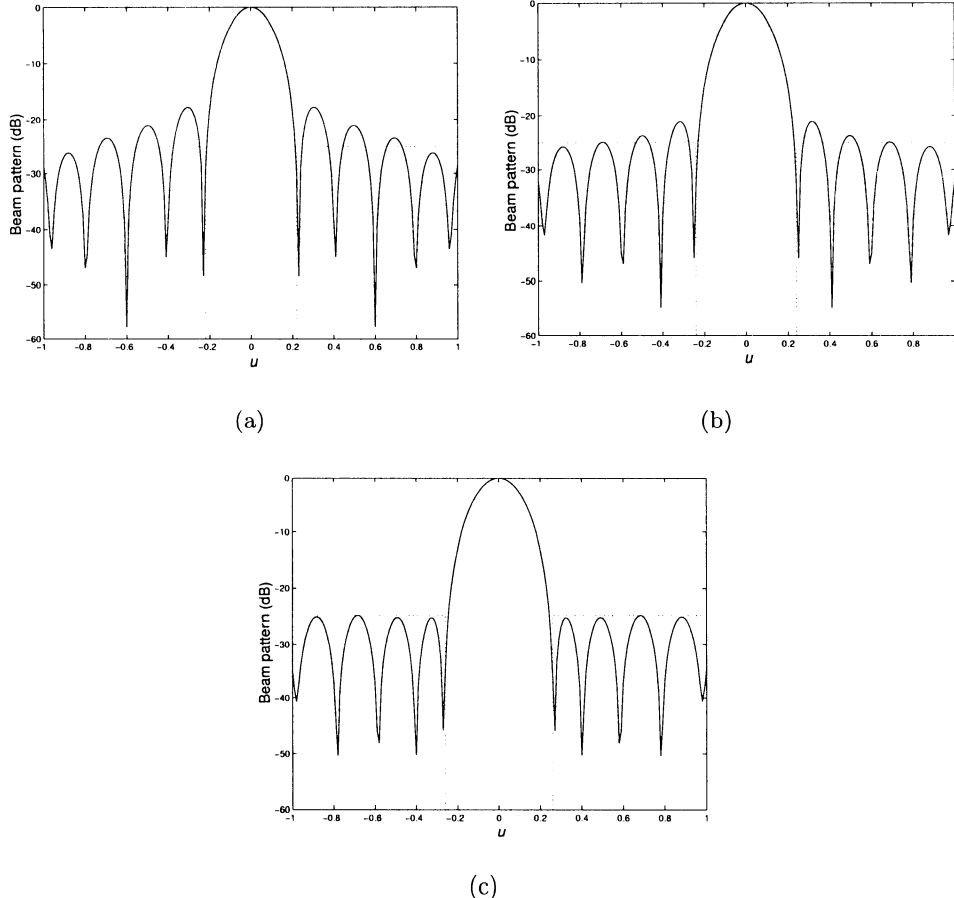


Figure 3.51 Beam pattern evolution for 10-element non-uniform linear array and -25-dB sidelobes. (a) First iteration; (b) fifth iteration; (c) 10th iteration.

The element locations for a particular trial are shown in Table 3.9. The beam pattern evolution is shown in Figure 3.51. Figure 3.51(a) is the initial pattern, Figure 3.51(b) is the fifth iteration, and Figure 3.51(c) is the tenth iteration.

The extension to non-uniform sidelobe control follows easily. We can also force nulls at specific locations. Both of our examples in this section considered linear arrays, but the technique also applies to arbitrary array geometries and non-isotropic sensors. In Chapter 7, we develop an adaptive version of the algorithm.

3.10 Beamspace Processing

All of the processing that we have discussed up to this point can be referred to as “element-space processing.” We weight (or filter in the wideband case) the signals arriving at each of the elements and sum the results to obtain an output signal.

In many cases, the number of elements, N , is very large and we find it useful to create a set of beams as a preliminary step to further processing. We then process the resulting beams. This procedure is referred to as beamspace processing and we will encounter it at various points in the text.

In this section, we consider three types of beamspace processing.

3.10.1 Full-dimension Beamspace

In this case we process the outputs of an N -element standard linear array to produce N orthogonal beams. The center beam is a conventional beam pointed at broadside ($u = 0$). We denote the weight vector as

$$\mathbf{w}^H(0) = \frac{1}{N} \mathbf{1}^T. \quad (3.321)$$

We form beams on either side of the center beam whose main response axes (MRAs) are shifted by $2/N$ in u -space.

For N even,

$$B_m(u) = \frac{1}{N} \frac{\sin \left[\frac{\pi N}{2} \left(u - \frac{2m}{N} \right) \right]}{\sin \left[\frac{\pi}{2} \left(u - \frac{2m}{N} \right) \right]}, \quad m = -\frac{N}{2} + 1, \dots, \frac{N}{2}. \quad (3.322)$$

There are N beams. The beam corresponding to $m = N/2$ is an endfire beam (it could also have been indexed as $m = -N/2$). In Figure 3.52(a), we show the beams in u -space. In Figure 3.52(b), we show the main lobe of the beams in θ -space.

For N odd,

$$B_m(u) = \frac{1}{N} \frac{\sin \left[\frac{\pi N}{2} \left(u - \frac{2m}{N} \right) \right]}{\sin \left[\frac{\pi}{2} \left(u - \frac{2m}{N} \right) \right]}, \quad m = -\frac{N-1}{2}, \dots, \frac{N-1}{2}. \quad (3.323)$$

In this case, there is no endfire beam. In Figure 3.53, we show the beams in u -space and the main lobes in θ -space for $N = 11$.

The MRA for the m th beam occurs at $2m/N$. All of the other beams have nulls at that point. This occurs because the weight vectors are orthogonal

$$\mathbf{w}^H(m)\mathbf{w}(l) = \frac{1}{N}\delta_{ml}. \quad (3.324)$$

The corresponding beams are also orthogonal:

$$B_m(u) = \mathbf{w}^H(m)\mathbf{v}(u), \quad (3.325)$$

and

$$\begin{aligned} \int_{-1}^1 B_m(u)B_l^*(u) du &= \mathbf{w}^H(m) \left(\int_{-1}^1 \mathbf{v}(u)\mathbf{v}^H(u) du \right) \mathbf{w}(l) \\ &= \mathbf{w}^H(m) \mathbf{I} \mathbf{w}(l) = \frac{1}{N}\delta_{ml}. \end{aligned} \quad (3.326)$$

The result in (3.324) implies that a signal arriving along the MRA of a particular beam will have no output in any other beam. However, a signal that is not along the MRA will appear in the sidelobes of the other beams.

We form an $N \times N$ matrix, \mathbf{B}_{bs}^H whose m th row is $\mathbf{w}^H(m)$. Then

$$\mathbf{x}_{bs} = \mathbf{B}_{bs}^H \mathbf{x}. \quad (3.327)$$

This operation is shown in Figure 3.54.

The matrix, \mathbf{B}_{bs}^H , is commonly referred to as Butler matrix [BL61] and is an invertible matrix. From (3.95), we observe that \mathbf{B}_{bs}^H is the DFT matrix. Thus,

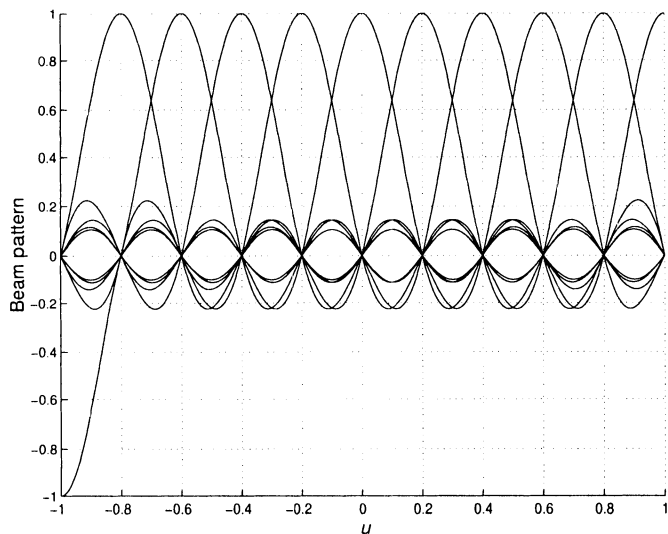
$$\mathbf{x} = [\mathbf{B}_{bs}^H]^{-1} \mathbf{x}_{bs}, \quad (3.328)$$

so we have not lost any information by the transformation. In the statistical literature, (3.327) is referred to as the DFT beamformer. Often this transformation makes the implementation of the resulting processing easier. In later chapters, we will develop beamspace adaptive arrays [AC76] and beamspace direction-of-arrival estimators.

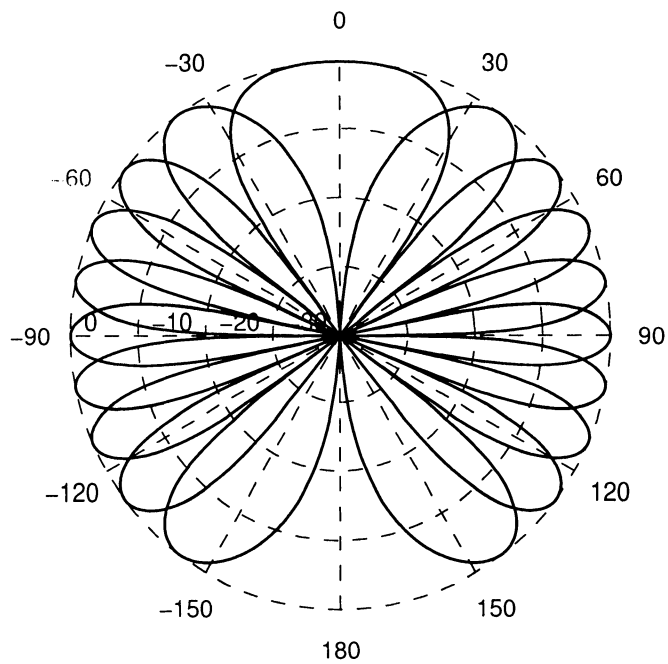
In most applications, we work with a reduced-dimension beamspace. We discuss this approach in the next section.

3.10.2 Reduced-dimension Beamspace

Consider the application shown in Figure 3.55. All of the signals of interest are contained in a region ψ_B . We can significantly reduce our subsequent processing if we form a set of beams that span the space.



(a)



(b)

Figure 3.52 Beam patterns: $N=10$; (a) u -space; (b) θ -space.

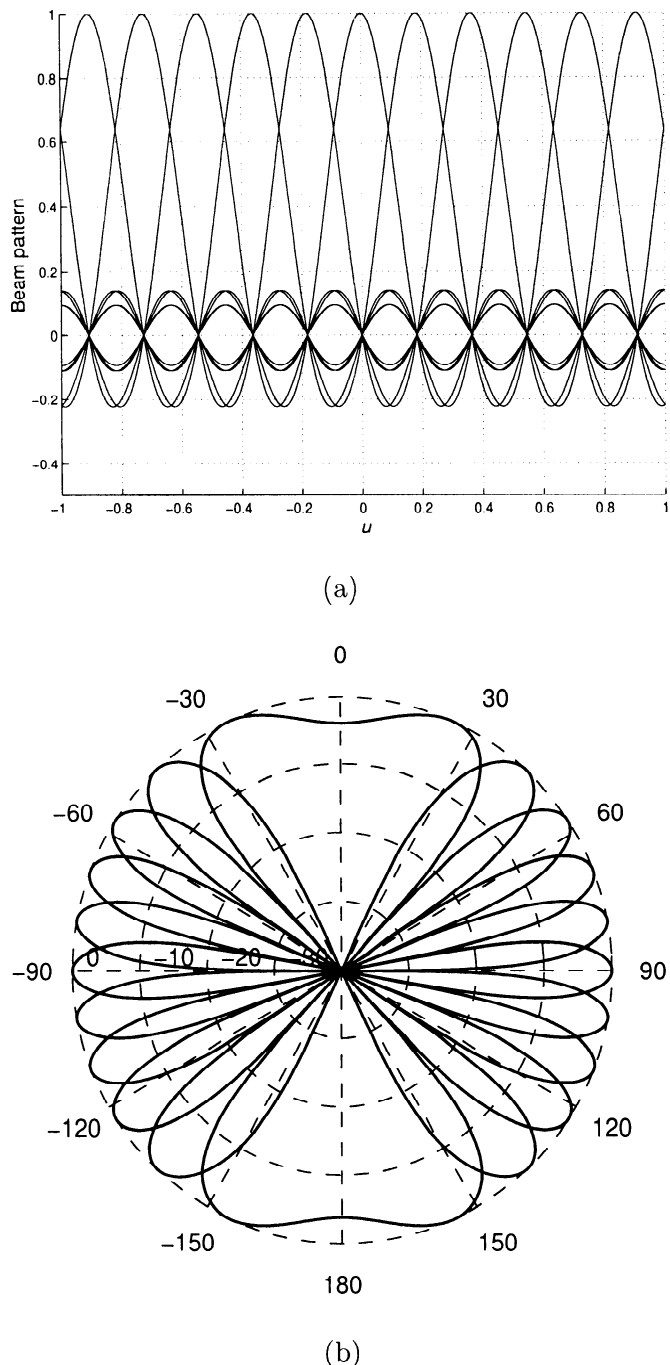


Figure 3.53 Beam patterns: $N=11$; (a) u -space; (b) θ -space.

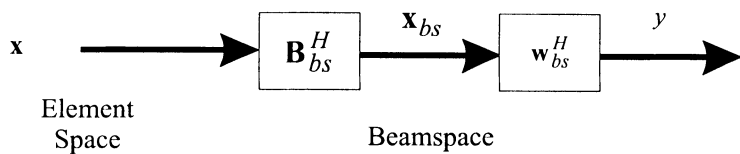


Figure 3.54 Butler beamformer.

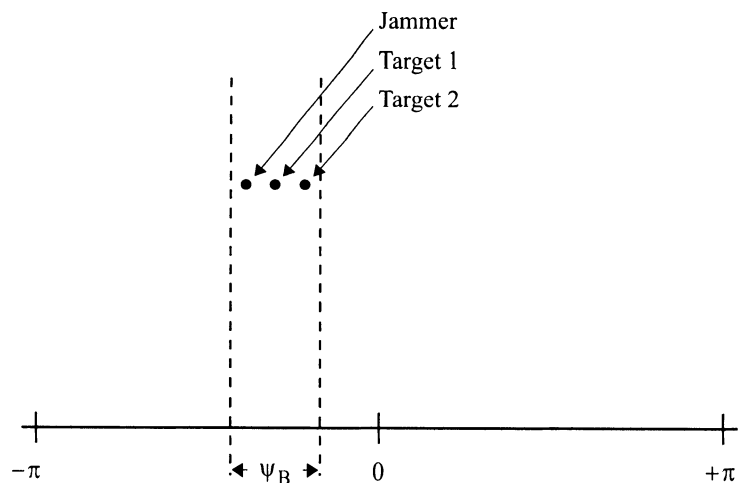


Figure 3.55 Reduced area of interest.

In practice, we normally are scanning the beams over some region in u -space. We form a beam fan consisting of N_{bs} beams and move the MRA of the center beam through u -space in $2/N$ increments. In Figure 3.56, we show several representative positions in u -space for a 7-beam fan and a 32-element standard linear array.

In most applications, we would like to use as few beams as possible without degrading the performance of the system. Later in the text we introduce appropriate statistical measures to quantify the degradation. In constructing the reduced-dimension beamspace we will consider different beamforming matrices in order to maximize performance. Several techniques are logical:

- (i) The conventional beamformer (or DFT) set as shown in Figure 3.56 is appropriate.
- (ii) In order to reduce out-of-sector interference, we can use low sidelobe beams such as Dolph-Chebychev or Taylor as the component beams. We would normally space the centers of the beams at equal intervals in ψ -space. The columns in the beamspace matrix are not orthogonal. In many applications, we need orthogonal columns. If we denote the original beamspace matrix as \mathbf{B}_{no} where the subscript “*no*” denotes that the columns are not orthogonal, then if we define the beamspace matrix as,

$$\mathbf{B}_{bs} = \mathbf{B}_{no} [\mathbf{B}_{no}^H \mathbf{B}_{no}]^{-\frac{1}{2}}, \quad (3.329)$$

the columns will be orthogonal. The transformation in (3.329) will increase the sidelobe level of the component beams by several dB.

- (iii) Another choice of component beams that have lower sidelobes than conventional beams are the weightings from Section 3.1 that generated beam patterns corresponding to weighted sums of shifted sinc functions. Specifically:
 - (a) $\cos^m(\pi\tilde{n}/N)$ (3.18)
 - (b) $\cos^2(\pi\tilde{n}/N)$ (3.18)
 - (c) Hamming (3.21)
 - (d) Blackman-Harris (3.23)

These weightings have the property that the out-of-sector zeros of each beam in the beam fan are the same. This property will be useful when we study parameter estimation in Chapters 8 and 9.

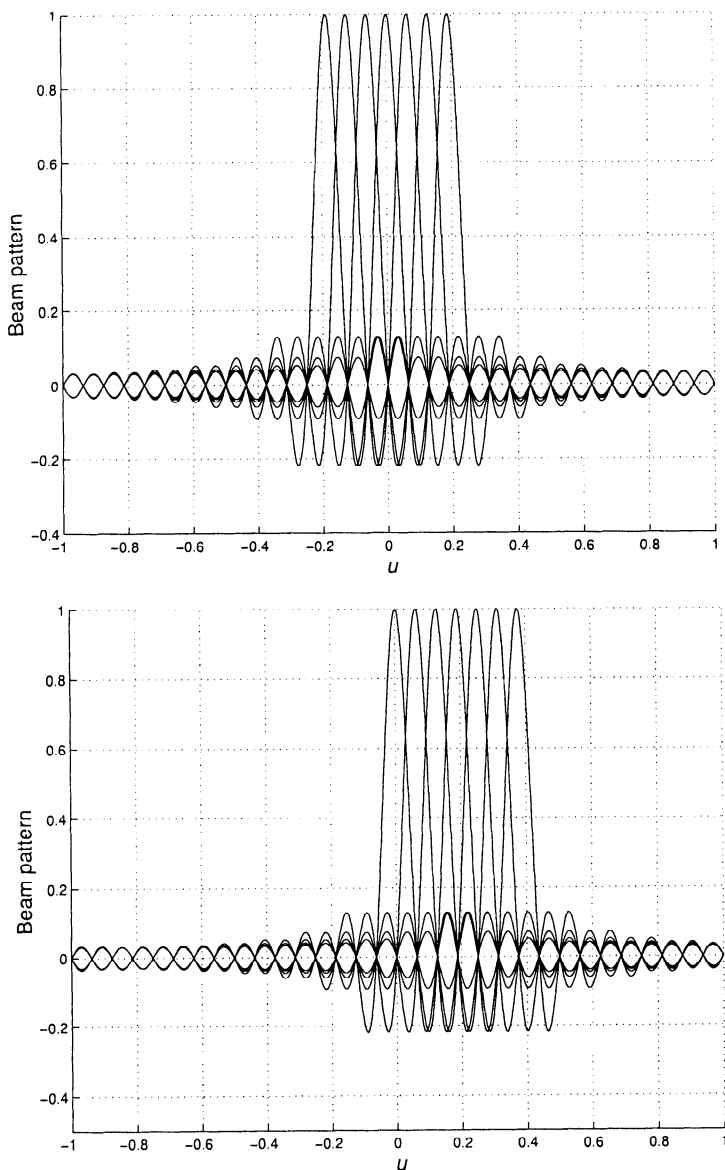


Figure 3.56 Scanning u -space with beam fans: $N = 32, N_{bs} = 7$; (a) center beam at $u = 0$; (b) center beam at $u = 6/N$.

- (iv) The first M discrete prolate spheroidal sequences developed in Section 3.1 ((3.25)–(3.35)) are logical candidates because of their power maximization characteristic.
- (v) We can develop a set of component beams by using the array manifold vector $\mathbf{v}(\psi)$ and its derivatives with respect to ψ , $\dot{\mathbf{v}}(\psi)$, $\ddot{\mathbf{v}}(\psi)$ evaluated at ψ_c , the location of the center of the beam fan.

Other choices appear in later discussions. The best choice depends on the environment and the specific objective of our array processor.

The final step is to process \mathbf{x}_{bs} , the output of the beamspace matrix to produce the array output y . We show the processing in Figure 3.54.

We define the beamspace array manifold vector as

$$\mathbf{v}_{bs}(\psi) = \mathbf{B}_{bs}^H \mathbf{v}_\psi(\psi). \quad (3.330)$$

If we use a 7×32 beamspace matrix whose rows correspond to shifted conventional beams, and the center beam is steered to ψ_c , then

$$\left[\mathbf{b}_{bs,m}^H \right]_n = \frac{1}{\sqrt{N}} \left[e^{-j(n-\frac{N-1}{2})(\psi_c-(m-4)\frac{2\pi}{N})} \right], \quad \begin{array}{l} n = 0, \dots, N-1, \\ m = 1, \dots, 7, \end{array} \quad (3.331)$$

and

$$[\mathbf{v}_\psi(\psi)]_n = e^{j(n-\frac{N-1}{2})\psi}, \quad n = 0, \dots, N-1. \quad (3.332)$$

Using (3.331) and (3.332) in (3.330) and, letting $\psi_c = 0$, gives

$$\mathbf{v}_{bs}(\psi) = \sqrt{N} \begin{bmatrix} \frac{\sin(\frac{N}{2}(\psi+3\frac{2\pi}{N}))}{\sin(\frac{1}{2}(\psi+3\frac{2\pi}{N}))} \\ \vdots \\ \frac{\sin(\frac{N}{2}(\psi-(m-4)\frac{2\pi}{N}))}{\sin(\frac{1}{2}(\psi-(m-4)\frac{2\pi}{N}))} \\ \vdots \\ \frac{\sin(\frac{N}{2}(\psi-3\frac{2\pi}{N}))}{\sin(\frac{1}{2}(\psi-3\frac{2\pi}{N}))} \end{bmatrix} = \sqrt{N} \begin{bmatrix} B_c\left(\psi + 3\frac{2\pi}{N}\right) \\ \vdots \\ B_c\left(\psi - (m-4)\frac{2\pi}{N}\right) \\ \vdots \\ B_c\left(\psi - 3\frac{2\pi}{N}\right) \end{bmatrix}. \quad (3.333)$$

Note that the beamspace array manifold vector is real. This result allows us to use real computation in many of our subsequent algorithms.

We process the output of the beamspace matrix, \mathbf{x}_{bs} , with a $1 \times N_{bs}$ matrix, \mathbf{w}_{bs}^H , to obtain a scalar output, y . The resulting beam pattern is

$$B_\psi(\psi) = \mathbf{w}_{bs}^H \mathbf{v}_{bs}(\psi). \quad (3.334)$$

In Chapters 6 through 9, we develop optimum beamspace processors for various applications and show the advantages of operating in a reduced-dimension beamspace.

3.10.3 Multiple Beam Antennas

In this case, the physical implementation of the antenna provides a set of multiple beams that span the wavenumber region of interest. Important examples of this case are the transmit and receive antennas on various military satellites (e.g., Mayhan [May76] or Ricardi [Ric76]). In those cases, we start the problem in beamspace.

3.10.4 Summary

We have introduced beamspace processing in this section. It is widely used in practical applications. One advantage is that the complexity of the subsequent processing is reduced significantly. By choosing a suitable beam fan we can usually minimize any loss in performance. We investigate those issues in later sections.

3.11 Broadband Arrays

In many applications, the array is required to process signals over a broad frequency band. One approach is to utilize an array with uniform spacing,

$$d = \frac{\lambda_u}{2}, \quad (3.335)$$

where λ_u is the wavelength of the highest frequency. We then use frequency-dependent weightings to process the beams. The difficulty with this approach is that the required number of sensors may be prohibitive. The spacing in (3.335) is required to avoid grating lobes. If we require that the width of the main lobe be constant across the frequency band of interest, then the total length must be proportional to the λ_l . From (2.109),

$$BW_{NN} = \alpha \frac{\lambda_l}{Nd}, \quad u\text{-space}, \quad (3.336)$$

where α is a constant dependent on the shading. Using (3.335) in (3.336) gives

$$N = \left(\frac{2\alpha}{BW_{NN}} \right) \frac{\lambda_l}{\lambda_u}, \quad (3.337)$$

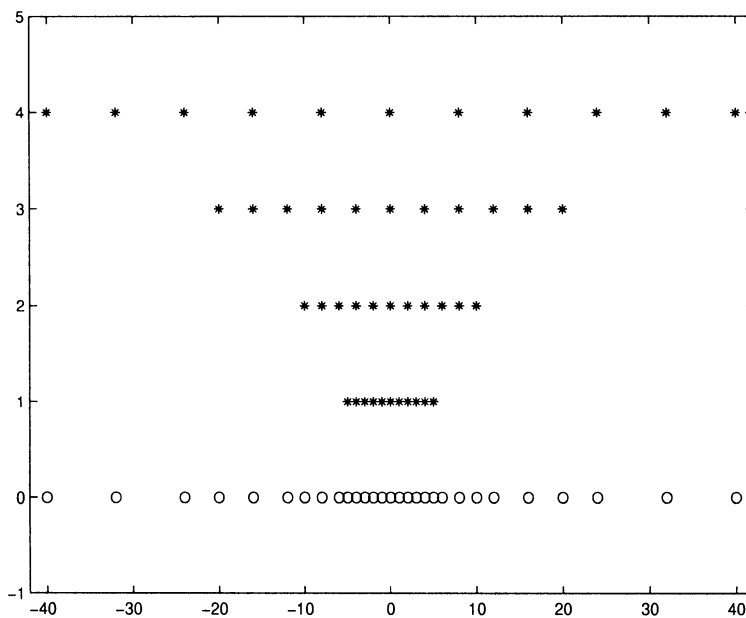


Figure 3.57 Nested arrays.

so the required number of elements is proportional to the band ratio. In this section, we discuss two techniques that utilize arrays with non-uniform element spacing.

The first technique uses a compound array consisting of a nested set of subarrays, each of which is designed for single frequency. The most common type of nested array is shown in Figure 3.57. The bottom subarray has N elements spaced at $d_1 = \lambda_u/2$, where λ_u is the wavelength at the highest frequency. In the figure, $N = 11$. The next subarray has N elements spaced at $d_2 = \lambda_u$, which corresponds to half-wavelength spacing at $f_u/2$. The third subarray has N elements spaced at $d_3 = 2\lambda_u$, which corresponds to half-wavelength spacing at $f_u/4$. The fourth subarray has N element spaced at $d_4 = 4\lambda_u$, which corresponds to half-wavelength spacing at $f_u/8$.

The total number of elements is

$$N_T = N + 3 \left(\frac{N+1}{2} \right), \quad N \text{ odd}, \quad (3.338)$$

and

$$N_T = N + 3 \frac{N}{2}, \quad N \text{ even}. \quad (3.339)$$

We process the highest octave, $f_u/2 < f < f_u$, with the first subarray, the next octave, $f_u/2 < f < f_u/4$ with the next subarray, and so forth.

We divide the output of each subarray into K frequency bins and use narrowband processing (complex weights) to create a beam in the frequency bin.³⁶ We consider two different weight techniques.

If we use conventional weighting, then the beam patterns are similar to those in Figure 2.20 for various d/λ values ranging from $d = \lambda/2$ to $d = \lambda/4$. In Figure 3.58, we show the beam patterns for $K=8$, where the frequency bins are centered at

$$f_k = f_l \left[1 + \frac{2k+1}{16} \right], \quad k = 0, \dots, 7. \quad (3.340)$$

Thus

$$\frac{d}{\lambda_m} = \frac{1}{4} \left(1 + \frac{2m+1}{16} \right), \quad m = 0, \dots, 7. \quad (3.341)$$

As we would expect, the beam narrows as the frequency increases. As we move from f_l to f_u , the BW_{NN} goes from $8/N$ in u -space to $4/N$ in u -space. This approach can be extended to any of the weightings developed earlier in the chapter. In all cases, the main-lobe width will decrease as we go up in frequency. Note that the beam patterns are repetitive in each octave because of the choice of the subarray.

A different technique is used if we want a constant beam pattern over each octave. The technique is described in Chou [Cho95] (see also [GE93] and [Tuc57]). We first define a desired beam pattern at f_l for a uniform linear array whose spacing is

$$d = \frac{\lambda_u}{2}, \quad (3.342)$$

and

$$\lambda_l = 2\lambda_u. \quad (3.343)$$

For example, if we use uniform weighting,

$$B_u(u) = \frac{1}{N} \frac{\sin\left(\frac{\pi N d}{\lambda_l} u\right)}{\sin\left(\frac{\pi d}{\lambda_l} u\right)} = \frac{1}{N} \frac{\sin(\pi N u)}{\sin \pi u}. \quad (3.344)$$

The beam pattern is shown in Figure 3.59 over the interval $-2 \leq u \leq 2$. Because $d = \lambda_l/4$, we need to consider the beam pattern over twice the

³⁶An important issue is the technique for combining the outputs of the different frequency bins to synthesize the output signal. This is discussed in Section 6.13.

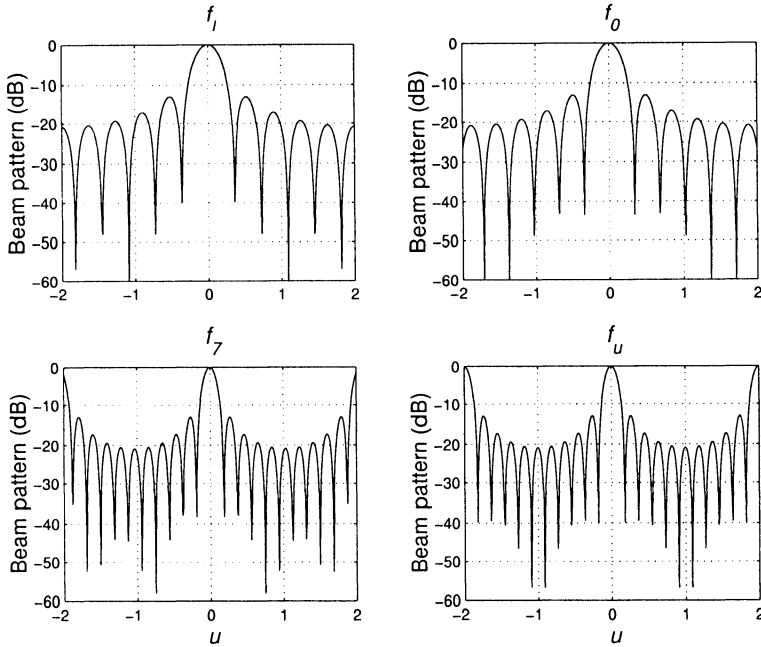


Figure 3.58 Beam patterns: $N=11$, $K=8$; f_0 and f_7 plus endpoint references f_l and f_u .

visible region. For each of the frequencies in (3.340), we sample the beam pattern at

$$u_n = \frac{c}{Nd \cdot f_k} n, \quad -\frac{N-1}{2} \leq n \leq \frac{N-1}{2}, \quad N \text{ odd}, \quad (3.345)$$

$$1 \leq k \leq K.$$

We perform an IDFT on the samples to obtain the weightings for that frequency bin f_k . We then take the DFT to find the beam pattern for frequency bin f_k . In Figure 3.60, we show the samples and resulting weightings for

$$f_0 = f_l(1 + 1/16), \quad (3.346)$$

and

$$f_7 = f_l(1 + 15/16). \quad (3.347)$$

We recall from Example 3.3.4 that we need samples outside the visible region to specify the weight vector when $d < \lambda/2$. In Figure 3.61, we show the resulting beam pattern over four octaves from 500 to 8000. The main lobe

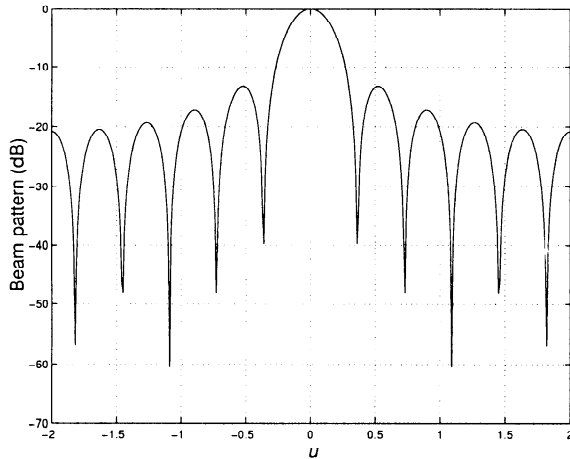


Figure 3.59 Desired beam pattern.

is essentially constant over the interval and there is only a slight variation in the sidelobes. The technique can be extended to other desired beam patterns by changing (3.344).

A possible disadvantage of the nested approach is that only a limited set of band ratios; 2, 4, 8, ⋯ are achievable.

An alternate approach that allows more flexibility in broadband array design is described in Doles and Benedict [DB88]. They use the asymptotic theory of unequally spaced arrays that was developed by Ishimaro (e.g., Ishimaru [Ish62], Ishimaru and Chen [IC65], and Chow [Cho65]). The resulting arrays have exponential spacing. The reader is referred to these references for discussions of the technique.

3.12 Summary

This completes our discussion of analysis and synthesis of the weight vectors for linear arrays. We have developed an extensive set of tools to carry out the process.

The majority of the chapter was devoted to two problems. In the first problem, we wanted to generate a pattern that had a narrow main lobe and low sidelobes. Sections 3.1 and 3.4 developed techniques for designing a weight vector that provided a suitable compromise between these conflicting objectives. The Dolph-Chebychev and Taylor weightings are widely used in classical array design and play an important role in the optimum array

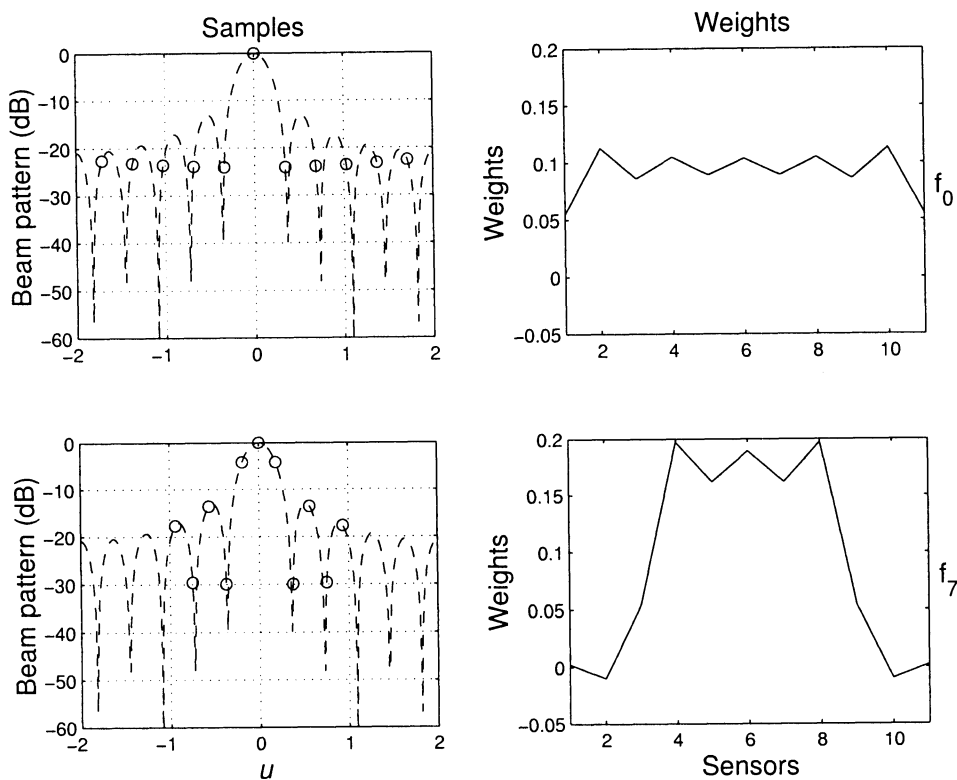


Figure 3.60 Samples and array weights; $N=11$, $K=8$, conventional desired pattern.

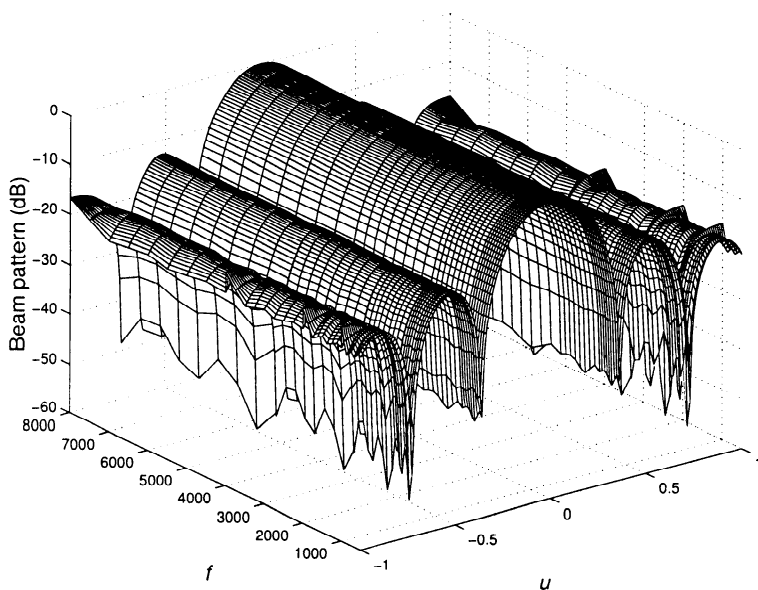


Figure 3.61 Beam patterns for broadband array: $N=11$, $K = 8$, $500 \leq f \leq 8000$, constant main lobe.

processing problem.

In the second problem, there is a desired beam pattern. In Sections 3.3, 3.5, 3.6, 3.7, and 3.9.3, techniques were developed to approximate the desired beam pattern. These techniques can be divided into three categories:

(i) Sampling techniques (Section 3.3)

For uniform linear arrays, this approach resulted in DFT and IDFT relations. The general sampling approach applies to arbitrary array geometries.

(ii) Minimax techniques (Sections 3.6 and 3.9.3)

These techniques impose hard constraints on the allowable deviation of the synthesized beam pattern from the desired beam pattern. They utilize an iterative technique to obtain the weight vector. The technique in Section 3.9.3 extends the hard constraint criterion of Sections 3.4 and 3.6 to arbitrary array geometries.

(iii) Least squares techniques (Sections 3.5 and 3.7)

Least squares techniques (generally with some type of constraints) are widely used in array design. The techniques are applicable to arbitrary array geometries. The least squares criterion leads to a quadratic minimization problem. In Sections 3.5 and 3.7, an analytic solution is available. The quadratic minimization approach applies to arbitrary arrays and is encountered frequently in subsequent discussions.

The remainder of the chapter discussed four other topics: difference beams, non-uniform linear arrays, beamspace processing, and broadband arrays.

Section 3.8 discussed the synthesis of difference beams with low sidelobes; these beams are widely used in applications where we want to estimate the angle of arrival of a plane-wave signal from a target and aim the array at the target. Section 3.9 discussed linear arrays with non-uniform spacing. The concept of a minimum redundancy linear array was introduced. Synthesis techniques for linear arrays with non-uniform spacing were developed. Section 3.10 developed the basic ideas of beamspace processing. Various beamspace applications will be discussed in subsequent chapters. Section 3.11 introduced some of the techniques for broadband array design. This topic is revisited in subsequent chapters.

Many of these techniques can be extended to planar arrays. Chapter 4 discusses planar arrays.

3.13 Problems

P3.1 Spectral Weighting

Problem 3.1.1

Consider a linear aperture of length L :

$$w(z) = 1 - \left(\frac{2z}{L}\right)^2, \quad -\frac{L}{2} \leq z \leq \frac{L}{2}. \quad (3.348)$$

Find the beam pattern, the HPBW, and height of the first sidelobe.

Problem 3.1.2

Consider a linear aperture of length L :

$$w(z) = \left(1 - \left(\frac{2z}{L}\right)^2\right)^2, \quad -\frac{L}{2} \leq z \leq \frac{L}{2}. \quad (3.349)$$

Find the beam pattern, the HPBW, and height of the first sidelobe.

Problem 3.1.3

Consider a linear aperture of length L :

$$w(z) = \left(1 - \left(\frac{2z}{L}\right)^2\right)^{\frac{1}{2}}, \quad -\frac{L}{2} \leq z \leq \frac{L}{2}. \quad (3.350)$$

Find the beam pattern, the HPBW, and height of the first sidelobe.

Problem 3.1.4

Consider a standard linear array with 9 elements.

- (a) Compute the DPSS weighting for $\psi_0 = 0.1\pi, 0.2\pi, 0.3\pi, 0.4\pi$.
- (b) Plot the resulting beam patterns.
- (c) Compute the HPBW, BW_{NN} , and the height of highest sidelobe.

Problem 3.1.5

Show that the beam pattern for the Kaiser weighting is proportional to

$$\frac{\sin \left[\beta \sqrt{\left(\frac{\psi}{\psi_\beta} \right)^2 - 1} \right]}{\sqrt{\left(\frac{\psi}{\psi_\beta} \right)^2 - 1}}, \quad (3.351)$$

where ψ_β is the approximate beamwidth of the main lobe.

Problem 3.1.6

The Lanczos weighting for a standard linear array is defined as

$$w_L(n) = \left\{ \frac{\sin \left[\frac{2\pi n}{(N-1)^2} \right]}{\frac{4\pi n}{(N-1)^2}} \right\}^L, \quad L > 0, \quad (3.352)$$

where the indexing is symmetric.

Plot the array weighting and corresponding beam pattern for several values of L .

Problem 3.1.7

Compute Δu_4 (see Problem 2.4.8) for:

- (a) Hann weighting
- (b) Hamming weighting
- (c) Blackman-Harris weighting

and compare to the HPBW.

Problem 3.1.8

Compute Δu_4 for:

- (a) Gaussian weighting
- (b) DPSS weighting
- (c) Kaiser weighting

and compare to the HPBW.

Problem 3.1.9

Consider an 11-element standard linear array with symmetric weighting

$$w_0 = 0.5, \quad (3.353)$$

$$w_n = w_{-n} = 1.0 + 0.5(n - 1), \quad n = 1, 2, \dots, 5. \quad (3.354)$$

- (a) Plot $B_\psi(\psi)$.
- (b) Where might this beam pattern be useful?

Problem 3.1.10

Consider an 11-element standard linear array with symmetric weighting,

$$w_n = 1.0, \quad n = 0, 1, 2, 3, \quad (3.355)$$

$$w_n = 0.6, \quad n = 4, \quad (3.356)$$

$$w_n = 0.2, \quad n = 5. \quad (3.357)$$

Compute and plot $B_\psi(\psi)$.

Problem 3.1.11

The Riesz (Bochner, Parzen) window [Har78] is defined as

$$w_n = 1.0 - \left| \frac{n}{N/2} \right|^2, \quad 0 \leq |n| \leq \frac{N}{2}. \quad (3.358)$$

- (a) Find and plot the beam pattern for $N = 10$.
- (b) Compute the HPBW, BW_{NN} , the height of the first sidelobe, the rate of sidelobe decrease, and the directivity.

Problem 3.1.12

The Riemann window is [Har78]

$$w_n = \frac{\sin \left[\frac{n}{N} 2\pi \right]}{\left[\frac{n}{N} 2\pi \right]}, \quad 0 \leq |n| \leq \frac{N}{2}, \quad (3.359)$$

and corresponds to the main lobe of a sinc function. Repeat Problem 3.1.11.

Problem 3.1.13

The de la Vallé-Poussin (Jackson, Parzen) window is a piecewise cubic curve obtained by self-convolving two triangles of half-extent or four rectangles of one-fourth extent. It is defined as

$$w_n = \begin{cases} 1.0 - 6 \left[\frac{n}{N/2} \right]^2 \left[1.0 - \frac{|n|}{N/2} \right], & 0 \leq |n| \leq \frac{N}{4}, \\ 2 \left[1.0 - \frac{|n|}{N/2} \right]^3, & \frac{N}{4} \leq |n| \leq \frac{N}{2}. \end{cases} \quad (3.360)$$

Repeat Problem 3.1.11.

Problem 3.1.14

The Tukey window [Har78], [Tuk67] is a cosine lobe of width $(\alpha/2)N$ convolved with a rectangle window of width $(1.0 - \alpha/2)N$. The window evolves from the rectangle to the

Hann window as the parameter α varies from unity to zero. The Tukey window is defined as

$$w_n = \begin{cases} 1.0, & 0 \leq |n| \leq \alpha \frac{N}{2}, \\ 0.5 \left[1.0 + \cos \left(\pi \frac{|n| - \alpha \frac{N}{2}}{(1-\alpha) \frac{N}{2}} \right) \right], & \alpha \frac{N}{2} \leq |n| \leq \frac{N}{2}. \end{cases} \quad (3.361)$$

- (a) Plot w_n and the corresponding beam pattern for $\alpha = 0.25, 0.50, 0.75$.
- (b) Compute the HPBW, BW_{NN} , the height of the first sidelobe, the rate of sidelobe decrease, and the directivity.

Problem 3.1.15

The Bohman window [Har78], [Boh60] is obtained by the convolution of two half-duration cosine lobes; thus its transform is the square of the cosine lobe transform. The window is defined as

$$w_n = \left[1.0 - \frac{|n|}{N/2} \right] \cos \left[\pi \frac{|n|}{N/2} \right] + \frac{1}{\pi} \sin \left[\pi \frac{|n|}{N/2} \right], \quad 0 \leq |n| \leq \frac{N}{2}. \quad (3.362)$$

Repeat Problem 3.1.11.

Problem 3.1.16

The Poisson window [Har78], [Bar64] is a two-sided exponential defined by

$$w_n = \exp \left(-\alpha \frac{|n|}{N/2} \right), \quad 0 \leq |n| \leq \frac{N}{2}. \quad (3.363)$$

Repeat Problem 3.1.11 for $\alpha = 2.0, 3.0$, and 4.0 .

Problem 3.1.17

The Hann-Poisson window is constructed as the product of the Hann and the Poisson windows. The family is defined by

$$w_n = 0.5 \left[1.0 + \cos \left(\pi \frac{n}{N/2} \right) \right] \exp \left(-\alpha \frac{|n|}{N/2} \right), \quad 0 \leq |n| \leq \frac{N}{2}. \quad (3.364)$$

Repeat Problem 3.1.11 for $\alpha = 0.5, 1.0$, and 2.0 .

Problem 3.1.18

The Cauchy (Abel, Poisson) window [Har78], [Akh56] is a family of windows parameterized by α and is defined as

$$w_n = \frac{1}{1 + \left(\alpha \frac{n}{N/2} \right)^2}, \quad 0 \leq |n| \leq \frac{N}{2}. \quad (3.365)$$

Repeat Problem 3.1.11 for $\alpha = 3.0, 4.0$, and 5.0 .

Problem 3.1.19

The Hamming, Hann, and Blackman windows are constructed from shifted conventional patterns. More generally, we can write

$$w_n = \sum_{m=0}^{N/2} a_m \cos \left(\frac{2\pi}{N} m \left(|n| - \frac{N-1}{2} \right) \right), \quad 0 \leq |n| \leq \frac{N}{2} \quad (3.366)$$

and

$$B_\psi(\psi) = \sum_{m=0}^{N/2} (-1)^m a_m \left[\Upsilon_C \left(\psi - \frac{2\pi}{N} m \right) + \Upsilon_C \left(\psi + \frac{2\pi}{N} m \right) \right]. \quad (3.367)$$

The Blackman window in the text uses $a_0 = 0.42$, $a_1 = 0.50$, $a_2 = 0.08$.

The “exact Blackman” window uses coefficients that place a zero exactly at $\psi = 3.5(2\pi/N)$ and $\psi = 4.5(2\pi/N)$. The coefficients are:

$$a_0 = \frac{7938}{18608} \doteq 0.42650971, \quad (3.368)$$

$$a_1 = \frac{9240}{18608} \doteq 0.49656062, \quad (3.369)$$

$$a_2 = \frac{1430}{18608} \doteq 0.07684867. \quad (3.370)$$

- (a) Repeat Problem 3.1.11 for these coefficients.
- (b) Compare to the Blackman window in the text and observe how a small change in w_n gives a significant change in the sidelobes.

Problem 3.1.20

Harris [Har76], [Har78] developed 4-term windows to achieve minimum sidelobe levels. The weighting is defined

$$w_m = a_0 - a_1 \cos \left(\frac{2\pi}{N} m \right) + a_2 \cos \left(\frac{2\pi}{N} 2m \right) - a_3 \cos \left(\frac{2\pi}{N} 3m \right), \quad m = 0, 1, 2, \dots, N-1. \quad (3.371)$$

Four examples are listed in the following table:

	3-Term (-67 dB)	3-Term (-61 dB)	4-Term (-92 dB)	4-Term (-74 dB)
a_0	0.42323	0.44959	0.35875	0.40217
a_1	0.49755	0.49364	0.48829	0.49703
a_2	0.07922	0.05677	0.14128	0.09392
a_3	—	—	0.01168	0.00183

Problem 3.1.21: Gaussian weightings

The Fourier uncertainty principle suggests that the optimum weighting for an infinitely long aperture has a Gaussian form. More precisely, for a given root-mean-square aperture extent, the weighting that generates the narrowest root-mean-square wavenumber response has a Gaussian function form. Moreover, the Gaussian weighting leads to a Gaussian array response that implies no sidelobes. The limiting factor for any implementation is the finite aperture extent that mitigates the consequences of the Fourier uncertainty principle, since the weighting must be terminated with a step discontinuity, however small it may be. The Gaussian weighting is a family of weightings parameterized by its width relative to the aperture length L . It is given by

$$w_\sigma(z) = \begin{cases} \frac{c(\sigma)}{L} e^{-\frac{1}{2}(\frac{z}{\sigma L})^2}, & |z| \leq \frac{L}{2}, \\ 0, & |z| > \frac{L}{2}, \end{cases} \quad (3.372)$$

where $c(\sigma)$ is a normalization constant such that response on the main response axis is unity (or equivalently, the area under the weighting is unity). The constant is given by

$$c(\sigma) = \left[2\sqrt{2\pi}\sigma(1 - Q\left(\frac{1}{2\sigma}\right)) \right]^{-1}, \quad (3.373)$$

where $Q(x)$ is the complementary error function for the Gaussian probability density.³⁷

The array weightings are

$$w_N(n) = w_N(z)|_{z=\frac{n}{N}}, \quad n = -\frac{N-1}{2}, \dots, \frac{N-1}{2}. \quad (3.374)$$

- (a) Plot the beam pattern for a standard 11-element linear array for $\sigma = 0.25, 0.177$, and 0.125 .
- (b) Compute the HPBW, BW_{NN} , and first sidelobe height for the three values of σ in part (a).
- (a) Discuss your results.

Problem 3.1.22: Binomial³⁸

Consider a standard N -element linear array steered to broadside. We want to synthesize a pattern whose zeros are all at $z = -1$. Thus,

$$\begin{aligned} B(z) &= (z+1)^{N-1} \\ &= z^{N-1} + \dots + a_n z^n + \dots + 1, \end{aligned} \quad (3.375)$$

where

$$a_n = \frac{(N-1)!}{n!(N-1-n)!} \quad (3.376)$$

is the binomial coefficient.

The resulting coefficients are given by Pascal's triangle.

$N = 1$				1			
$N = 2$				1	1		
$N = 3$				1	2	1	
$N = 4$				1	3	3	1
$N = 5$				1	4	6	4
$N = 6$				1	5	10	10
$N = 7$				1	6	15	20
$N = 8$				1	7	21	35
$N = 9$				1	8	28	56
$N = 10$	1	9	36	84	126	126	84
							36
							9
							1

(3.377)

- (a) Plot the beam pattern for $N = 10$. Compute the HPBW and the tolerance factor.
- (b) Discuss the behavior for large N .

P3.2 Array Polynomials and the z -Transform

Problem 3.2.1 [Bal82]

A 3-element array is placed along the z -axis. Assuming the spacing between the elements is $d = \lambda/4$ and the relative amplitude excitation is equal to $a_1 = 1, a_2 = 2, a_3 = 1$:

³⁷ $Q(x) = \frac{1}{\sqrt{2\pi}} \int_x^\infty e^{-\frac{x^2}{2}} dx$, which was defined as $erfc_*(x)$ in [DEMT I], [VT68], [VT01a].

³⁸The binomial distribution was originally suggested by Stone [Sto]. He proposed that the amplitudes be proportional to the coefficients of a binomial series of the form of (3.375).

- (a) Find the nulls of the beam pattern where the interelement phase shift ψ_T (2.127) is 0° , 60° , and 120° .
- (b) Plot the beam patterns.

Problem 3.2.2

Design a linear array of isotropic elements placed along the z -axis such that the zeros of the array factor occur at $\theta = 0^\circ$, 60° , and 120° . Assume that the elements are spaced $d = \lambda/4$ apart and that the interelement phase shift between them is 0° .

- (a) Find the required number of elements.
- (b) Determine their excitation coefficients.
- (c) Write the array factor.
- (d) Plot the array factor pattern.

Problem 3.2.3

Consider a linear array along the z -axis. Assume that $d = \lambda/2$. The nulls in the array factor are specified to be 0° , 60° , and 120° .

- (a) Find the minimum number of array elements.
- (b) Specify the array weighting.
- (c) Find and plot the array factor.

Problem 3.2.4

Consider a standard 21-element linear array. Plot the zeros in the z -plane for the following array weighting functions:

- (a) Triangular
- (b) Cosine
- (c) Raised cosine
- (d) Cosine²
- (e) Cosine³
- (f) Cosine⁴

Problem 3.2.5

Consider a standard 21-element linear array. Plot the zeros in the z -plane for the following array weighting functions:

- (a) Raised cosine-squared
- (b) Hamming
- (c) Blackman-Harris

Problem 3.2.6

Consider a standard 15-element linear array. Plot the zeros in the z -plane for the following array weighting functions:

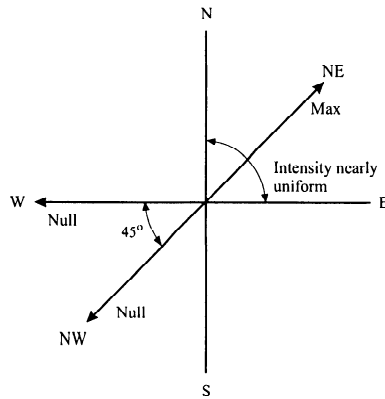


Figure 3.62 Four-tower broadcast array pattern requirements. [Adapted from [Kra88]]

- (a) DPSS ($\psi_0 = 0.15\pi, 0.25\pi$, and 0.5π)
- (b) Kaiser ($\beta = 2$ and 8)

Problem 3.2.7 [Bal82]

The z -plane array factor of an array of isotropic elements placed along the z -axis is given by

$$AF = z(z^4 - 1). \quad (3.378)$$

Determine the

- (a) Number of elements of the array. Indicate any elements with zero weighting (null elements).
- (b) Position of each element (including that of null elements) along the z -axis.
- (c) Magnitude and phase (in degree) of each element.
- (d) Angles where the pattern will equal zero when the total array length (including null elements) is 2λ .

Problem 3.2.8 [Kra88]

Four-tower BC array. A broadcasting station requires the horizontal plane pattern indicated in Figure 3.62. The maximum field intensity is to be radiated northeast with as little decrease as possible in field intensity in the 90° sector between north and east. No nulls are permitted in this sector. Nulls may occur in any direction in the complementary 270° sector. However, it is required that nulls must be present for the directions of due west and due southwest, in order to prevent interference with other stations in these directions.

Design a four-vertical-tower array to fulfill these requirements. The currents are to be equal in magnitude in all towers, but the phase may be adjusted to any relationship. There is also no restriction on the spacing or geometrical arrangements of the towers. Plot the beam pattern.

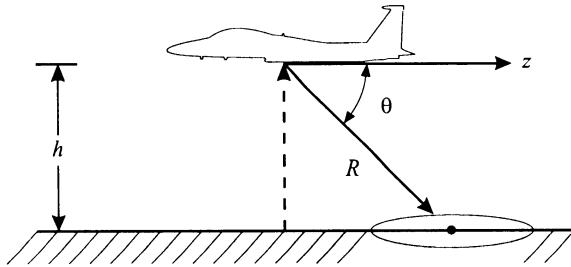


Figure 3.63 Cosecant pattern.

P3.3 Pattern Sampling in Wavenumber Space

The cosecant beam pattern is encountered in a number of applications. The next four problems, which are taken from [Bal82], use the Woodward procedure to synthesize these patterns.

Problem 3.3.1 [Bal82]

In target-search, grounding-mapping radars, and in airport beacons it is desirable to have the echo power received from a target, of constant cross section, to be independent of its range R .

Generally, the far-zone field radiated by an antenna is given by

$$|E(R, \theta, \phi)| = C_0 \frac{|F(\theta, \phi)|}{R}, \quad (3.379)$$

where C_0 is a constant. According to the geometry of Figure 3.63,

$$R = \frac{h}{\sin \theta} = h \csc \theta. \quad (3.380)$$

For a constant value of ϕ , the radiated field expression reduces to

$$|E(R, \theta, \phi = \phi_0)| = C_0 \frac{|F(\theta, \phi = \phi_0)|}{R} = C_1 \frac{|f(\theta)|}{R}. \quad (3.381)$$

A constant value of field strength can be maintained provided the radar is flying at a constant altitude h and the far-field antenna pattern is equal to

$$f(\theta) = C_2 \csc(\theta).$$

This is referred to as a cosecant pattern, and it is used to compensate for the range variations. For very narrow beam antennas, the total pattern is approximately equal to the space or array factor. Design a line source, using the Woodward method, whose array factor is given by

$$AF(\theta) = \begin{cases} 0.342 \csc(\theta), & 20^\circ \leq \theta \leq 60^\circ, \\ 0, & \text{elsewhere.} \end{cases} \quad (3.382)$$

Plot the synthesized pattern for $L = 20\lambda$, and compare it with the desired pattern.

Problem 3.3.2 [Bal82]

Repeat the design of Problem 3.3.1 for a linear array of $N = 21$ elements with a spacing of $d = \lambda/2$ between them.

Problem 3.3.3 [Bal82]

For some radar search applications, it is more desirable to have an antenna that has a square beam for $0 \leq \theta \leq \theta_0$, a cosecant pattern for $\theta_0 \leq \theta \leq \theta_m$, and is zero elsewhere. Design a line source, using the Woodward method with an array factor of

$$AF(\theta) = \begin{cases} 1, & 15^\circ \leq \theta \leq 20^\circ, \\ 0.342 \csc(\theta), & 20^\circ \leq \theta \leq 60^\circ, \\ 0, & \text{elsewhere.} \end{cases} \quad (3.383)$$

Plot the synthesized pattern for $L = 20\lambda$, and compare it with the desired pattern.

Problem 3.3.4 [Bal82]

Repeat the design of Problem 3.3.3 using the Woodward method, for a standard linear array of 41 elements.

Problem 3.3.5

Repeat the design problem in Problem 3.3.1 using the Woodward method.

Problem 3.3.6

Repeat the design problem in Problem 3.3.2 using the Woodward method.

Problem 3.3.7

Design a standard linear array with $N = 21$ when the desired array factor is

$$AF_d(\theta) = \sin^3 \theta, \quad 20^\circ \leq \theta \leq 60^\circ. \quad (3.384)$$

Use the Woodward procedure.

P3.4 Minimum Beamwidth for Specified Sidelobe Level**Problem 3.4.1**

Show that the Dolph-Chebychev procedure and the Riblet-Chebychev procedure lead to the same beam pattern for $d = \lambda/2$.

Problem 3.4.2

Consider a standard 10-element linear array pointed at broadside.

- (a) Find the Dolph-Chebychev weightings for sidelobes of -20 dB, -30 dB, and -40 dB.
- (b) Plot the resulting beam pattern and compute the HPBW, BW_{NN} , and the directivity.
- (c) Plot the roots in the z -plane.

Problem 3.4.3

Repeat Problem 3.4.2 for a 20-element linear array with $d = \lambda/4$. Repeat parts (a)-(b).

- (c) Find the Riblet-Chebychev weighting for the same sidelobe requirements and compare the BW_{NN} .

Problem 3.4.4

Compute the HPBW of the Chebychev array in Problem 3.4.2 when it is scanned to $\theta = 60^\circ$.

Problem 3.4.5

Consider a standard 7-element linear array pointed at broadside.

- (a) Find the Dolph-Chebychev weightings for sidelobe of -20 dB, -30 dB, and -40 dB.
- (b) Plot the resulting beam pattern and compute the HPBW, BW_{NN} , and the directivity.

Problem 3.4.6

[Kra88] Calculate the Dolph-Chebychev distribution of a six-source broadside standard linear array for $R = 5, 7$, and 10 .

Problem 3.4.7

Consider a standard 5-element linear array. The array is aimed at broadside.

- (a) Find the Dolph-Chebychev weightings for -20 dB sidelobes.
- (b) Plot the resulting beam pattern.
- (c) Find the HPBW and BW_{NN} .

Problem 3.4.8

Consider an 8-element linear array with $d = 3\lambda/4$. The array is aimed at broadside.

- (a) Find the Dolph-Chebychev weightings for -40 dB sidelobes.
- (b) Plot the resulting beam pattern.
- (c) Find the HPBW and BW_{NN} .

Problem 3.4.9

Consider a standard linear array with $N = 15$.

- (a) Repeat Problem 3.4.2.
- (b) Repeat part (a) for Taylor weighting with $\bar{n} = 6$.

Problem 3.4.10

Consider the model in Example 3.4.2. Find and plot the aperture weighting function and the corresponding beam pattern.

Problem 3.4.11 (continuation)

- (a) Plot the beam pattern for the corresponding linear array with $d = \lambda/4$ and $N = 17$.
- (b) Plot the beam pattern for the corresponding linear array with $d = \lambda/2$ and $N = 9$.

Problem 3.4.12 (continuation)

Instead of finding the weighting of the discrete array by sampling the continuous weighting, find a discrete weighting so that the nulls of the two patterns are matched (e.g., [Ell81]).

Problem 3.4.13

Consider a 41-element standard linear array. Design a beam pattern using a Villeneuve \bar{n} weighting with a maximum -30 -dB sidelobe.

- (a) Plot the beam pattern for $\bar{n} = 6$.
- (b) How does the pattern change as a function of \bar{n} ?
- (c) Find the array weights for the pattern in part (a).

Problem 3.4.14

Repeat Problem 3.4.13 for -35 -dB maximum sidelobes.

Problem 3.4.15

- (a) Calculate the directivity of a standard N -element linear array pointed at broadside using a Dolph-Chebychev weighting.
- (b) Plot the directivity index DIB versus N for sidelobe levels of $-15, -20, -30, -40$, and -60 dB. Let N vary from 10 to 1000.

Problem 3.4.16

Repeat Problem 3.4.15 for a Villeneuve \bar{n} weighting with $\bar{n} = 6$.

Problem 3.4.17

Derive a simple expression for the BW_{NN} of a SLA using Dolph-Chebychev weighting. Plot BW_{NN} versus SLL in dB for $N = 10$.

Problem 3.4.18

In order to find the Chebychev weights, Stegen [Ste53] used the following technique. The array coefficients are represented by an inverse DFT,

$$a_n = \frac{1}{N} \sum_{m=-\frac{N-1}{2}}^{\frac{N-1}{2}} p_m e^{j \frac{2\pi}{N} nm} \quad (3.385)$$

for N odd. The p_m correspond to equally spaced samples of the beam pattern in ψ -space.

If the pattern corresponds to a Chebychev polynomial, then

$$p_m = T_{N-1}(x_0 \cos \frac{m\pi}{N}). \quad (3.386)$$

Using (3.386) in (3.385) gives an expression for the coefficients,

$$\begin{aligned} a_n &= \frac{1}{RN} \left\{ R + 2 \sum_{m=1}^{\frac{N-1}{2}} T_{N-1} \left(x_0 \cos \frac{m\pi}{N} \right) \cdot \left(\cos \frac{2\pi}{N} mn \right) \right\}, \\ n &= 0, 1, \dots, \frac{N-1}{2}, \end{aligned} \quad (3.387)$$

for N odd. Similarly,

$$\begin{aligned} a_n &= \frac{2}{RN} + \left\{ \frac{R}{2} \sum_{m=1}^{\frac{N}{2}} T_{N-1} \left(x_0 \cos \frac{m\pi}{N} \right) \cdot \left(\cos \frac{\pi}{N} (2n-1)m \right) \right\}, \\ n &= 0, 1, \dots, \frac{N}{2}, \end{aligned} \quad (3.388)$$

for N even.

Use this approach to find the weights in Example 3.4.1.

P3.5 Least Squares Error Pattern Synthesis

Problem 3.5.1

The desired $B_D(\theta)$ is uniform on $-\pi/4 \leq \theta \leq 3\pi/4$. Use the Fourier transform method to find the aperture weighting function for a linear aperture of length $L = 5\lambda$ and $L = 10\lambda$.

- (a) Plot the resulting beam pattern.
- (b) Calculate the resulting maximum sidelobe.
- (c) Calculate BW_{NN} .
- (d) Calculate the peak overshoot in the main-lobe region.

Problem 3.5.2

Repeat Problem 3.5.1 for a standard linear array with $N = 11$ and $N = 21$.

Problem 3.5.3

Assume that $B_d(\theta)$ is uniform on $-30^\circ \leq \theta \leq 60^\circ$. Repeat Problem 3.5.1.

Problem 3.5.4

Assume that $B_d(\theta)$ is uniform on $30^\circ \leq \theta \leq 60^\circ$. Repeat Problem 3.5.2.

Problem 3.5.5

The desired beam pattern is uniform on $-\pi/\sqrt{2} \leq \psi \leq \pi/\sqrt{2}$ and zero elsewhere.

- (a) Find the Fourier coefficients for $N = 11$ and $N = 21$.
- (b) Use a Hann window. Plot the resulting beam pattern. Compare δ , the main-lobe overshoot, and $\Delta\psi$, the transition distance.
- (c) Repeat part (b) using a Hamming window.
- (d) Assume $N = 21$. Use a Kaiser window. Find β to match the overshoot in part (b). Plot the resulting beam pattern. What is $\Delta\psi$?
- (e) Repeat part (d) and match the overshoot in part (c).

Problem 3.5.6

Consider the model in Example 3.5.2.

- (a) Use a DPSS window with $\psi_0 = \pi/6$. Plot the resulting beam pattern and compare to Figure 3.33(a).
- (b) What is the effect of varying ψ_0 on the window?

P3.6 Minimax Design

Problem 3.6.1

Consider the model in Example 3.6.1 ($N = 11$) with $\delta_p/\delta_s = 10$. Assume δ_p is chosen to match the Hamming window in Example 3.5.2.

- (a) Use the Parks-McClellan-Rabiner algorithm to design the optimum weighting and plot the resulting beam pattern.
- (b) What $\Delta\psi = \psi_p - \psi_s$. Compare this result with $\Delta\psi$ found in Example 3.6.1.

Problem 3.6.2

Utilize the techniques in Section 3.6.2 to repeat Problem 3.6.1 for the case when $N = 10$.

Problem 3.6.3

Consider a standard linear array. Assume $20 \log_{10} \delta_p = -53$ dB and $\delta_p/\delta_s = 10$. Assume the Parks-McClellan-Rabiner algorithm is used to design the array weighting.

Plot $\Delta\psi$ as a function of N , the number of array elements.

P3.7 Null Steering

Problem 3.7.1

Consider a standard 41-element linear array with a Chebychev pattern (-40 dB sidelobe). In Example 3.7.3, we placed four nulls at $u = 0.22, 0.24, 0.26$, and 0.28 . An alternative strategy is to place a first- and second-order null at $u = 0.235$ and 0.265 . Find the resulting beam pattern and compare to Example 3.7.3.

Problem 3.7.2

Consider a standard 21-element linear array. We require a null at ψ_0 . $B_d(\psi)$ corresponds to uniform weighting.

- (a) Find the least squares approximation to $B_d(\psi)$ subject to this null constraint.
- (b) Plot the beam pattern for $\psi_0 = 3\pi/N$, $\psi_0 = 2\pi/N$, $\psi_0 = \pi/N$, and $\psi_0 = 0.5\pi/N$. Discuss your results.

Problem 3.7.3

Consider a linear array that consists of two segments: (i) an 11-element standard linear array centered at $z = 0$; and (ii) two 5-element standard linear arrays centered at $z = \pm 7.5\lambda$.

- (a) Assume that the 21 elements are weighted uniformly. Plot the beam pattern and discuss the grating structure.
- (b) We denote the beam pattern in part (a) as $B_d(\psi)$. We require a null at $\psi = 0.5\pi/N$. Find the least squares approximation to $B_d(\psi)$ subject to the null constraint.

P3.8 Asymmetric Beams

Problem 3.8.1

Assume N is even. Let the $w_n, n = 1, 2, \dots, N/2$ correspond to Hamming weighting, and

$$w_{-n} = -w_n. \quad (3.389)$$

- (a) Find and plot the resulting beam pattern.
- (b) Find the slope at the origin and the height of the first sidelobe.

Problem 3.8.2

We can divide an asymmetric (N even) array polynomial into two components:

$$B(z) = B_1(z) B_2(z), \quad (3.390)$$

where

$$B_1(z) = \frac{1 - z^{-1}}{2}, \quad (3.391)$$

and

$$B_2(z) = \sum_{n=0}^{N-2} b_2(n) z^{-n}, \quad (3.392)$$

and thus

$$B_1(\psi) = \sin\left(\frac{\psi}{2}\right). \quad (3.393)$$

- (a) Use this approach to find the beam pattern for uniform weighting.
- (b) Use this approach to design an asymmetric Hann beam pattern.

Problem 3.8.3 (continuation)

Assume $N = 10$. Then $B_2(z)$ is an eighth-order polynomial.

- (a) Choose the coefficients to achieve a Dolph-Chebychev weighting with -40 dB sidelobes.
- (b) Plot the resulting beam pattern.
- (c) Calculate the slope at the origin.

Problem 3.8.4 (continuation)

Assume that the beam pattern in Problem 3.8.3 is $B_d(\psi)$. Find the least squares approximation to $B_d(\psi)$ with a zero-order null constraint at $\psi_0 = 5\pi/N$.

P3.9 Spatially Non-uniform Linear Arrays

Problem 3.9.1

Consider a 4-element non-uniform linear array whose element spacings are $d, 3d, 2d$.

- (a) Plot the beam pattern for uniform weighting.
- (b) Uniform weighting corresponds to $w_1 = w_2 = w_5 = w_7 = 1/4$ and $w_3 = w_4 = w_6 = 0$ in a standard linear array. Plot the autocorrelation of \mathbf{w} with itself.

Problem 3.9.2

Consider a 5-element non-uniform linear array whose element spacings are $d, 3d, 5d, 2d$. Repeat Problem 3.9.1.

Problem 3.9.3 (continuation)

Consider the array in Problem 3.9.2. Use the algorithm in Section 3.9.3 to design a beam pattern with -20 dB sidelobes.

Problem 3.9.4

- (a) Consider a standard linear array with 21 elements. Use the technique in Section 3.9.3 to design a beam pattern that maximizes the directivity subject to a -35-dB constraint of the sidelobe. Describe your algorithm.
- (b) Compare the resulting BW_{NN} with that of a 21-element SLA using Dolph-Chebychev weighting.

P3.10 Beamspace Processing**Problem 3.10.1**

Consider a 32-element standard linear array and a 7×32 beamspace matrix whose rows use conventional weighting. We want to implement the null steering techniques in beamspace. Assume

$$B_d(\psi) = \mathbf{v}_{bs}^H(0)\mathbf{v}_{bs}(\psi). \quad (3.394)$$

We want to place a null at ψ_I while minimizing the least squares error between the desired beam pattern and the beam pattern containing the null.

- (a) Let $\psi_I = 3/32$. Find \mathbf{w}_{bs}^H and plot the resulting beam pattern.
- (b) Repeat part (a) for $\psi_I = 7/32$ and $\psi_I = 13/32$.
- (c) Let

$$B_d(\psi) = \mathbf{v}_{bs}^H(\psi_T)\mathbf{v}_{bs}(\psi). \quad (3.395)$$

Repeat part (a) for $\psi_T = 1/32$ and $\psi_I = 5/32$.

Problem 3.10.2

In many applications, we require

$$\mathbf{B}_{bs}^H \mathbf{B}_{bs} = \mathbf{I}. \quad (3.396)$$

If we use a Taylor weighting, the rows of the beamspace matrix are not orthonormal. We denote this matrix as \mathbf{B}_{no}^H . We pass the output of \mathbf{B}_{no}^H through an $N_{bs} \times N_{bs}$ matrix \mathbf{H}_w . We denote the cascade of the two processors as

$$\mathbf{B}_{bs}^H = \mathbf{H}_w \mathbf{B}_{no}^H. \quad (3.397)$$

- (a) Show that if

$$\mathbf{H}_w = [\mathbf{B}_{no}^H \mathbf{B}_{no}]^{-1/2}, \quad (3.398)$$

then \mathbf{B}_{bs}^H satisfies the orthonormality condition. Is \mathbf{H}_w unique?

- (b) Consider the 7×32 beamspace matrix whose rows have Taylor weighting. Verify the above result numerically.
- (c) Plot the beam patterns for the orthogonal beams. Discuss the sidelobe behavior.

Problem 3.10.3

Consider an 32-element standard linear array and a $N_{bs} \times N$ beamspace processor where rows are orthonormal conventional beams.

We want to generate a beam pattern corresponding to the $\cos^{N_{bs}}$ -element-space weighting in (3.18).

- (a) Consider the case when N_{bs} is even. Assume the beam sector is centered at $u_s = 0$. Find the required beam steering directions and beamspace weights for $N_{bs} = 2, 4$, and 6. Plot the resulting beam patterns and calculate the HPBW, BW_{NN} , D_N , and the height of the first sidelobe.
- (b) Repeat part (a) for $N_{bs} = 3, 5$, and 7.

Problem 3.10.4 (continuation Problem 3.10.3)

Repeat Problem 3.10.3 for the case in which the desired beam pattern corresponds to the Hamming beam pattern in (3.21). In this case, $N_{bs} = 3$.

Problem 3.10.5 (continuation Problem 3.10.3)

Repeat Problem 3.10.3 for the case in which the desired beam pattern corresponds to the Blackman-Harris beam pattern in (3.23). In this case, $N_{bs} = 5$.

Problem 3.10.6 (continuation Problem 3.10.5)

Extend the results of Problem 3.10.5 to the case when $N_{bs} = 7$.

Problem 3.10.7 (continuation, Example 3.10.3)

Consider a standard 32-element linear array and the 6×32 beamspace processor in Example 3.10.3. We use an asymmetric beamspace weighting,

$$[\mathbf{w}_{bs}]_m = -[\mathbf{w}_{bs}]_{M-m}, \quad m = 1, 2, 3. \quad (3.399)$$

- (a) Plot the beam pattern for real constant weights. Plot both $B_{bs}(u)$ on a linear scale and $|B_{bs}(u)|$ in dB.
- (b) Consider various other weightings that trade-off slope at the origin versus sidelobe behavior.

P3.11 Broadband Arrays

Problem 3.11.1

Consider the compound array with nested subarrays shown in Figure 3.57. Each subarray has $N = 11$ elements. In some applications, we want to place a null at a specific point in u -space over the entire octave. Assume that we use $K = 8$ frequency bins.

The desired beam pattern corresponds to conventional weighting in each bin (Figure 2.20). Design a beamformer that provides a least squares approximation to the desired beam pattern (e.g., Section 3.7) with a null at $u = 0.30$ in each bin.

Problem 3.11.2

Consider the compound array with nested subarrays shown in Figure 3.57. Assume that we use $K = 8$ frequency bins.

Design a beamformer using the Riblet-Chebychev algorithm in each frequency bin. Plot the resulting beam pattern in each bin.

Bibliography

- [AC76] S. P. Applebaum and D. J. Chapman. Adaptive arrays with main beam constraints. *IEEE Trans. Antennas Propag.*, vol. AP-24, pp. 650–662, September 1976.

- [AGGS98] Y. I. Abramovich, D. A. Gray, A. Y. Gorokhov, and N. K. Spencer. Positive-definite Toeplitz completion in DOA estimation for nonuniform linear antenna arrays—Part I: Fully augmentable arrays. *IEEE Trans. Signal Process.*, vol.SP-46, pp. 2458–2471, September 1998.
- [Akh56] N. I. Akhiezer. *Theory of Approximation*. Ungar, New York, 1956.
- [AL69] V. D. Agrawal and Y. T. Lo. Distribution of sidelobe level in random arrays. *Proc. IEEE*, vol.57, pp. 1764–1765, October 1969.
- [All61] J. L. Allen. Some extensions of the theory of random error effects on array patterns. Technical Report 36, M.I.T. Lincoln Laboratory, Lexington, Massachusetts, November 1961.
- [AS65] M. Abramowitz and I. A. Stegun. *Handbook of Mathematical Functions*. Dover Publications, New York, 1965.
- [ASG99a] Y. I. Abramovich, N. K. Spencer, and A. Y. Gorokhov. Positive-definite Toeplitz completion in DOA estimation for nonuniform linear antenna arrays—Part II: Partially augmentable arrays. *IEEE Trans. Signal Process.*, vol.SP-47, pp. 1502–1521, June 1999.
- [ASG99b] Y. I. Abramovich, N. K. Spencer, and A. Y. Gorokhov. Resolving manifold ambiguities in direction-of-arrival estimation for nonuniform linear antenna arrays. *IEEE Trans. Signal Process.*, vol.SP-47, pp. 2619–2643, October 1999.
- [Bag76] A. B. Baggeroer. Space-time processes and optimal array processing. Technical Report 506, Navy Undersea Center, San Diego, California, December 1976.
- [Bal82] C. A. Balanis. *Antenna Theory Analysis and Design*. Wiley, New York, 1982.
- [Bar64] N. K. Bary. *A Treatise on Trigonometric Series*, volume 1. Macmillan, New York, 1964.
- [Bar89] D. K. Barton. *Modern Radar System Analysis*. Artech House, Boston, 1989.
- [Bay68] E. T. Bayliss. Design of monopulse antenna difference patterns with low side lobes. *Bell Syst. Tech. J.*, vol.47, pp. 623–640, 1968.
- [BL61] J. Butler and R. Lowe. Beam forming matrix simplifies design of electronically scanned antennas. *Electron. Des.*, vol.9, pp. 120–133, April 1961.
- [Bla65] R. B. Blackman. *Linear Data-Smoothing and Prediction in Theory and Practice*. Addison-Wesley, Reading, Massachusetts, 1965.
- [Boh60] H. Bohman. Approximate Fourier analysis of distribution functions. *Ark. Mat.*, vol.4, pp. 99–157, 1960.
- [Bro88] E. Brookner, editor. *Aspects of Modern Radar*. Artech House, Boston, 1988.
- [BVG00] K. L. Bell, H. L. Van Trees, and L. J. Griffiths, Adaptive beampattern control using quadratic constraints for circular array STAP. *8th Annual Workshop on Adaptive Sensor Array Processing (ASAP 2000)*, M.I.T. Lincoln Laboratory, Lexington, Massachusetts, pp. 43–48, March 2000.
- [Che66] E. W. Cheney. *Introduction to Approximation Theory*. McGraw-Hill, New York, 1966.
- [Cho65] Y. L. Chow. On grating plateaux of nonuniformly spaced arrays. *IEEE Trans. Antennas Propag.*, vol.13, pp. 208–215, 1965.

- [Cho95] T. Chou. Frequency-independent beamformer with low response error. *Proc. ICASSP*, Detroit, Michigan, vol.5, pp. 2995–2998, 1995.
- [DB88] J. H. Doles and F. D. Benedict. Broad-band array design using the asymptotic theory of unequally spaced arrays. *IEEE Trans. Antennas Propag.*, vol.AP-36, pp. 27–33, January 1988.
- [Dol46] C.L. Dolph. A current distribution for broadside arrays which optimizes the relationship between beamwidth and sidelobe level. *Proc. IRE*, vol.34, pp. 335–348, June 1946.
- [Duf89] E. C. Dufort. Pattern synthesis based on adaptive array theory. *IEEE Trans. Antennas Propag.*, vol.AP-37, pp. 1017–1018, 1989.
- [Ell63] R. S. Elliott. Beamwidth and directivity of large scanning arrays. *Microwave J.*, Appendix B, vol.6, pp. 53–60, 1963.
- [Ell75] R. S. Elliott. Design of line source antennas for narrow beamwidth and asymmetric low sidelobes. *IEEE Trans. Antennas Propag.*, vol.AP-23, pp. 100–107, January 1975.
- [Ell81] R. S. Elliott. *Antenna Theory and Design*. Prentice-Hall, Englewood Cliffs, New Jersey, 1981.
- [Er92] M. H. Er. Array pattern synthesis with a controlled mean-square sidelobe level. *IEEE Trans. Signal Process.*, vol.SP-40, pp. 977–981, April 1992.
- [FS74] D. C. Farden and L. L. Scharf. Statistical design of nonrecursive digital filters. *IEEE Trans. Acoust., Speech, Signal Processing*, vol.ASSP-22, pp. 188–196, June 1974.
- [GE93] M. M. Goodwin and G. W. Elko. Constant beamwidth beamforming. *Proc. ICASSP*, Minneapolis, Minnesota, vol.1, pp. 169–172, 1993.
- [GM55] E.N. Gilbert and S.P. Morgan. Optimum design of directive antenna arrays subject to random variations. *Bell Syst. Tech. J.*, vol.34, pp. 637–663, May 1955.
- [HA70] E. L. Hixson and K. T. Au. Wide-bandwidth constant beamwidth acoustic array. *J. Acoust. Soc. Am.*, vol.48, p.117, July 1970.
- [Han66] R.C. Hansen, Editor. *Microwave Scanning Antennas (Array Theory and Practice)*, vol.II, Chapter 1, p. 27. Academic Press, New York, 1966.
- [Han85] R. C. Hansen. Aperture efficiency of Villeneuve \tilde{n} arrays. *IEEE Trans. Antennas Propag.*, vol.AP-33, pp. 666–669, June 1985.
- [Han92] R. C. Hansen. Array pattern control and synthesis. *Proc. IEEE*, vol.80, pp. 141–151, January 1992.
- [Han98] R.C. Hansen, Ed. *Phased Array Antennas*. Wiley, New York, 1998.
- [Har61] R. F. Harrington. Sidelobe reduction by nonuniform element spacing. *IEEE Trans. Antennas Propag.*, vol.AP-9, pp. 187–192, March 1961.
- [Har76] F. J. Harris. High-resolution spectral analysis with arbitrary spectral centers and adjustable spectral resolutions. *J. Comput. Elec. Eng.*, vol.3, pp. 171–191, 1976.
- [Har78] F. J. Harris. On the use of windows for harmonic analysis with the discrete fourier transform. *Proc. IEEE*, vol.66, pp. 51–83, January 1978.

- [Hau68] R. A. Haubrich. Array design. *Bull. Seismol. Soc. Am.*, vol.58, pp. 977–991, June 1968.
- [HTL72] H. S. Hersey, D. W. Tufts, and J. T. Lewis. Interactive minimax design of linear phase nonrecursive digital filters subject to upper and lower function constraints. *IEEE Trans. Audio Electroacoust.*, vol.AU-20, pp.171–173, June 1972.
- [IC65] A. Ishimaru and Y. S. Chen. Thinning and broadbanding antenna arrays by unequal spacings. *IEEE Trans. Antennas Propag.*, vol.AP-13, pp. 34–42, January 1965.
- [Ish62] A. Ishimaru. Theory of unequally spaced arrays. *IRE Trans. Antennas Propag.*, vol.AP-10, pp. 691–702, November 1962.
- [JD93] D. H. Johnson and D. E. Dudgeon. *Array Signal Processing*. Prentice-Hall, Englewood Cliffs, New Jersey, 1993.
- [Joh93] R. C. Johnson. *Antenna Engineering Handbook*. McGraw-Hill, New York, 3rd edition, 1993.
- [Kai74] J. F. Kaiser. Nonrecursive digital filter design using the I_0 -Sinh window function. In *Proc. IEEE Int. Symp. Circuit Syst.*, San Francisco, California, pp. 20–23, 1974.
- [KK66] F. F. Kuo and J. F. Kaiser, editors. *System Analysis by Digital Computer*. Wiley, New York, 1966.
- [KPT60] D. D. King, R. F. Packard, and R. K. Thomas. Unequally spaced broad-band antenna arrays. *IRE Trans. Antennas Propag.*, vol.AP-8, pp. 380–385, July 1960.
- [Kra88] J. D. Kraus. *Antennas*. McGraw-Hill, New York, 2nd edition, 1988.
- [Kre71] J. L. Kreuzer. A synthetic aperture coherent imaging technique. *Acoust. Hologr.*, vol.3, pp. 287–315, 1971.
- [Kum92] W. H. Kummer. Basic array theory. *Proc. IEEE*, vol.80, pp. 127–139, January 1992.
- [Lin92] D. A. Linebarger. A fast method for computing the coarray of sparse linear arrays. *IEEE Trans. Antennas Propag.*, vol.AP-40, pp. 1109–1112, September 1992.
- [LL59] Y. T. Lo and S. W. Lee, editors. *Antenna Handbook Theory, Applications and Design*. Van Nostrand Reinhold, New York, 1959.
- [LL93a] Y. T. Lo and S. W. Lee, editors. *Antenna Handbook (Antenna Theory)*, vol.2, Chapman & Hall, New York, 1993.
- [LL93b] Y. T. Lo and S. W. Lee, editors. *Antenna Handbook (Applications)*, vol.3, Chapman & Hall, New York, 1993.
- [LL93c] Y. T. Lo and S. W. Lee, editors. *Antenna Handbook (Fundamentals and Mathematical Techniques)*, vol.1, Chapman & Hall, New York, 1993.
- [LL93d] Y. T. Lo and S. W. Lee, editors. *Antenna Handbook (Related Issues)*, vol.4, Chapman & Hall, New York, 1993.
- [LMT76] J. T. Lewis, R. Murphy, and D. W. Tufts. Design of minimum noise digital filters subject to inequality constraints using quadratic programming. *IEEE Trans. Acoust., Speech, Signal Processing*, vol.ASSP-24, pp.434–436, October 1976.

- [Lo63] Y. T. Lo. Sidelobe level in non-uniformly spaced antenna arrays. *IEEE Trans. Antennas Propag.*, vol.AP-11, p. 511, July 1963.
- [Lo64a] Y. T. Lo. A mathematical theory of antenna arrays with randomly spaced elements. *IRE Trans. Antennas Propag.*, vol.AP-12, pp.257–268, May 1964.
- [Lo64b] Y. T. Lo. A probabilistic approach to the problem of large antenna arrays. *Radio Sci.*, vol.68D, pp. 1011–1019, September 1964.
- [Lo68] Y. T. Lo. Random periodic arrays. *Radio Sci.*, vol.3, pp. 425–436, May 1968.
- [LP61] H. J. Landau and H. O. Pollak. Prolate spheroidal wave functions, Fourier analysis, and uncertainty: II. *Bell Syst. Tech. J.*, vol.40, pp. 65–84, January 1961.
- [LP62] H. J. Landau and H. O. Pollak. Prolate spheroidal wave functions, Fourier analysis, and uncertainty: III. *Bell Syst. Tech. J.*, vol.41, pp. 1295–1336, July 1962.
- [LST93] D. A. Linebarger, I. H. Sudborough, and I. G. Tollis. Difference bases and sparse sensor arrays. *IEEE Trans. Inform. Theory*, vol.IT-39, pp. 716–721, March 1993.
- [Ma74] M. T. Ma. *Theory and Applications of Antenna Arrays*. Wiley, New York, 1974.
- [Maf62] A. L. Maffet. Array factors with nonuniform spacing parameters. *IRE Trans. Antennas Propag.*, vol.AP-10, pp. 131–136, March 1962.
- [Mai94] R. J. Mailloux. *Phased Array Antenna Handbook*. Artech House, Boston, 1994.
- [May76] J. T. Mayhan. Nulling limitations for a multiple-beam antenna. *IEEE Trans. Antennas and Propag.*, vol.AP-24, pp. 769–779, November 1976.
- [MC63] T. M. Maher and D. K. Cheng. Random removal of radiators from large linear arrays. *IEEE Trans. Antennas Propag.*, vol.AP-11, pp. 106–112, March 1963.
- [McN85] D. A. McNamara. Optimum monopulse linear array excitations using Zolotarev polynomials. *Electron. Lett.*, vol.21, pp. 681–682, 1985.
- [McN93] D. A. McNamara. Direct synthesis of optimum difference patterns for discrete linear arrays using Zolotarev distributions. *Proc. IEE*, vol.MAP-140, pt. H, pp. 495–500, December 1993.
- [McN94] D. A. McNamara. Performance of Zolotarev and modified-Zolotarev difference pattern array distributions. *Proc. IEE*, vol.MAP-141, pp. 37–44, February 1994.
- [Mil85] T. A. Milligan. *Modern Antenna Design*. McGraw-Hill, New York, 1985.
- [MK93] S. K. Mitra and J. F. Kaiser, editors. *Handbook for Digital Signal Processing*. Wiley, New York, 1993.
- [MP73] J. H. McClellan and T. W. Parks. A unified approach to the design of optimum FIR linear phase digital filters. *IEEE Trans. Circuit Theory*, vol.CT-20, pp. 697–701, 1973.
- [MPR73] J. H. McClellan, T. W. Parks, and L. R. Rabiner. A computer program for designing optimum FIR linear phase digital filters. *IEEE Trans. Audio Electroacoust.*, vol.AU-21, pp. 506–526, 1973.

- [MR79] J. H. McClellan and C. M. Rader. *Number Theory in Digital Signal Processing*. Prentice-Hall, Englewood Cliffs, New Jersey, 1979.
- [MTL75] R. A. Mucci, D. W. Tufts, and J. T. Lewis. Beam pattern synthesis for line arrays subject to upper and lower constraining bounds. *IEEE Trans. Antennas Propag.*, pp. 732–734, September 1975.
- [MTL76] R. A. Mucci, D. W. Tufts, and J. T. Lewis. Constrained least-square synthesis of coefficients for arrays of sensors and FIR digital filters. *IEEE Trans. Aerosp. Electron. Syst.*, vol.AES-12, pp. 195–202, March 1976.
- [OC90] C. A. Olen and R. T. Compton, Jr. A numerical pattern synthesis algorithm for arrays. *IEEE Trans. Antennas Propag.*, vol.AP-38, pp. 1666–1676, October 1990.
- [OS89] A. V. Oppenheim and R. W. Schafer. *Discrete-Time Signal Processing*. Prentice-Hall, Englewood Cliffs, New Jersey, 1989.
- [PB72] A. Papoulis and M. S. Bertran. Digital filtering and prolate functions. *IEEE Trans. Circuit Theory*, vol.CT-19, pp. 674–681, November 1972.
- [PL69] A. R. Panicali and Y. T. Lo. A probabilistic approach to large circular and spherical arrays. *IEEE Trans. Antennas Propag.*, vol.AP-17, pp. 514–522, July 1969.
- [PM72a] T. W. Parks and J. H. McClellan. Chebyshev approximation for nonrecursive digital filters with linear phase. *IEEE Trans. Circuit Theory*, vol.CT-19, pp. 189–194, 1972.
- [PM72b] T. W. Parks and J. H. McClellan. A program for the design of linear phase finite impulse response digital filters. *IEEE Trans. Audio Electroacoust.*, vol.AU-20, pp. 195–199, 1972.
- [PPL90] D. Pearson, S. U. Pillai, and Y. Lee. An algorithm for near-optimal placement of sensor elements. *IEEE Trans. Inform. Theory*, vol.IT-36, pp. 1280–1284, November 1990.
- [Pra82] S. Prasad. On an index for array optimization and the discrete prolate spheroidal functions. *IEEE Trans. Antennas Propag.*, vol.AP-30, pp. 1021–1023, September 1982.
- [PRLN92] J. G. Proakis, C. M. Rader, F. Ling, and C. L. Nikias. *Advanced Digital Signal Processing*. Macmillan Publishing Company, New York, 1992.
- [RG75] L. R. Rabiner and B. Gold. *Theory and Application of Digital Signal Processing*. Prentice-Hall, Englewood Cliffs, New Jersey, 1975.
- [Rho63] D. R. Rhodes. The optimum line source for the best mean-square approximation to a given radiation pattern. *IEEE Trans. Antennas Propag.*, vol.AP-11, pp. 440–446, July 1963.
- [Rib47] H. J. Riblet. A current distribution for broadside arrays which optimizes the relationship between beamwidth and side-lobe level. *Proc. IRE*, vol.35, pp. 489–492, May 1947.
- [Ric64] J. R. Rice. *The Approximation of Functions, volume 1. Antenna Handbook*. Addison-Wesley, Reading, Massachusetts, 1964.
- [Ric76] L. J. Ricardi. A summary of methods for producing nulls in an antenna radiation pattern. Technical Report, M.I.T. Lincoln Laboratory, Lexington, Massachusetts, August 1976.

- [RMP75] L. R. Rabiner, J. H. McClellan, and T. W. Parks. FIR digital filter design techniques using weighted Chebychev approximation. *Proc. IEEE*, vol.63, pp. 595–610, April 1975.
- [Ruf93] C. S. Ruf. Numerical annealing of low-redundancy linear arrays. *IEEE Trans. Antennas Propag.*, vol.AP-41, pp. 85–90, January 1993.
- [Ruz52] J. Ruze. The effect of aperture errors on the antenna pattern. *Nouvo Cimento*, Suppl. 3(9), pp. 364–380, 1952.
- [San60] S. S. Sandler. Some equivalence between equally and unequally spaced arrays. *IRE Trans. Antennas Propag.*, vol.AP-8, pp. 498–500, September 1960.
- [Sch43] S. A. Schelkunoff. A mathematical theory of linear arrays. *Bell Syst. Tech. J.*, vol.22, pp. 80–107, 1943.
- [SK82] J. C. Sureau and K. J. Keeping. Sidelobe control in cylindrical arrays. *IEEE Trans. Antennas Propag.*, vol.AP-30, pp. 1027–1031, September 1982.
- [Sko69] M. I. Skolnik. Nonuniform arrays. In Collin and Zucke, editors, *Antenna Theory*, Part I, chapter 6. McGraw-Hill, New York, 1969.
- [Sko80] M. I. Skolnik. *Introduction to Radar Systems*. McGraw-Hill, New York, 1980.
- [Sko90] M. I. Skolnik, editor. *Radar Handbook*. McGraw-Hill, New York, 2nd edition, 1990.
- [Sle64] D. Slepian. Prolate spheroidal wave functions, Fourier analysis, and uncertainty: IV. *Bell Syst. Tech. J.*, vol.46, pp. 3009–3058, November 1964.
- [Sle65] D. Slepian. Some asymptotic expansions for prolate spheroidal wave functions. *J. Math. Phys.*, vol.44, pp. 99–140, June 1965.
- [Sle78] D. Slepian. Prolate spheroidal wave functions, Fourier analysis, and uncertainty, V: The discrete case. *Bell Syst. Tech. J.*, vol.57, pp. 1371–1430, May-June 1978.
- [SP61] D. Slepian and H. O. Pollak. Prolate spheroidal wave functions, Fourier analysis, and uncertainty: I. *Bell Syst. Tech. J.*, vol.40, pp. 43–64, January 1961.
- [SS65] D. Slepian and E. Sonnenblick. Eigenvalues associated with prolate spheroidal wave functions of zero order. *Bell Syst. Tech. J.*, vol.44, pp. 1745–1760, October 1965.
- [ST81] W. L. Stutzman and G. A. Thiele. *Antenna Theory and Design*. Wiley, New York, 1981.
- [Ste53] R. J. Stegen. Excitation coefficients and beamwidths of Tschebyscheff arrays. *Proc. IRE*, vol.41, pp. 1671–1674, November 1953.
- [Ste72] B. D. Steinberg. The peak sidelobe of the phased array having randomly located elements. *IEEE Trans. Antennas Propag.*, vol.AP-20, pp. 312–320, March 1972.
- [Ste76] B.D. Steinberg. *Principles of Aperture and Array System Design*. Wiley, New York, 1976.
- [Ste82] H. Steyskal. Synthesis of antenna patterns with prescribed nulls. *IEEE Trans. Antennas Propag.*, vol.AP-30, pp. 273–279, March 1982.
- [Sto] J. S. Stone. United States Patents No. 1,643,323 and No. 1,715,433.

- [Tay53] T. T. Taylor. One parameter family of line sources producing modified Sin U/U patterns. Technical Report 324, Hughes Aircraft Co., Culver City, California, 1953.
- [Tay55] T. T. Taylor. Design of line-source antennas for narrow beamwidth and low sidelobes. *IRE Trans. Antennas Propag.*, vol.AP-3, pp. 16–28, January 1955.
- [Tay69] G. D. Taylor. Approximation by Functions Having Restricted Ranges III. *J. Math. Anal. Appl.*, vol.27, pp.241–248, 1969.
- [TF70] D. W. Tufts and J. T. Francis. Designing digital low-pass filters: comparison of some methods and criteria. *IEEE Trans. Audio Electroacoust.*, vol.AU-18, pp. 487–494, December 1970.
- [TG92] C-Y. Tseng and L. J. Griffiths. A simple algorithm to achieve desired patterns for arbitrary arrays. *IEEE Trans. Signal Process.*, vol.SP-40, pp. 2737–2746, November 1992.
- [TW70] G. D. Taylor and M. J. Winter. Calculation of best restricted approximations. *SIAM J. Numer. Anal.*, vol.2, pp. 248–255, 1970.
- [Tuc57] D. G. Tucker. Arrays with constant beam-width over a wide frequency-range. *Nature*, vol.180, pp. 496-497, September 1957.
- [Tuf75] D. W. Tufts. Comments on FIR digital filter design techniques using weighted Chebyshev approximation. *Proc. IEEE*, vol.63, p.1618, November 1975.
- [Tuk67] J. W. Tukey. An introduction to the calculations of numerical spectrum analysis. *Spectral Analysis of Time Series*, pp. 25–46, 1967.
- [Unz60] H. Unz. Linear arrays with arbitrarily distributed elements. *IRE Trans. Antennas Propag.*, vol.AP-8, pp. 222–223, March 1960.
- [Vil84] A. T. Villeneuve. Taylor patterns for discrete arrays. *IEEE Trans. Antennas Propag.*, vol.AP-32, pp. 1089–1093, October 1984.
- [VT68] H. L. Van Trees. *Detection, Estimation, and Modulation Theory, Part I*. Wiley, New York, 1968.
- [VT01a] H. L. Van Trees. *Detection, Estimation, and Modulation Theory, Part I*. Wiley Interscience, New York, 2001.
- [Wee68] W. L. Weeks. *Antenna Engineering*. McGraw-Hill, New York, 1968.
- [Wil62] R. E. Willey. Space tapering of linear and planar arrays. *IRE Trans. Antennas Propag.*, vol.AP-10, pp. 1369–1377, July 1962.
- [Wol37] I. Wolf. Determination of the radiating system which will produce a specified directional characteristic. *Proc. IRE*, vol.25, pp. 630–643, May 1937.
- [Woo46] P. M. Woodward. A method for calculating the field over a plane aperture required to produce a given polar diagram. *J. IEE*, vol.93, pt. IIIA, pp. 1554–1558, 1946.
- [ZI98] P. Y. Zhou and M. A. Ingram, A new synthesis algorithm with application to adaptive beamforming, *9th IEEE Workshop on Stat. Signal and Array Process.*, Portland, Oregon, September 1998.
- [ZI99] P. Y. Zhou and M. A. Ingram, Pattern synthesis for arbitrary arrays using an adaptive array method, *IEEE Trans. Antennas Propag.*, vol.AP-47, pp. 862–869, May 1999.
- [Zio95] L. J. Ziomek. *Fundamentals of Acoustic Field Theory and Space-Time Signal Processing*. CRC Press, Boca Raton, Florida, 1995.

Copyright of Optimum Array Processing is the property of John Wiley & Sons, Inc. 2002 and its content may not be copied or emailed to multiple sites or posted to a listserv without the copyright holder's express written permission. However, users may print, download, or email articles for individual use.